CHAPTER I:
Introduction

Memories are the scaffolding that hold our personal histories, declarative facts, and procedural knowledge. Consolidation, the process by which memories are stored and stabilized against disruption, is evolutionarily conserved across species. However, for a process that is so crucial for survival, researchers' ability to clarify the mechanistic basis of memory formation has been notoriously difficult. [1] A major handicap in understanding this intricate process is that there is an inherent difficulty in characterizing the many, dynamic changes that occur across the brain-that lead to consolidation.

In one of the earliest attempts to explain memory, René Descartes postulated that when the brain wished to recall something "animal spirits" emerged from deep within the brain and burrowed through the cortex to free the memory traces that were kept within the folds.[2] While this notion may seem outlandish, at this point in history there was no fully satisfactory explanation as to how unseen messages were transmitted through the brain. Nearly 300 years after Descartes, scientists were still trying to find the specific location of memories in the brain. In his seminal work, Karl Lashley sought the location of memory 'engrams' –physical representations of

memories in the brain.[3] Lashley successfully trained rats to run a maze, after which he lesioned parts of the cortex in attempt to physically remove the memory of the maze. He made several lesions across the entirety of the cortex but was unable to disrupt maze learning until roughly 40% of the cortex had been destroyed.[3] While he was unsuccessful in his endeavor to physically isolate memories, Lashley's failure suggested that memories are not stored in discrete locations in the brain, but rather globally distributed across many regions. [4,5] But what does that mean for our understanding of what, exactly, a memory *IS*? The word memory is, according to Google, the "*faculty by which the mind stores and remembers information",* that is, an active process as opposed to a discrete entity. Thus, understanding the way in which information is stored is a critical question for modern research on memory.

The first, and definitely most famous, clinical insight into how episodic memory is stored was patient H.M. In the 1950's H.M. underwent experimental psychosurgery to treat debilitating seizures. Ultimately, the bilateral lesioning of his temporal lobe removed roughly 2/3 of his hippocampus, which we know now is a processing center for episodic memories.[6] Following his surgery, H.M.'s reasoning, understanding, and recall of distant past events were unaffected, but he suffered a loss of recently acquired memories (i.e., retrograde amnesia) and was completely unable to form lasting memories of new experiences (anterograde amnesia). [7,8] Of important note was that H.M.'s cognitive deficits were only episodic in that his ability to learn procedures remained intact; however, he could not recall learning them. This showed that memories of recent experiences are sensitive to disruption for a window of time after

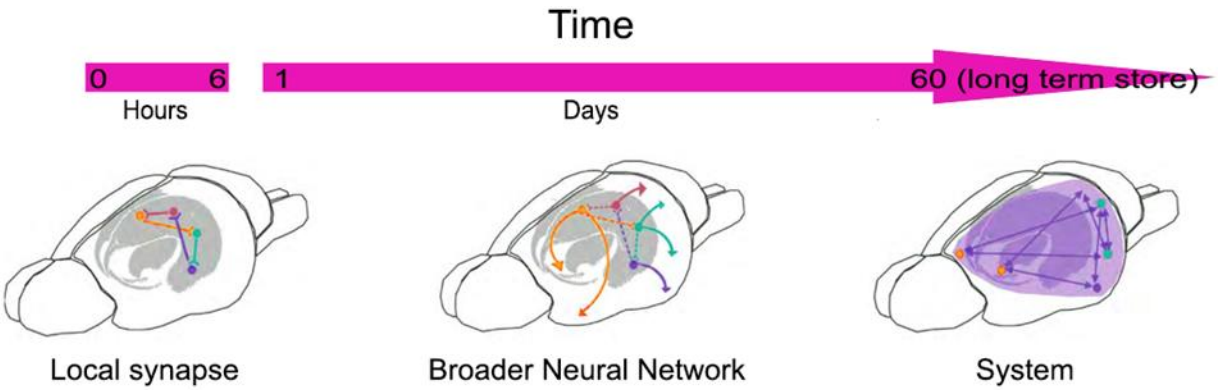

Figure 1.1: Two stage model of memory processing. In the first hours following acquisition, a memory trace is represented in the hippocampus (highlighted in gray) in a specific subset of cells, or engram. The memory trace is then gradually integrated via synaptic connections to other brain regions, including cortical areas outside the hippocampus which were not involved in initial memory acquisition. Over time, the memory trace is distributed and stored throughout the neocortex (shown in purple). Modified from Aton SJ, Seibt J, & Frank, M (Encyclopedia of Life Sciences 2009)

acquisition; memories can be impaired or enhanced during this critical memory consolidation window. [8] The labile state of memories in this window may have evolved as a way for recently-learned information to be combined with previous and future experiences, making learning an ongoing, active, and flexible process.[9] While H.M. was unable to make new memories, details from his past and things he had learned long before his surgery (e.g. riding a bike in childhood) remained intact.[9] This implicates the hippocampus as the first processing step for new episodic information before it can be moved to long-term store. This new information is initially encoded in the hippocampus, after which it is gradually transferred to a more stable, permanent store in the neocortex. [1,10] This is known as the 'two-stage memory model' of long-term memory formation. [11] **(Figure 1.1)** While many have studied how this process is regulated, the exact mechanism of information transfer remains unknown. One compelling candidate is that sleep is a mode of offline processing that promotes a systems-wide consolidation of memory. [11]

1.1 Sleep

Hermann Ebbinghaus, who pioneered the experimental study of learning, noted that forgetting, or disruption of consolidation, was a function of time- in that it is very rapid at first but becomes progressively slower as time goes on. [12] However, in his research, he also noted that there was a time between 8 hours and 24 hours following acquisition, where there was a decreased incidence of forgetting compared to other time points, for which he had explained as experimental error. [13] However, what Ebbinghaus failed to note was that his experimental subjects spent the majority of that interval sleeping.

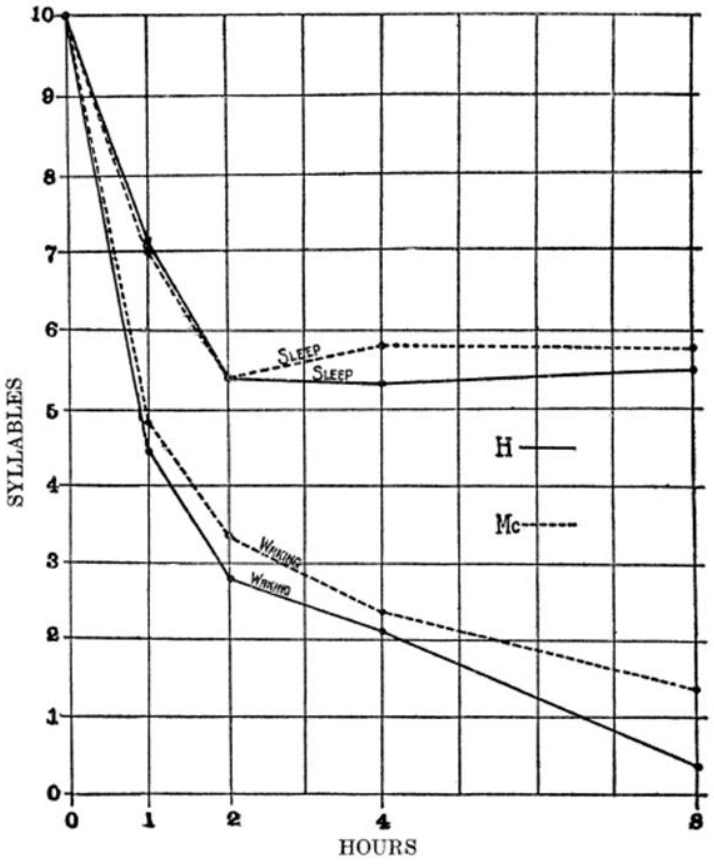

Figure 1.2: Recall over time curves for waking vs. sleeping subjects. Average Number of Syllables Reproduced by each patient (dashed and solid lines represent each patient) at various time-intervals of sleep and waking. From Jenkins and Dallenbach (1924) *The American Journal of Psychology*

Building off of the work of Ebbinghaus, the first empirical evidence linking sleep to memory was performed in 1924 by Jenkins and Dallenbach, where they taught participants a series of nonsense syllables which they asked them to recall hours later. During the interval the participants were either allowed to sleep or were kept awake. The authors noted that there was a marked difference in the rate of forgetting between sleep and waking. [13] **(Figure 1.2)** The recall curves of the waking experiments take a familiar form: a sharp decline which becomes progressively flatter. However, the form of the curves of the sleep experiments differs in that after a small initial decline, the curves flatten and a high and level of recall is maintained thereafter.[13] This suggests that sleep has a role beyond simply slowing the passive forgetting of information; instead sleep may make representations of memories more robust and thus less vulnerable to interference as time passes. [14]

However, sleep is a perplexing behavior as t precludes the ability to find a mate, prevents the gathering resources, and actively makes organisms vulnerable to predation. [15] So why sleep? While the exact biological functions of sleep remain a mystery, its consistent phenomenology and conservation across species makes it an important behavioral process to study.[16] Further research over the past century has shown that sleep plays an essential role in promoting various forms of memory consolidation and also promotes plasticity in brain circuits *in vivo.* [17] However, our biological understanding of ***how*** and ***why*** sleep contributes to cognitive function has advanced very little. This is due, in part, to the myriad of changes occurring simultaneously in the sleeping brain - including changes in neuronal firing patterns, oscillatory activity, and patterns of reactivation.

1.1.1 Sleep architecture

Unlike the nature of memory consolidation, the structure of sleep has been well characterized over the past century. What early sleep researchers like Jenkins and Dallenbach did not know was that sleep comprises two distinct brain states: rapid eye movement (REM) sleep and non-rapid eye movement (NREM) sleep (alternatively referred to in Chapter II of this document as slow wave sleep- SWS). Theses stages differ in frequency and intensity of many behavioral properties such eye movements, muscle tone, and dreaming.[18] During REM sleep, electromyographic (EMG) recordings - which record muscle movement - show complete muscle atonia. **(Figure 1.3a)** However NREM sleep shows some movement of the animal and sometimes the perceptible rhythm of a heartbeat. **(Figure 1.3b)** Wakefulness is characterized by lots of muscle movement, as evident from robust EMG recordings. **(Figure 1.3c)**

Sleep differs not only in behavior, but also in the unseen changes occurring *within* the brain. Local field potential (LFP) recordings are signals generated by the summed electrical current flowing from thousands or even millions of cells within a given brain region. Cortical LFP rhythms show that REM sleep consists of low voltage activity, resembling wakefulness. [18] NREM sleep, however, is characterized by high voltage, slow oscillations, known as slow-wave sleep (SWS). [19] NREM and REM occur sequentially, and progress in cycles over the course of sleep. Across species bouts of each state and cycles between them vary in length. For example, in humans, sleep is generally organized into a single nocturnal period, with ~90 min NREM-REM cycles. The early part of sleep each night is dominated by NREM

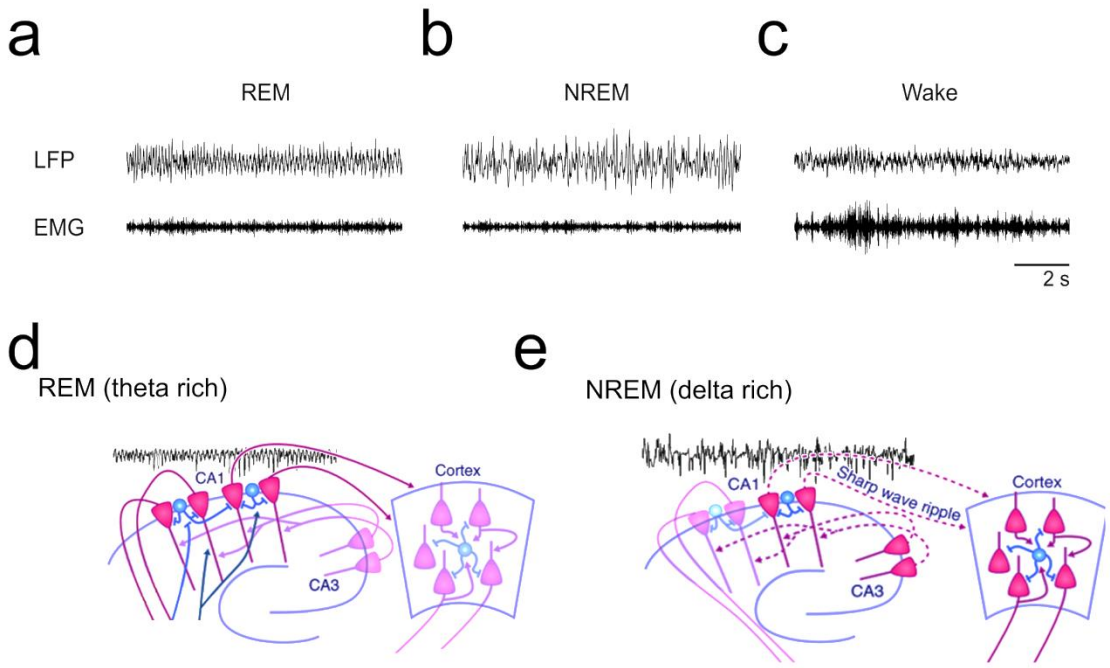

Figure 1.3: Sleep architecture in C57BL/6J mice. Representative LFP and EMG traces in show typical activity during **(a)** NREM, **(b)** REM, **(c)** and wake **(d)** Theta oscillations are locally processed in the hippocampus with the cortex receiving input from CA1 that show theta oscillatory activity. Dark lines are active signals, faded lines are indicative of inactive pathways during specified state. **(e)** Delta oscillations arise from activity throughout the cortex. SPWRs in the hippocampus are correlated with the phase of delta oscillations in cortex, making them an attractive candidate for relay of 'two-step model' of consolidation. Dashed lines are contributing signals. Image modified from Headley, Paré, (2017)

sleep with REM bouts becoming longer as the night progresses. [20] In rodents, however, NREM and REM are compressed into much shorter windows (lasting ~20 min or less). The rodents most frequently studied in a lab setting - rats and mice - are nocturnal, sleep on and off ~12 hours a day in these short bouts, intermittent with bouts of wakefulness.

1.1.2 Sleep-associated network oscillations: REM theta

The oscillatory brain activity patterns of REM and NREM sleep have been extensively characterized, and these patterns are different from both one another and network activity patterns seen in wakefulness. **(Figure 1.3a-c)** REM sleep is dominated by the identified theta (4-12 Hz) rhythm, which is generated within the hippocampus. [10,21] **(Figure 1.3a, d)** Theta has been implicated in coordinating communication between hippocampal neurons, as local properties of theta such as peak frequency, coherence, and entrainment of unit activity are uniform throughout the hippocampus. **(Figure 1.3 d)** These characteristics make it an attractive feature to study as a potential mechanism to promote learning and memory formation, which is hippocampus dependent. [7,19–21] Theta-frequency oscillations of network activity are relayed from the hippocampus to target structures, such as the cortex, evidence of which include increases in coherence between the prefrontal cortex and hippocampus (i.e., entrainment of prefrontal neurons by hippocampally-generated theta) following learning.[22] **(Figure 1.3d)** Early studies investigating sleep's role in memory consolidation focused on REM sleep and the consequences of REM sleep deprivation by repeatedly waking subjects at the first signs of REM sleep. However, an important caveat associated with this approach (and for that matter, all sleep deprivation studies)

is that repeated awakenings cause stress, which itself influences memory function. [23] However, REM deprivation following training disrupts retention of learning to a greater extent than does a control for stress. Taken together, these studies suggested REM sleep in some way facilitates subsequent learning. [24] Additionally, with prolonged REM sleep deprivation, NREM sleep is also fragmented and disrupted.

1.1.3 Sleep-associated network oscillations: NREM delta

While REM sleep is dominated by rhythmic theta oscillations, cortical activity patterns in NREM sleep consist mostly of slow (0.5–4-Hz) delta oscillations and thalamocortical spindles (7-15 Hz waxing and waning events). [25,26] Delta oscillations reflect alternating periods of depolarization and hyperpolarization that are synchronized across the cortex. [27] **(Figure 1.3e)** Cortical delta oscillations also interact with hippocampal activity, with cells in hippocampus synchronizing with cortical delta and spindle oscillations. [28] There are several lines of evidence pointing to the importance of delta oscillations for consolidation. If a subject is presented with a set of stimuli to be subsequently recalled, an intervening sleep period consisting of only high-delta NREM will often increase the number of remembered items. [29] Selective experimental manipulation of slow wave activity in human subjects is sufficient to impair hippocampal activity and cognitive performance during subsequent memory tasks, suggesting slow waves may be necessary for optimal hippocampal circuit function. [25] Additionally, manipulations that increase the strength of delta in the cortex boost long term memory storage. [28,31] Critically, these oscillatory characteristic of NREM seem to interact with features of REM sleep in the context of memory formation. For example, overnight improvement is strongly correlated with both the amount of delta in the first quarter of

the night and the amount of REM sleep later on, and these features together can predict the extent of memory consolidation in human subjects. [32]

1.1.4 Sharp wave ripple complexes

Delta and theta are not the only sleep-associated network activity changes associated with memory consolidation. Sharp-wave ripples (SPWRs) are phenomena that also occur during NREM sleep and are also thought to promote memory consolidation. [33] SPWRs consist of two coordinated events, the first of which, sharp waves, occur as high-amplitude events within hippocampal area CA1 (representing the simultaneous arrival of many excitatory post-synaptic potentials [EPSPs] from area CA3); these events occur at a rate less than 1 Hz across NREM. Following the arrival of this EPSP barrage, high frequency (~150Hz) ripple oscillations emerge locally within CA1. **(Figure 1.3d)** SPWRs thus create great synchrony of firing in CA1 pyramidal cells and interneurons. [21,34,35] SPWRs are thought to be important for the transfer of information from the hippocampus to the neocortex, as firing between areas such as CA1 and temporal and frontal cortex are highly synchronous during these events. [36,37] Importantly, the frequency and amplitude of SPWRs increase during NREM in the ~1 h following a learning task. [38] Furthermore, experimental suppression of NREM SPWRs over several days in rats results in spatial learning impairments. [33] One prominent hypothesis in the field is that during post-learning sleep there exists a critical 'rehearsal' period and that bursts of SPWRs help to facilitate the selective reactivation of previously activated cell assemblies, to promote long-term memory consolidation. [39] Because the precise timing of action potentials among local groups of cells is an important means by

which information is encoded, understanding the changes in network oscillations that follow learning may shed light on the means by which memory is consolidated. [35,40,41]

1.2 Contextual fear memory as a model of episodic memory formation

One of the most common paradigms used in modern neuroscience to study episodic-like memory in an animal model is contextual fear conditioning (CFC). **(Figure 1.4a)** CFC begins with placement of a mouse or rat into a novel environment (a chamber distinct from the home cage) which it can freely explore After a period of free exploration, the animal is given a mild foot shock. This pairing of a conditioned stimulus (the context- environment of the arena) with an unconditioned stimulus (shock) represents the encoding stage of contextual fear memory (CFM). Following the shock, the animal is placed back into its home cage; during which time the memory can then either undergo a process of consolidation (stabilization for long-term storage) or be forgotten. [42] Some period of time later (in many studies, the following day but as short as a few hours and as long as several days after), the animal is placed back into the shock-associated environment, and the memory is accessed. If the animal recognizes the context as one in which foot shock was delivered, it exhibits a behavior referred to as contextual freezing (a state of alert immobility with no movement aside from respiration). This behavior is quantified as the metric of CFM. **(Figure 1.4b-c)** CFM is dependent on hippocampal network activity, as post-training lidocaine infusion into region CA1 of dorsal hippocampus (i.e., to silence local synapses) CFM. [43] **(Figure 1.4b)** CFM consolidation is also blocked by post-training sleep deprivation (SD) at early time points (within the first 5 h) after CFC.[44] **(Figure 1.4c)**

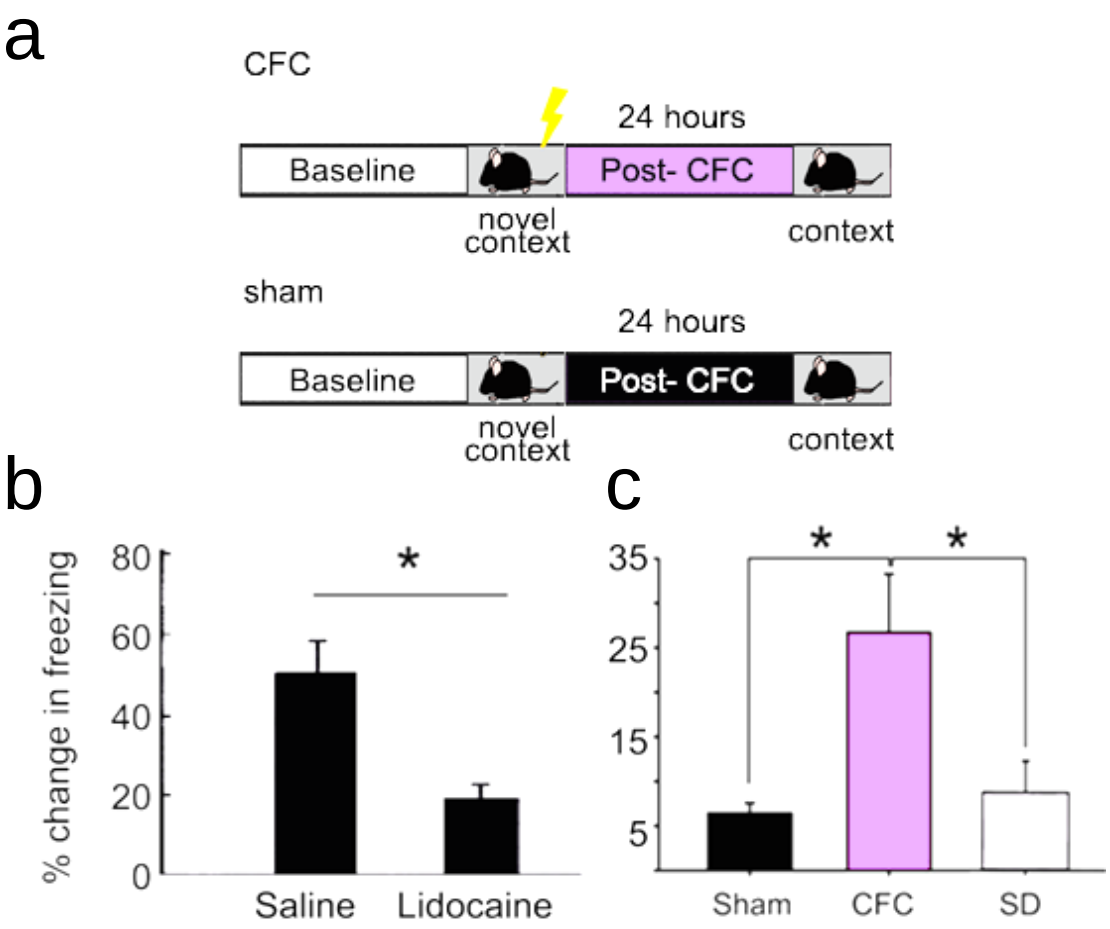

Figure 1.4: Contextual fear conditioning is hippocampus and sleep dependent. (a) Schematic of learning paradigm. Mouse is recorded from in its home cage for basal activity level prior to placement in a novel context. There, after a brief period of exploration, it is given a foot shock. The mouse is then placed back in its home cage for 24-h prior to assessment of freezing behavior when placed again in the novel context. A variation of CFC controlling for context is sham training, which puts the mouse in a novel context, but does not pair it with a foot shock, which does not induce CFM **(c).**[45] **(b)** Electrical inhibition of CA1 synapses after training decreases CFM, while saline injection does not. Modified from *Daumas et al.* (*Learning and Memory* 2005) **(c)** CFM is also dependent on post-training sleep, as 6-h of sleep deprivation abolishes learning behavior.

However, sleep deprivation 5–10 h after CFC does not disrupt CFM, suggesting a critical consolidation window exists in the hours immediately after training, where sleep and hippocampal network activity are necessary for memory stability. [16,17] While it is known sleep is necessary for consolidation of CFM, relatively little is known about the CA1 network activity patterns associated with CFM consolidation, or the role that sleep plays in regulating these dynamics.

1.3 The hippocampus

The hippocampus is located beneath the cerebral cortex and in primates in the medial temporal lobe. The first illustrations of the hippocampus in the 16th century likened the curved structure to a seahorse, and from the Greek word meaning seahorse "hippocampus" it received its name. **(Figure 1.5a)** The hippocampus contains two main subregions: the hippocampus proper (CA [*cornu ammonis,* or Ram's horn, from its curved shape]) and the anatomically and functionally distinct dentate gyrus (DG). The dorsal hippocampus (DH), ventral hippocampus (VH) serve different functions, send projections to different brain areas, and have different circuit anatomy. [46] The dorsal hippocampus has been shown to be of critical importance for both spatial and verbal memory as well as the learning of conceptual information. [47]

Input to the dorsal hippocampus from multiple cortical and subcortical structures (e.g. thalamic nuclei, medial septum) comes from the entorhinal cortex (EC) via the perforant path (PP). **(Figure 1.5b)** Neurons in the EC project to the DG, with additional collaterals projecting to the CA3 subfield. Granule cells in the DG project to the CA3 field of the hippocampus via the mossy fiber (mf) pathway. The CA3's

pyramidal cells project to the CA1 through Schaffer collaterals (Sc). **(Figure 1.5b)** This trisynaptic circuit is a primarily feedforward circuit with very little feedback, making it a compelling clinical and scientific experimental testing-ground for understanding learning.

1.3.1 Network activity in the hippocampus during consolidation

Recent data suggest that sleep promotes the adaptive changes to the strength of synaptic connections between neurons which are thought to underlie long-term memory formation. [48] Hebbian theory postulates that repetition of firing relationships between two cells (in close proximity) will induce lasting changes increasing the stability of the connection between these cells. [49] A prominent hypothesis in the field is that coordinated activation of specific populations of hippocampal neurons is sufficient for subsequent recall. According to this hypothesis, hippocampus-dependent memory formation takes place in two main steps. First, the hippocampus rapidly encodes memories during an experience in wakefulness. Then, during 'offline periods', memory traces are reactivated by the hippocampus, facilitating both reinforcement of synaptic connections between memory-encoding neurons, and allowing information transfer to longer term storage. [50] However, much less is known about how these dynamics are coordinated in the hippocampus and throughout the brain in the hours following learning.

Abundant recent data suggest that a specific region of the dorsal hippocampus, CA1, is critical for the consolidation of CFM and other memories immediately following learning. [40,51–53] CA1 contains heterogeneous ensembles of neurons of which 80-90% are glutamatergic principal (pyramidal) cells (PCs); the activity of which is tightly

controlled by local GABA-ergic, inhibitory interneurons (10-20% of population). [54–56] **(Figure 1.5c)** Many studies have shown GABAergic interneuron dysfunction may be associated with pathologies with disrupted cognition such as schizophrenia, Parkinson's and Alzheimer's disease. [57] While PCs are better studied with regard to information processing (e.g., in sensory systems), in the hippocampus and elsewhere in the brain, interneurons show much larger cell diversity compared to PCs. For example, each sub-class of interneurons receives distinct inputs from different parts of the hippocampus, and sends inhibition to different cellular and sub-cellular targets. As a result, they are well-positioned to play a major functional role in coordinating the control of activity within local hippocampal subfields. [58–60] **(Figure 1.5d)**

1.3.2 Parvalbumin-positive interneurons

GABAergic interneurons are thought to play a major functional role in coordinating activity in local hippocampal PCs, in both health and disease. [59–61] While the connectivity and major synaptic properties of CA1 hippocampal PCs are widely studied, the inhibitory control of CA1 is still not as well understood. While relatively few in number (making up only ~2.6% of the CA1 neuronal population) **(Figure 1.5e-f)** parvalbumin expressing (PV+) fast-spiking (FS) interneurons each innervate large numbers of pyramidal cells. [62] Thus, from an anatomical standpoint, they are uniquely well-suited to coordinate ensemble activity and spike timing within neuronal ensembles. These cells receive excitatory input via Schaffer collaterals from CA3, entorhinal cortex, and amygdala and send their axonal projections laterally to the somata and

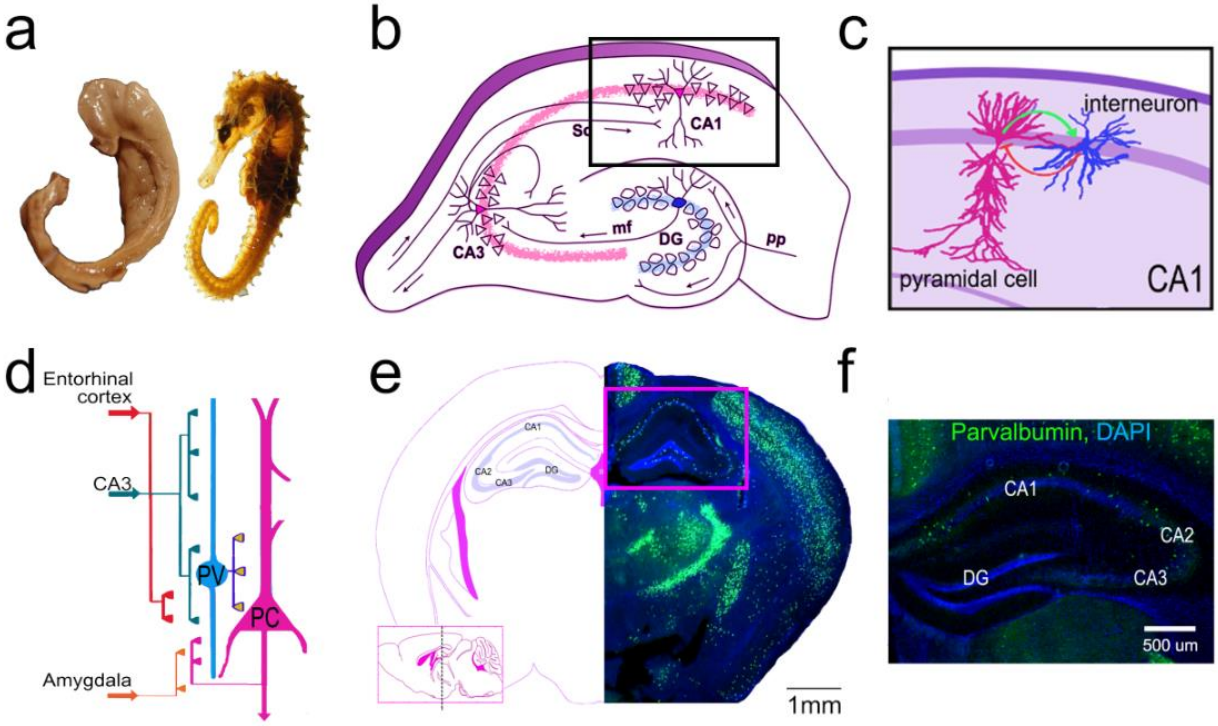

Figure 1.5: Circuitry and parvalbumin positive interneurons in the dorsal hippocampus (a) The curved shape of the primate hippocampus resembles a seahorse, for which it was named. Image from László Seress, 1980. **(b)** Schematic of tripartite synaptic circuit that make up the dorsal hippocampus. pp= preforant path, mf= mossy fibers, Sc= Schaffer collaterals. Modified from Yassa and Stark (*Trends Neurosci.* 2011) **(c)** Schematic of CA1 enlarged from black box in panel b. Positioning of PC cells (pink) and interneurons (blue) in CA1 **(d)** Schematic of inputs received from multiple brain regions by PV+ interneuron dendrites (shown in blue) and PV+ interneuron axon synapses (shown in purple) on PC cells. **(e)** Coronal view of mouse brain at a section 2 mm, posterior of Bregma (inset shows where slice was made) showing PV+ interneuron tagged with green fluorescent protein (GFP). PV+ interneurons are ubiquitous throughout the brain. **(f)** Enlargement of region in the pink box from panel (e), showing preferential localization of PV+ interneurons in CA1.

proximal dendrites of the PCs in CA1. [59,63] **(Figure 1.5d)** PV+ interneurons uniformly fire phase-locked to theta oscillations (firing at the rising peak of theta) in the CA1network *in vivo*. [64,65] They also appear to be critically involved in the induction and maintenance of these oscillations. [66–68] Because these oscillations are hypothesized to promote Hebbian plasticity within coherently firing cell ensembles PV+ interneurons could mediate synaptic changes as a function of the oscillatory activity they control. [4,69]

1.4 Coordinated network dynamics

To understand the oscillatory dynamics leading to memory formation, we can use two metrics to define how neurons and networks are connected in the brain: anatomical and functional.[70] While anatomical connectivity refers to physical (e.g. synaptic) links between cells or brain regions, functional connectivity refers to temporal relationships between neural activity patterns at different locations. [71,72] The control of functional connectivity is thought to be essential for the majority of sophisticated brain functions and its pathologies. [73–75] Memory impairments associated with aging, dementia, mental retardation syndromes, and epilepsy are all associated with impaired intra-hippocampal and hippocampal-cortical functional connectivity. [74,76] In animal models of these disorders cognitive impairments do not generally arise from changes in neuronal firing rates, but rather from abnormal patterns of cell-cell synchronization in local circuits. [77,78] Studies of hippocampal circuits have also demonstrated dynamic changes in functional connectivity among hippocampal neurons during, and after, novel experiences. [79]

1.4.1 Offline reactivation as a means by which memory is reinforced

Recent studies have found that during NREM sleep, traces of neuronal activity patterns from preceding behavior can be observed in rat hippocampus and neocortex, usually during SPWRs. [80,81] The reactivation of these patterns is typically seen in spike-timing-based cross-correlations within a population of simultaneously recorded neurons. [82] Using this sort of measurement, temporally sequenced ensemble firing rate patterns seen during behavior have been reported to reemerge during REM episodes in rats. [83] These events are hypothesized to be generated in the hippocampus as a function of sleep oscillatory events - SPWRs during NREM and theta in REM. The work in this dissertation is aimed at testing the hypothesis that during learning, a specific subset of cells (Lashley's engram) is activated and has temporally coordinated firing. During subsequent sleep (an offline period), state-specific network oscillations coordinated by PV+ interneurons structure the spike timings of these and other cells within CA1. This temporal synchrony of spike timings assists in memory reinforcement, as well as information transfer from the hippocampus to cortex, where it then can be accessed in the future. **(Figure 1.6)**

1.5 Outline

The aim of this dissertation is to explore the coordination of network dynamics that regulate sleep-dependent CFM consolidation in mice. Using a combination of behavioral analysis, electrophysiological recordings, pharmacogenetic and optogenetic manipulations, and computational tools I have investigated the complex network dynamics that promote learning.

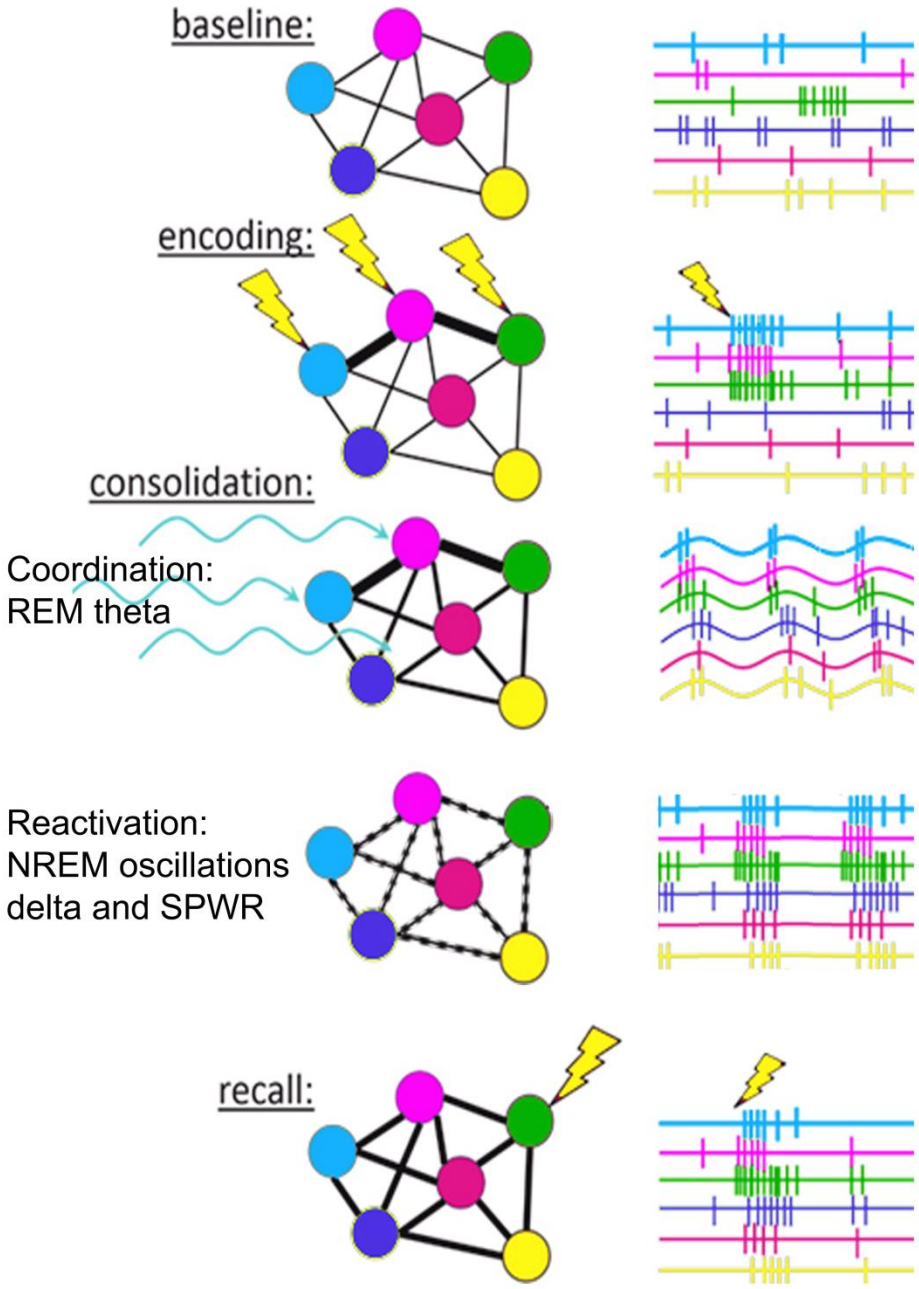

Figure 1.6 Model of Sleep-dependent consolidation. (a) Prior to learning; there is a basal connectivity of the network, with individual neurons firing at unique frequencies. **(b)** Upon initiation of learning, encoding, the introduction of heterogeneity (memory trace) into the network activates a subset of cells and increases firing of those neurons. **(c)** Consolidation is facilitated, via regulated spike timing, aided by sleep-associated network oscillation. This oscillatory activity synchronizes spike timings of all the cells within the local cluster. **(d)** After a period of consolidation, presumably assisted by offline reactivation of this cell ensemble, there is now a globally distributed representation of new memory **(e)** This memory is accessed during recall.

In **Chapter II**, I investigate naturally-occurring changes in CA1 network dynamics following CFC. I show that in C57Bl/6 mice, during CFM consolidation there are increases in CA1 neuronal firing and in hippocampal delta and theta oscillations during post-training sleep. Additionally, for the first time, we employ a novel metric for assessing the stability of functional communication patterns between neurons over timescales relevant to learning (i.e., many hours). I show that post- CFC stabilization of the CA1 network happens preferentially after learning, and particularly during post-learning NREM sleep. This work was published in *Frontiers in Systems Neuroscience* in 2014.

Collaborative work with the Zochowski lab in the Department of Physics is the focus of **Chapter III**. This chapter emphasizes methodologies to explore and quantify network dynamics in time series data. I discuss how in collaboration with the Zochowski lab, we have evolved a published functional network similarity metric into a tertiary analysis of network stability. This metric is applied to work in all subsequent chapters. Part of this chapter has been submitted for publication.

Specific mechanisms controlling CA1 network dynamics during CFM consolidation is investigated in **Chapter IV** I tested the role PV+ interneurons play in state-specific patterns of hippocampal activity. Pharmacogenetic tools in combination with chronic *in vivo* recording were used to characterize neuronal and network activity changes during CFM consolidation. Pharmacogenetic inhibition of PV+ FS-interneurons after CFC leads to impaired CFM consolidation. While this treatment caused no significant changes in sleep architecture, inhibiting PV+ interneurons in CA1 attenuates post-CFC delta, theta, and SPWR activity increases associated with learning in control

mice. Functional connectivity within CA1 also becomes unstable following PV+ interneuron inhibition. I also show that a period of rhythmic activation of PV+ interneurons (at theta frequency) is sufficient to stabilize CA1 dynamics, and strengthen functional connectivity between CA1 neurons, for hours afterward. Taken together, these data suggest that activity among CA1 PV+ interneurons is required for establishing network dynamics that underlie sleep-dependent CFM consolidation. These findings were published in *Nature Communications* in 2017.

To further clarify the state-specific role of PV+ interneurons in CFM consolidation, I employed state-targeted optogenetic manipulations of PV+ interneuron activity in CA1 following learning in **Chapter V**. I found that PV+ interneuron activity during NREM sleep, but not wake or REM sleep, is critical for CFM consolidation. Most striking is rhythmic stimulation of CA1 PV+ interneurons is sufficient to rescue CFM from deficits caused by sleep deprivation. This suggests that PV+ interneurons amplify NREM sleep-associated CA1 network oscillations to regulate spike timing in a manner that could promote systems-level memory consolidation. These findings are in preparation for a forthcoming publication.

CHAPTER II:

CA1 hippocampal network activity changes during sleep-dependent memory consolidation

This chapter includes the manuscript: **Ognjanovski N,** Maruyama D, Lashner N, Zochowski M, Aton SJ. (2014) CA1 hippocampal network activity changes during sleep-dependent memory consolidation. Front Syst Neurosci. 2014; 8: 61. doi:10.3389/fnsys.2014.00061

Abstract:

A period of sleep over the first few hours following single-trial contextual fear conditioning (CFC) is essential for hippocampally-mediated memory consolidation. Recent studies have uncovered intracellular mechanisms required for memory formation that are affected by post-conditioning sleep and sleep deprivation. However, almost nothing is known about the circuit-level activity changes during sleep that underlie activation of these intracellular pathways. Here we continuously record neuronal activity from the CA1 region of freely-behaving mice to characterize neuronal and network activity changes occurring during active memory consolidation. C57BL/6J mice were implanted with custom stereotrode recording arrays to monitor activity of

individual CA1 neurons, local field potentials (LFPs), and electromyographic activity. Sleep architecture and state-specific CA1 activity patterns were assessed during a 24 h baseline recording period, and for 24 h following either single-trial CFC or Sham conditioning. We find that consolidation of CFC is not associated with significant sleep architecture changes, but is accompanied by long-lasting increases in both CA1 neuronal firing and theta (4-12 Hz) frequency LFP activity. These changes occurred in both sleep and wakefulness, and may drive synaptic plasticity within the CA1 network during memory formation. We also find that functional connectivity within the CA1 network, assessed through functional clustering analysis (FCA) of spike timing relationships among recorded neurons, becomes more stable during consolidation of CFC. This increase in network stability was not present following Sham conditioning, was most evident during post-CFC slow wave sleep, and was negligible during post-CFC wakefulness. Thus in the interval between encoding and recall, slow wave sleep may stabilize the hippocampal contextual fear memory trace by promoting CA1 network stability.

2.1 Introduction

Sleep plays an essential role in promoting various forms of memory consolidation[42] and plasticity in brain circuits *in vivo.* [42,84–86] Recent work has taken advantage of single-trial training paradigms in rodents to assess sleep effects on memory processes dependent on circuit plasticity. An example is single-trial contextual fear conditioning (CFC) in mice (placement in a novel context, followed by foot shock), which results in a long-lasting fearful memory of the conditioned context, measured as contextual freezing behavior upon return to the CFC context. In this paradigm, sleep

within the first 5 hours following CFC is an absolute requirement for long-term contextual fear memory (CFM) consolidation. [44,87,88]

Recent work has been aimed at understanding the relationship between sleep and the intracellular events required for both synaptic plasticity and memory formation. The cellular mechanisms underlying CFM *in vivo* are also critical for long-term potentiation (LTP) of CA1 hippocampal synapses *in vitro*. CFM consolidation requires both CA1 network activity, and the activation of kinase and protein synthesis pathways, in the hours immediately following CFC. [43] [89–91] Because these pathways are also required for CA1 LTP, one possibility is that sleep interferes with CFM consolidation by disrupting synaptic potentiation in CA1. Recent studies have clarified intracellular events in the hippocampus during sleep vs. sleep loss and have defined how intracellular signaling pathways are altered by sleep deprivation to impair CFM. [8892] The pathways disrupted in the hippocampus by sleep loss (*e.g.*, mTOR-mediated activation of protein synthesis, kinase-mediated protein phosphorylation) are essential for CA1 LTP, and critically, sleep deprivation itself interferes with CA1 LTP. [87] [88,92]

In contrast to our increasing understanding of the cellular and molecular effects of sleep and sleep deprivation in the hippocampus, almost nothing is known about how the hippocampal network activity changes unique to sleep contribute to memory consolidation. Two hippocampal network oscillations - theta (4-7 Hz) and sharp-wave/ripple (150-200 Hz) events - are hypothesized to promote episodic memory consolidation; these oscillations occur most prominently during rapid eye movement (REM) sleep and slow wave sleep (SWS), respectively. [33,38,93,94] However, very little is known about the role of such oscillations in sleep-dependent memory consolidation.

Even less is known about whether activity changes among individual hippocampal neurons occur during memory consolidation. Recent *in vitro* studies suggest that membrane excitability increases in CA1 neurons follow initial learning, and that long-term (*i.e*., 72 h) sleep deprivation reduces membrane excitability. [87] [95,96] However, it remains unclear how such changes are expressed *in vivo*, or what role sleep might play in regulating *in vivo* activity changes.

Clarification of how hippocampal network activity changes *in vivo* during active memory consolidation was accomplished using continuous stereotrode recording of CA1 neuronal firing and local field potential (LFP) activity in mice. Recordings spanned a 24-h baseline period and for 24 h following either single-trial CFC or (as a control for behavioral procedures not associated with CFM) sham conditioning. We assessed how neuronal and network activity in CA1 was altered as a function of behavioral state and active CFM consolidation. Specifically, we quantified state-specific changes in CA1 neurons' firing rates and power spectral density in CA1 local field potentials (LFPs) following either CFC or sham conditioning (placement in a novel context without associated foot shock). We also assessed changes in the temporal dynamics of functional communication between CA1 neurons in the hippocampal network as a function of CFC and behavioral state.

2.2 Materials and Methods

2.2.1 Mouse handling and surgical procedures

All animal husbandry and surgical/experimental procedures were approved by the University of Michigan UCUCA board for animal care and use. Throughout all experimental procedures, mice were kept on a 12 h: 12 h light: dark cycle (lights on at 8 AM), and were given food and water *ad lib*.

At age 2-6 months, male C57Bl/6J mice (Jackson) were implanted with custom-built, driveable headstages (EIB-36, Neuralynx) under isoflurane anesthesia, using previously-described techniques. [84] Each headstage was composed of two bundles (each approximately 200 µm in diameter, spaced 1-1.5 mm apart) of 7 stereotrodes each (25-µm nichrome wire, California Fine Wire) placed within right-hemisphere CA1. Reference and ground electrodes (silver-plated copper wire, Alpha Wire) were placed over left-hemisphere hippocampus and cortex, and 3 EMG electrodes were placed deep in the nuchal muscle.

2.2.2 Recording procedures

Chronic stereotrode recording was carried out using general procedures described previously. [84] After 1 week of postoperative recovery, mice housed in their home cages were placed within a sound-attenuated sleep-recording chamber (Med Associates), and headstages were connected to a lightweight cable and commutator to record neural signals. Over a 3-5 day period, mice were habituated to the recording chamber and were handled daily for at least 10 minutes. During this time, stereotrode bundles were slowly advanced into the hippocampus in 10-20 µm steps, until stable

recordings were obtained (indicated by continuous presence of spike waveforms on channels for at least 24 h. Following this period of habituation and electrode advancement, all experiments began with a 24-h baseline recording period, starting at lights-on. Signals from each electrode were split and differentially filtered to obtain spike data (200Hz-8kHz) and local field potential/electroencephalographic data (LFP/EEG; 0.5Hz-200Hz) at each recording site. Data were amplified at 20×, digitized, further digitally amplified at 20-100×, and recorded using Plexon Omniplex hardware and software (Plexon Inc.; Dallas, TX).

2.2.3 Contextual fear conditioning (CFC)

Following 24-h baseline recording (within 1 h of lights-on), mice underwent either CFC[44] or Sham conditioning (n = 6 per group). Mice were placed in a novel conditioning chamber with walls made of clear Plexiglas and a shock grid floor. Chamber walls and floor were cleaned with 70% ethanol both prior to and immediately following conditioning. Mice were placed into the chamber and allowed to explore freely for either 150 s (CFC mice) or 180 s (Sham mice). CFC mice then received a 2-s foot shock (0.75 mA; administered via a Med Associates Aversive Stimulator/Scrambler), and were left in the conditioning chamber for an additional 28 s. Throughout these procedures, mice were continuously video monitored using Plexon Cineplex software. Following conditioning, mice were returned to their home cage in the sleep-recording chamber and underwent an additional 24-h period of undisturbed recording prior to contextual fear behavioral assessment.

24 h following contextual fear or sham conditioning, mice were returned to the conditioning chamber for 5 min, during which behavior was continuously video monitored. Freezing behavior (and CFM) was subsequently assessed from video recordings using previously-described methods. [88] To quantify CFM in each mouse, context-specific freezing was quantified as a change in the percentage of total recording time spent in stereotyped freezing behavior between the 5-min test period and the initial 150- or 180-s training period (*i.e*., % time spent freezing at test - % time spent freezing at baseline).

2.2.4 Sleep/wake, firing rate, and LFP analysis

Intrahippocampal LFP and nuchal EMG signals were used to assign polysomnographic data into periods of REM sleep, SWS, and waking states over 10-s intervals using custom software. The proportion of time spent in REM, SWS, and waking (and mean bout duration for each state) was calculated during the baseline and post-conditioning recording periods using standard conventions. [84]

Single-neuron data were discriminated offline using standard principle-component based procedures (Offline Sorter; Plexon). Individual neurons were tracked throughout each experiment on the basis of spike waveform, relative spike amplitude on the two stereotrode recording wires, and neuronal subclass (*e.g*., FS vs. principal). [84] Only those neurons that were verifiably recorded throughout each experiment (*i.e.*, those that were stably recorded across 24-h baseline and 24-h post-conditioning recording) were included in analyses of ongoing network activity.

For each reliably-discriminated neuron, mean firing rates were calculated separately within each behavioral state (REM, SWS, and wakefulness) across the 24-h baseline period and 24-h post-conditioning period. Mean firing rates in each state were then calculated in 6-h windows across each recording period. Firing rate changes after conditioning were then expressed for each neuron as a percent change from baseline in each 6-h window. LFP power was similarly averaged within each state in 6-h windows, and changes in power at each frequency band were quantified from raw LFP traces as a percent change from baseline within each window. For quantitative analysis of LFP changes, changes from baseline were summed across the following frequency bands for each mouse: delta (0.5-4 Hz), theta (4-7 Hz), and gamma (25-50 Hz).

2.4.5 Functional clustering algorithm and network stability analysis

To assess network communication changes in the hippocampus (following conditioning, and as a function of behavioral state), we used a functional clustering algorithm (FCA) to assess network structure based on firing patterns among CA1 neurons. [97] The FCA is a reduction-based algorithm, in which pairwise correlations between neurons in a network are calculated and the most strongly correlated pairs are iteratively merged together into a single spike train. The clustering stops when the most highly correlated pair among the remaining spike trains no longer exceeds a set threshold. Pairwise correlations were calculated based on the average minimum time between the spikes of the two trains (with shorter times indicating greater correlation), normalized with reference to uncorrelated (Poisson) spike trains with the same firing rate. This normalization removes the frequency-dependence of the average minimum time metric and allows comparisons to be made between cells with distinct firing rates.

FCA was combined with the normalized average minimal time measure to generate dendrograms, which were used to characterize the functional connectivity structure among recorded CA1 neurons within a given interval of time.

Dendrograms were generated for the entire population of stably recorded CA1 neurons across each 1-min recording interval. Dendrogram distance values were assigned to each pair of cells, with values between 0 and 1 corresponding to the highest and lowest possible correlation between spike trains. In order to put more importance on strongly connected values than weakly connected values, a monotonically decreasing function, -log(x), was used to flip small distance values into values of high importance and weight down the distance values near threshold (*i.e.*, 1). Thus dendrogram distance values were transformed into vectors. Stability of the network dendrogram structure was assessed by applying cosine similarity to vectors filled with the weighted pairwise dendrogram values. This similarity analysis yielded values between -1 and 1, indicating the level of similarity between dendrogram structures from adjacent 1-minute recording intervals. The resulting minute-to-minute similarity values were averaged over the entire 24-h duration of baseline and post-conditioning recording. Changes in average stability between the baseline and post-conditioning periods were calculated separately using data from all behavioral states, from epochs of SWS only, and from epochs of wakefulness only. Due to the relative infrequency and short duration of REM epochs (which usually lasted less than 1 min each) there was an insufficient number of successive recording epochs to reliably calculate network stability changes specifically within REM epochs, or effectively compare REM stability changes with those of the other states.

2.3 Results

2.3.1 CFC induces contextual fear memory without altering sleep behavior.

Contextual fear memory (CFM) was assessed using previously described methods[88]. As anticipated, mice receiving a foot shock in the context of exploring a novel test chamber (CFC) showed significantly increased freezing behavior when returned to the same environment 24 h later ($p < 0.05$ for CFC vs. Sham, Student's *t*-test; **Figure 2.1a**). While CFM consolidation is known to require sleep behavior, neither CFC nor Sham conditioning caused significant changes in subsequent sleep architecture (*i.e*., % of time spent in SWS, REM, or wakefulness, or mean duration of SWS, REM or wakefulness bouts) from the baseline recording period (**Figure 2.1b**). Two-way repeated-measures ANOVA found no significant effect of either group (Sham vs. CFC) or time relative to training (baseline vs. post-conditioning) on sleep architecture measures. Thus the role of sleep in promoting CFM consolidation is not associated with either overall increases in sleep time, alterations in SWS:REM sleep time ratio, or greater sleep continuity following CFC.

2.3.2 CFM consolidation is associated with increased CA1 neuronal activity

To assess changes in neuronal activity associated with CFM consolidation, firing patterns of individual CA1 hippocampal neurons were tracked continuously over the 24 h baseline recording period and for 24 h following conditioning. Firing rate changes

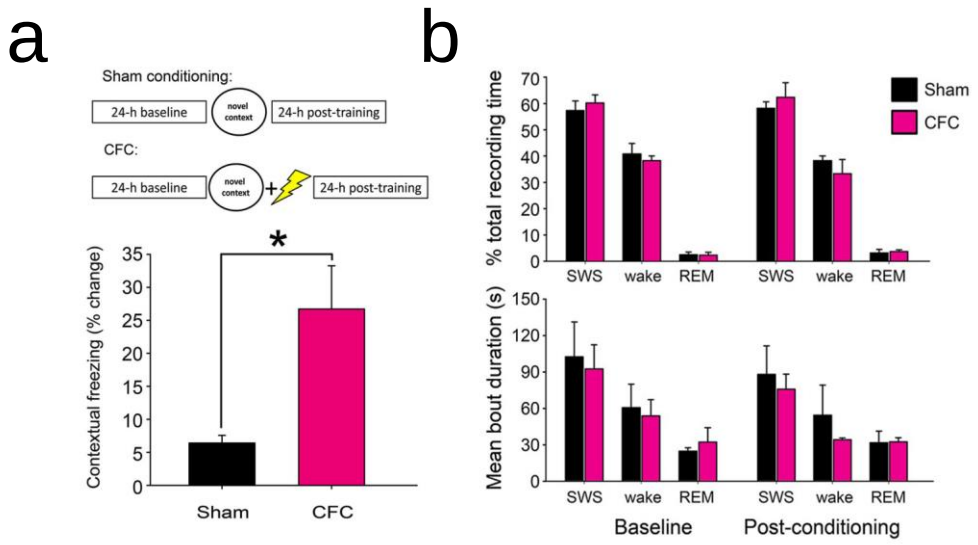

Figure 2.1: CFC initiates fear memory formation without significantly altering sleep-wake behavior. (a) Experimental overview and quantification of context-specific freezing in Sham and CFC mice (n = 6 per group). * indicates $p < 0.05$, Student's t-test. **(b)** Sleep architecture in the 24 h following CFC was not significantly altered, either relative to pre-CFC baseline, or relative to the 24 h following Sham conditioning. Effects of group (Sham vs. CFC) and time relative to training (baseline vs. post-conditioning) on % total recording time or bout duration for each state, *N.S.*, 2-way RM ANOVA.

associated with Sham conditioning and CFC were assessed among those neurons stably recorded across the entire baseline and p.1ost-conditioning periods (from which representative example data is shown in **Figures 2.2a-b**). CA1 firing rates for CFC mice increased significantly in all behavioral states within the first hours following CFC (**Figure 2.3a**; main effect of conditioning $p < 0.005$, $p < 0.001$, and $p < 0.05$ for wake, REM, and SWS, respectively; conditioning × time interaction $p < 0.001$, *N.S.*, and $p < 0.001$ for wake, REM, and SWS, respectively, two-way RM ANOVA). These early post-CFC firing rate changes were not uniform across the population of CA1 neurons. While the majority of neurons recorded from CFC mice (>60%) showed firing rate increases across all states, 25–35% showed decreases, and a much smaller minority (<5% of neurons from all recordings) showed no change (less than 5% increase or decrease from baseline; **Figure 2.3b**). Post-CFC firing rate changes were maintained across the 24 h period following CFC (**Figure 2.3c**; main effect of conditioning $p < 0.05$, $p < 0.01$, and $p < 0.005$ for wake, REM, and SWS, respectively; conditioning × time-of-day interaction $p < 0.005$, $p < 0.001$, and $p < 0.005$ for wake, REM, and SWS, respectively, two-way RM ANOVA).

In contrast, firing rates for Sham mice did not change significantly during REM or wakefulness after Sham conditioning (main effect of conditioning *N.S.*, two-way RM ANOVA), and showed a slight but significant decrease after Sham conditioning within SWS ($p < 0.05$, two-way RM ANOVA). When firing rate changes post-conditioning were expressed as a percent change from baseline, significant differences between Sham and CFC were evident, with mean increases of >50% present in all states immediately

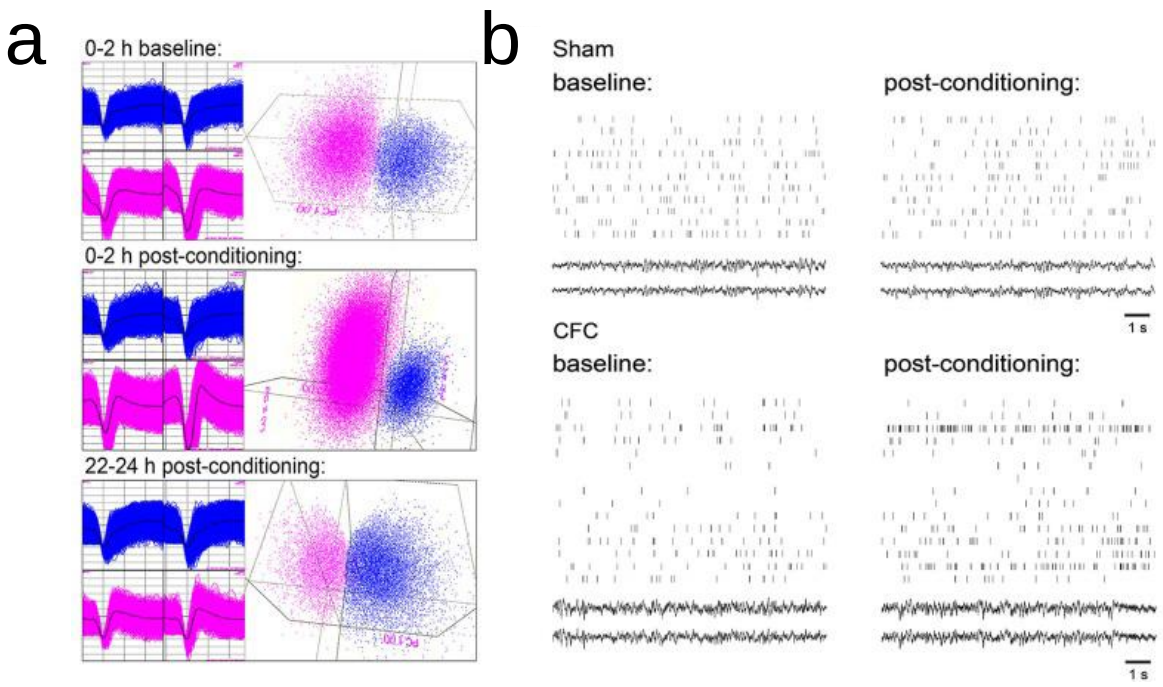

Figure 2.2: CA1 neuronal spiking and field potential recordings. (a) Representative spike waveforms for two CA1 neurons which were continuously recorded on a single stereotrode and reliably discriminated across 24 h baseline and 24 h post-CFC periods (left), and mapping of spike waveform clusters in three-dimensional principal component space (right). Data shown comprise waveforms collected over 2 h windows, either 24 prior to CFC (top), immediately following CFC (middle), or immediately prior to contextual fear assessment (bottom). **(b)** 10 s rasters of firing for all CA1 neurons stably recorded from a representative mouse in Sham and CFC conditions (and corresponding LFPs). Rasters are taken from intervals of SWS within the first hour of both the baseline and post-conditioning periods.

after conditioning (**Figure 2.3d**). The tendency for increased firing among CA1 neurons after CFC was present throughout the entire 24 h post-conditioning recording period. Thus the duration of firing rate changes we see *in vivo* (lasting at least 24-h following conditioning) is consistent with the reported time course of CA1 neurons' intrinsic excitability changes observed *in vitro* after classical conditioning in various rodent models. [95,96,98]

2.3.3 CA1 field activity is altered during CFM consolidation

To determine how hippocampal network activity patterns are affected during CFM consolidation, raw spectral power for CA1 LFPs were compared in each behavioral state between corresponding 6-h time windows in the baseline and post-conditioning periods (**Figure 2.4**). Comparisons of percent changes in LFP power at each frequency band showed clear differences between CFC and Sham mice. The most striking and consistent difference was an increase theta (4-12 Hz) frequency activity, which was present in all states (REM, SWS, and wakefulness) throughout the post-CFC recording period (**Figure 2.4**).

To determine how hippocampal network activity patterns are affected during CFM consolidation, raw spectral power for CA1 LFPs were compared in each behavioral state between corresponding 6 h time windows in the baseline and post-conditioning periods (**Figure 2.4a**). Comparisons of percent changes in LFP power across frequency bands showed clear differences between CFC and Sham mice. To characterize these differences, power spectral changes from baseline were summed

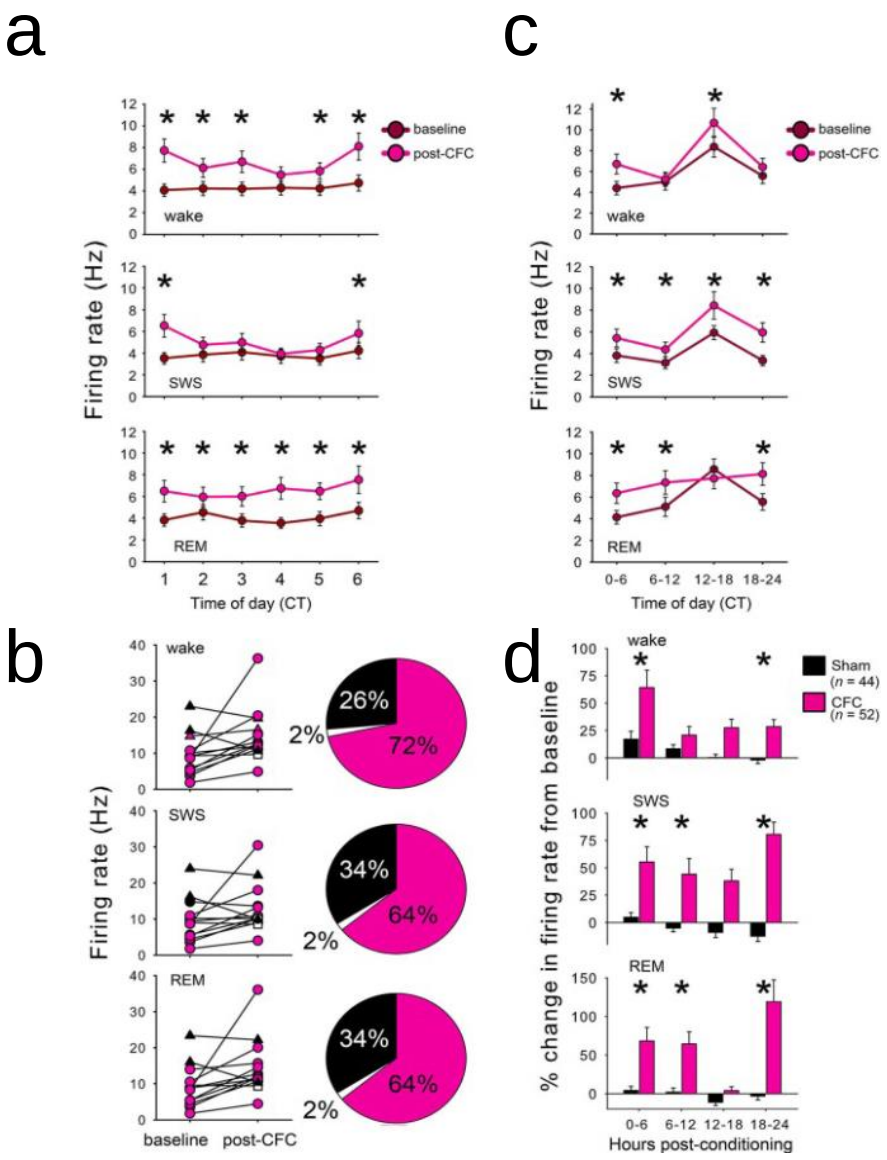

Figure 2.3: CFC induces long-lasting increases in CA1 neuronal firing rates. (a) Mean firing rates for CA1 neurons increased significantly across the first 6-h during the post-CFC recording period. For all 3 states, main effect of conditioning $p < 0.05$; conditioning × time-of-day interaction $p < 0.005$, 2-way RM ANOVA). (b) Early post-CFC firing rate changes were not uniform across the population of CA1 neurons. Cells that increase across a state are shown in pink, cells that decrease in black, and cells showing no change (<5%) in firing rate from baseline are shown in white. **(c)** Post-CFC firing rate changes were maintained across the 24 h period following CFC **(d)** CFC and Sham conditioning differentially affected firing rate. Post-conditioning firing rates for each neuron were expressed as a % change from the corresponding period of baseline recording. Effects of group (Sham vs. CFC) and time relative to training (baseline vs. post-conditioning) $p < 0.001$ for each state, 2-way RM ANOVA. * indicates $p < 0.05$, Holm-Sidak *post hoc* test for baseline vs. post-CFC comparisons.

across delta (0.5–4 Hz), theta (4–12 Hz), and gamma (25–50 Hz) frequency bands. In the first 6 h post-conditioning, CFC showed smaller increases in delta-activity than Sham mice during both wakefulness and SWS, and larger increases in REM (**Figures 2.4a-b**).

At subsequent time points, delta-power showed larger increases in CFC mice than Sham mice—an effect that was present across all states (main effect of conditioning $p < 0.01$, $p < 0.001$, and *N.S.* for wake, REM, and SWS, respectively; conditioning × time-of-day interaction $p < 0.001$ for all states, two-way RM ANOVA). Theta-frequency activity showed even larger increases following CFC, which were present in REM and wakefulness (but not SWS) throughout the post-CFC recording period (main effect of conditioning $p < 0.005$, $p < 0.001$, and *N.S.* for wake, REM, and SWS, respectively; conditioning × time-of-day interaction $p < 0.005$ for REM, *N.S.* for wake and SWS, two-way RM ANOVA). Because the range of theta-frequencies reported here is broader than that published in some studies (which can be restricted to a range as narrow as 4–7 Hz), we also compared changes in the 4–7 Hz band, with nearly identical results (main effect of conditioning $p < 0.001$, $p < 0.001$, and *N.S.* for wake, REM, and SWS, respectively; conditioning × time-of-day interaction $p < 0.001$, $p < 0.05$, and *N.S.* for wake, REM, and SWS, respectively, two-way RM ANOVA). Slight increases in gamma were also present following CFC, but these changes were restricted to REM (main effect of conditioning $p < 0.001$; conditioning × time-of-day interaction $p < 0.001$, two-way RM ANOVA).

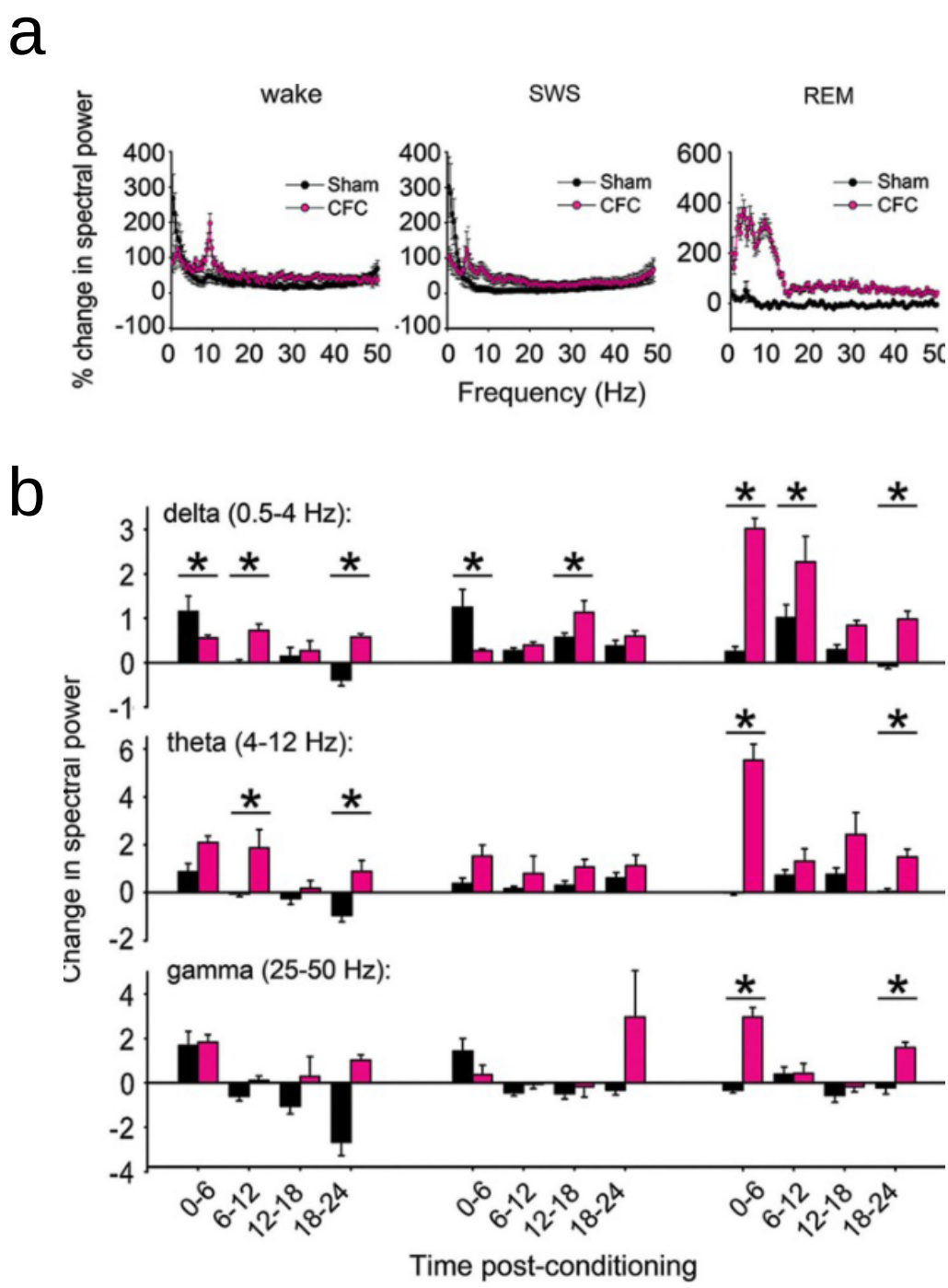

Figure 2.4: CFC induces long-lasting increases in CA1 theta (4-12 Hz) oscillatory activity. (a) Changes in spectral power (between baseline and post-conditioning recording periods) are shown from 0-50 Hz over successive 6-h time windows in wakefulness, SWS, and REM. **(b)** While the largest post-CFC changes were seen in the theta frequency range during REM (with relative increases peaking at around 8-10 Hz), significant increases were also present in the same frequency band following CFC in both wakefulness and SWS.

2.3.4 CA1 network structure is stabilized during CFM consolidation

Recent quantitative analysis of hippocampal immediate-early gene expression has indicated that activity across the network of CA1 neurons during rest reflects the specific network activation patterns generated in prior waking experience. [99] This suggests that a memory trace, or engram, may be continuously present in CA1 at the level of network activation (and perhaps network functional connectivity) long after a learning experience ends. To test whether this is true of the CA1 network following CFC, we used a functional clustering algorithm (FCA) to quantify functional connectivity between CA1 neurons. [97] We also used minute-to-minute comparisons of CA1 network functional connectivity to quantify the stability of network activity patterns at baseline and after conditioning.

Stability of network functional structure was assessed over time by comparing FCA-generated network architecture between successive 1 min intervals across the entire baseline and post-conditioning periods (**Figure 2.5a)** The term “stability” in this case means the similarity (in time) of functional connectivity among recorded neurons. In this sense, more stable networks maintain similar functional clusters over time (i.e., the same neurons remain within given functional clusters, and neither the number of clusters nor the joining distance change significantly). Using this metric, average minute-to-minute stability values were calculated across each recording period, and changes in average stability across the recorded CA1 network post-conditioning were expressed as a percent change from baseline in each mouse. CA1 network structure stability increased significantly after conditioning in CFC mice, but not in Sham mice

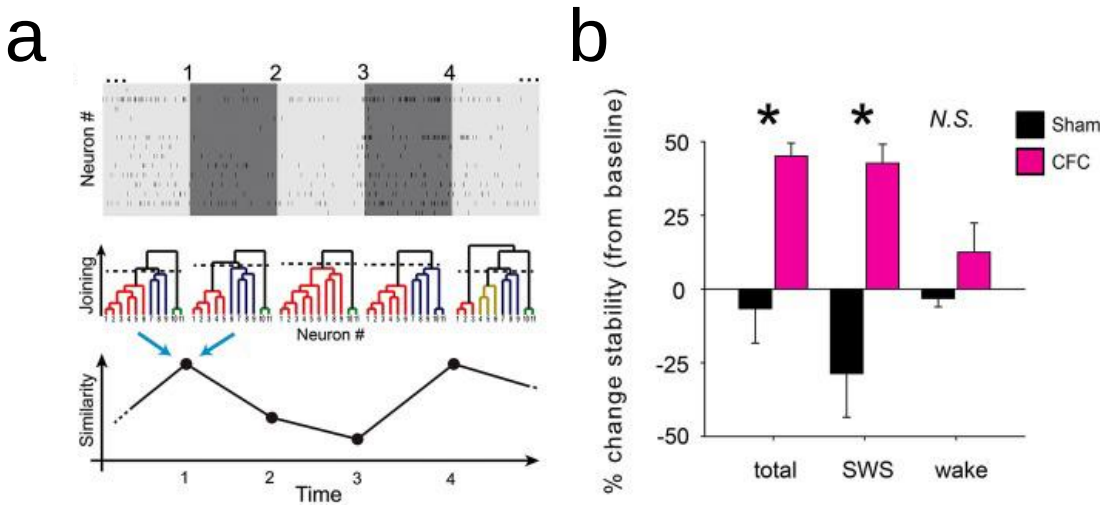

Figure 2.5: CA1 network communication becomes more stable during SWS following CFC. (a) Schematic depiction of the stability analysis. Recorded spike trains are divided into adjoining 60-s intervals (top). Functional clustering analysis (FCA) is performed on every interval (middle). The stability of network connectivity is established from the evaluation of the similarity of neuronal functional clustering between consecutive intervals (bottom). **(b)** Changes in mean network stability (from baseline to post-conditioning periods) are shown for Sham and CFC mice. While significant differences in stability changes were seen between the two groups when analysis was carried out across all states (total) or across intervals occurring in SWS, no significant stability differences seen for analysis over intervals of wakefulness (wake).

(**Figure 2.5b**). This stability increase was evident when all successive 1 min intervals were included in stability analysis, regardless of behavioral state, and also when only intervals spent in SWS were analyzed separately ($p < 0.01$ and $p < 0.005$ respectively for all-state and SWS-specific analysis, Student's *t*-test). However, the same stability increase was not seen across post-CFC intervals of wakefulness (stability changes for CFC vs. Sham *N.S.*, Student's *t*-test). Stability across REM intervals could not be separately assessed due to the relatively brevity and infrequency of REM episodes, which reduced the reliability of stability measurements.

2.4 Discussion

These studies were aimed at assessing sleep-associated changes in CA1 network activity that might contribute to the sleep-dependence of contextual fear memory (CFM) consolidation. We found that single-trial CFC induces CFM without causing significant alterations in sleep architecture over the 24-h CFM consolidation period. However, CFC leads to three long-lasting changes in either the activity of individual CA1 neurons or the interactions of these neurons within the hippocampal network. These changes are discussed in detail below:

2.4.1 Post-CFC firing rate increases in CA1 neurons

First, we find that neuronal firing rates increase immediately after CFC *in vivo*, and remain elevated over the course of 24 h of post-CFC recording. This increase was specific to CFC, as similar firing rate changes were not seen after Sham conditioning, where exploration of a novel context is not paired with foot shock. Critically, the time

course of these changes is similar to that of excitability changes measured *in vitro* in mouse, rat, and rabbit CA1 neurons following aversive conditioning. [95,96]

Recent studies of the underlying mechanisms for these changes have shown that aversive conditioning leads to decreased expression of KCNN2, an apamin-sensitive small conductance calcium-activated potassium channels (SK), in the hippocampus, which has previously been implicated in LTP. [100] Activation of SK channels blocks conditioning-induced excitability changes in both CA1 pyramidal neurons and interneurons, and impairs learning. [100] Because SK channels play a critical role in regulating after hyperpolarizing currents and thus, firing rates in CA1 excitability changes associated with SK channel reductions may mediate firing rate increases we see *in vivo* after CFC. [101] Critically, sleep may play an important role in maintaining conditioning-induced reductions in SK channel expression. A recent study examining sleep- and sleep deprivation-mediated gene expression changes found that expression of KCNN2 is reduced during sleep and increased during sleep deprivation in multiple brain areas. [102] Such a mechanism may explain the effect of sleep loss in reducing membrane excitability in CA1.

What effect do firing rate increases have on the hippocampal network during CFM consolidation? While CA1 network activity in the hours following CFC is essential for CFM, the role of increased activity in the consolidation process is unknown. [43] One possibility is that increased firing rates among CA1 neurons drives synaptic plasticity in the network throughout the post-CFC consolidation window. Firing rate contributes to the sign (LTP or LTD) of spike-timing-dependent plasticity, and for some CA1 synapses, firing rate appears to be more important than pre-vs.-postsynaptic spike timing for

determining the sign of plasticity. [103] [104] Based on available data from *in vitro* studies, it seems plausible that the increase in firing we observe after CFC *in vivo* biases CA1 neurons toward synaptic potentiation. Interference with cellular pathways required for synaptic potentiation in the hours following CFC (through either drug treatments, or behaviorally, through sleep deprivation) impairs CFM consolidation. [88,89] Because synaptic potentiation clearly plays an important role in long-term memory formation, it stands to reason that enhanced neuronal firing could promote consolidation through this mechanism.

2.4.2 Post-CFC increases in theta oscillations

Second, we find that theta-frequency activity in CA1 is specifically increased in the range of 6-12 Hz following CFC (relative to Sham conditioning), with a time course similar to that seen for firing rate changes. CA1 neurons show natural oscillations in membrane potential *in vitro* that resonate with exogenous input at theta frequencies between, and CA1 theta oscillations *in vivo* are specifically augmented during novel experiences which engage the hippocampus.[105] [106] Because theta frequency stimulation can induce LTP in CA1 *in vitro*, and driving theta oscillations in the hippocampus *in vivo* promotes memory consolidation, it is tempting to speculate that these oscillations drive the network plasticity underlying memory formation. [94] [107] Our data suggest that naturally-occurring enhancements in theta-frequency CA1 oscillations accompany CFM consolidation. These increases are most prominent following CFC in REM sleep (a state in which prominent hippocampal theta-oscillations are a consistent feature), but are also clearly present in wakefulness. These findings raise two questions. First, what network changes underlie these long-term increases in theta-

frequency activity? One possibility is that CFC leads to rapid alterations in hippocampal inputs (e.g., input from the medial septum) which could subsequently drive theta-activity more robustly in CA1. [108] Another is that CFC alters intra-hippocampal network connectivity, which could lead to more coherent theta-oscillatory activity. While our current data do not address the former, our analyses of CA1 network structure (see below) suggest that the latter possibility is plausible. A second question is whether, and how, these oscillations contribute to memory consolidation. As is true for increases in neuronal firing, it seems plausible that enhancing theta-oscillations could promote consolidation by creating optimal conditions for synaptic potentiation within hippocampal circuits. Moreover, because increased theta-frequency coherence between the hippocampus and other brain areas (e.g., the amygdala and prefrontal cortex) is specifically associated with other forms of memory consolidation, it is also possible that enhanced CA1 theta-rhythms could drive systems-level memory consolidation during sleep. [22 42,91]

2.4.3 Post-CFC stabilization of the CA1 network

The third change we observe in CA1 after CFC is a significant stabilization of functional connectivity within the CA1 network. Network stability increases after conditioning were not seen in any of the Sham mice, but were present in all CFC mice. Importantly, significant increases in network stability after CFC were not seen during periods of wakefulness, but were clearly seen in SWS. Thus increased network stability is one feature of network activity that is associated specifically with sleep during CFM consolidation. Because sleep is necessary for long-term memory formation in this system, it stands to reason that network-level changes associated with sleep are critical

for the consolidation process. Stabilization of spike-timing relationships within CA1 may be a plausible strategy for preserving a memory trace (*i.e.*, an engram) of CFC during consolidation. In this case, the memory trace would be weakened by replacing sleep with wakefulness (*i.e.*, with sleep deprivation) - which could provide a network-level mechanistic explanation for why sleep deprivation disrupts mnemonic function.

"Replay" of experience-associated sequences of network activity during subsequent rest has been hypothesized to play an important role in memory consolidation. [16] However, most studies of replay involve recording activity patterns from animals following repetition of a relatively familiar task; *i.e*., the animals under study have been trained over a period of days to weeks prior to recording. Thus the replay described in these studies is not temporally associated with consolidation of new memories; it might more fairly be described as occurring following practice of a very familiar task. In almost no case has sequential pattern reactivation been demonstrated in the context of active consolidation of memory following a novel learning experience. The stabilization of network activity patterns we see following CFC may be a true network-level correlate of *de novo* memory consolidation. The fact that it is associated specifically with a behavioral state required for consolidation suggests that it may play a functional role in protecting memory traces at their most labile state, immediately following encoding.

Taken together, the neuronal and network activity changes we have found comprise one of the first descriptions of, naturally occurring, *in vivo* electrophysiological changes corresponding to active memory consolidation. Future studies will be aimed at better understanding whether similar network level changes occur following learning in

other brain structures, the role of sleep in promoting these changes, as well as which network-level changes are necessary, and sufficient, for memory consolidation and what regulates these changes.

CHAPTER III:

Quantifying the functional network dynamics underlying memory formation

This chapter includes figures and text modified from the manuscript: Skilling Q, Maruyama D, **Ognjanovski N**, Aton SJ, Zochowski M. Structurally-induced functional network stability as a mechanism for systems memory consolidation.

3.1 Introduction

How information is encoded and stored in neural circuits is a long-standing question in neuroscience. Memory formation is an evolutionarily conserved process; in order to survive, animals routinely store fleeting experiences into memories that can last a lifetime. However, understanding how these experiences are encoded and stored long term by the circuits of the brain has been a historical conundrum.[3] In particular, uncovering the network dynamics leading to memory formation has been notoriously difficult. [1] A major handicap in understanding this intricate process is that there is an inherent difficulty in characterizing the many facets of network signaling changes- whether biological, physical, or computational - which could play a role in consolidation.

The main objective of this theoretical chapter is to critically address some of the current metrics employed to aid in understanding the neural network dynamics associated with consolidation. With advancing technology allowing data collection from increasing numbers of simultaneously recorded neurons across different brain regions, and over longer recording periods, it has become increasingly challenging for experimentalists to identify and quantify these changes. Interdisciplinary approaches may optimize the information extracted from biological data sets, to address questions relating to network dynamics leading to memory formation. [79] Computational modeling can be used to establish testable predictions, and new quantitative methodologies will allow investigators to characterize network dynamic changes more rapidly and more sensitively. In this chapter I introduce the reader to current mathematical approaches to understanding network dynamics, and the shortcomings when applying these metrics to large data sets. In addition, I introduce a novel metric developed with collaborators in the University Of Michigan Department Of Physics that has optimized our analysis of how network connectivity and dynamics are changing following learning. Using these tools, we hope to obtain novel insight into how the brain encodes and stores information.

3.2 Quantifying functional connectivity between neurons: how and why?

Connectivity refers to a pattern of structural links -anatomical connectivity- or of statistical dependencies -functional connectivity- between nodes in a network, or for biological system- neurons in the brain**.** While assessing anatomical connectivity ("connectomics") is becoming increasingly high-throughput thanks to recent technological advances, for the most part this can only be done in postmortem tissue -

not in the living brain. Functional connectivity, on the other hand, can be measured *in vivo* and is dynamic. One general strategy for understanding network communication in the context of information processing is to first quantify communication (i.e., functional connectivity) in a pairwise manner between recorded neurons. One can then characterize how the pattern of communication between neurons changes over time which can then be related to a particular processes or task. Such measureable changes in communication may either be the cause, or the result, of spike-timing-dependent plasticity. [103][103] Different methods have been employed to characterize information flow between neurons based on their respective activity patterns. These metrics fall into two broad categories: directed measures and non-direction biased connectivity.

3.2.1 Directional connectivity

Directional couplings indicate causality. Directional connectivity metrics are notable because they differentiate effects of one neuron, or continuous voltage signal [e.g. a local field potential], on another. [109] (see schematic example: **Figure 3.1a**) Granger causality (GC) is a powerful method for identifying directed functional interactions from time-series data by using the event history of one time series to try to explain the events of the other time series (X→Y). [110] Causality can then be used to identify sequences of connected neurons with elevated synaptic strengths that are embedded in a realistic spiking network model. [111] These interactions are bidirectional, and are usually task specific, meaning that the structural connectivity within a certain area dictated the function of that process. GC, however, removes the network-centric hypothesis when describing information flow in the brain, that there is a global

representation of a locally processed stimulus. [112] As a result, GC has several hiccups in trying to assess dynamics of a changing network where multiple factors, such as timing of different oscillations occurring during sleep states, which are thought to drive network changes leading to stability.[22,113]

Transfer entropy (TE) is another directional connectivity model, very similar to GC. [114] TE measures directed information transfer between jointly dependent processes, but is time-asymmetric, meaning that while GC is a predictive model where X→Y, TE is framed in terms of resolution of uncertainty of these variables- where for X & Y, Y has as much fate in determining its dynamics as X does. [112] This helps to resolve the idea of global information storage. A problem associated with TE, however, is that it is computationally intensive. [115] Additionally, with TE and the analysis of spike times, an experiment can only use one time delay. This is problematic because delays between an action potential and a post-synaptic potential typically span a large range (1-20ms) in mammals. [103] Adjusting time bins to larger delays could sacrifice temporal resolution, which in the case of analysis of discreet state windows is, like GC, a problem for our analysis.

3.2.2 Non-direction biased connectivity

Quantification of communication between neurons can also be quantified in a way which does not make conclusions regarding the direction of information flow – referred to as non-direction based metrics. [116] **(Figure 3.1b)** Often times communication takes place among neural populations located in in brain areas across vast (synaptic or actual) distances. Due to sheer size and number of connections that cross multiple brain

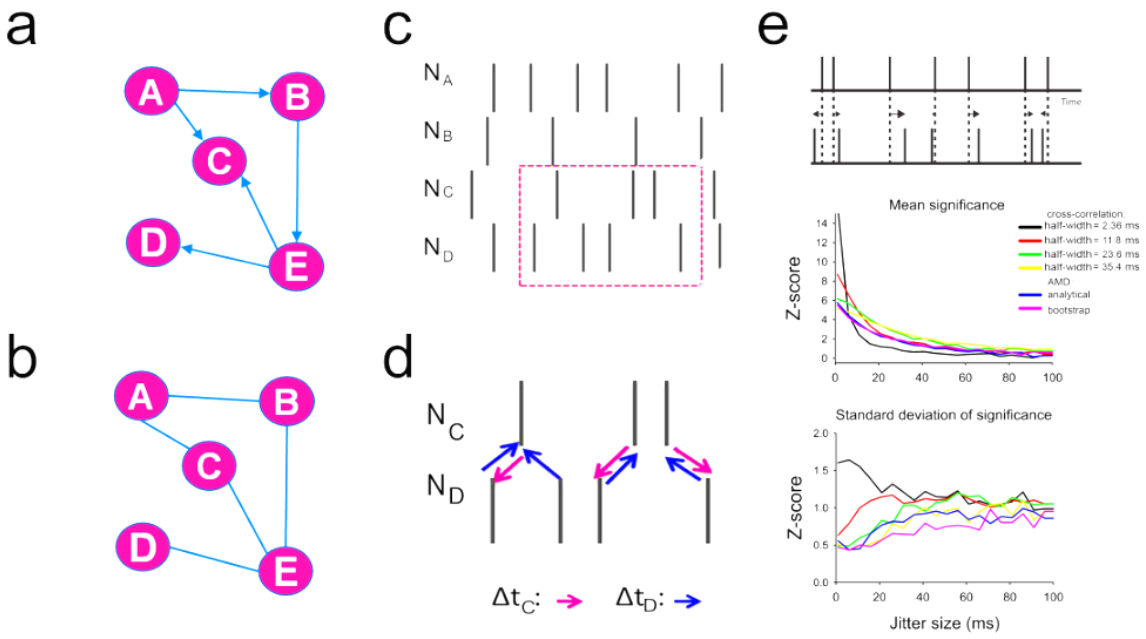

Figure 3.1: Average minimum distance (AMD) as a non-direction based communication metric. (a) Schematic of directed connectivity for five nodes in a network **(b)** Schematic of directed connectivity for the same five nodes in network (a), but connections are non-direction based **(c)** Example raster plots of 4 recorded neurons, from which AMD is measured **(d)** Pairwise AMD values are calculated between spikes of 2 neurons C and D over 1-min intervals. The closest spike of neuron D to the closest given spike of neuron C (blue arrows) and vice versa (pink arrows). Cells with smaller AMD are thought to be more functionally connected. **(e)** AMD and cross-correlation measures were compared for quantifying functional connectivity of two simulated spike trains. ***Top:*** The first 1-s, 30-spike train was generated randomly. The second train was generated by introducing jitter to the times of spikes from the first train. The amount of jitter was varied systematically between 1 and 100 ms, to determine how this variable (which should decrease with stronger functional connectivity) affects the two measures. ***Middle:*** Comparison of significance of functional connectivity measures for the two spike trains, across a range of jitter sizes. Cross-correlation significance between the two trains was calculated at 0 lag based on bootstrapping with 100 randomized spike trains, and Gaussian convolution of various half-widths. For comparison, AMD significance was calculated both analytically and using a similar bootstrapping technique. ***Bottom:*** Standard deviation of functional connectivity significance values was estimated over 100 repetitions using randomized spike trains. Across a range of jitter sizes, AMD metrics provide a more reliable estimate of significance.

regions, as well as not knowing the exact connectivity patterns of individual synapses, non-direction based connectivity seems to suit our analysis best, as connectivity is inferred from deviations from statistical independence between the unique (sometimes even spatially remote) neuronal units. This type of connectivity represents statistical relationships between neurons and can be assessed by such metrics as cross-correlations, coherence, or average minimum distance.

Spike field coherence is used to understand temporal dynamics of spike timings in non-directed networks. [22] This is a favorable approach because multi-unit activity is easily recorded over populations of cells and this data can be used to determine how oscillatory activity is related to spike timing. However, a fault in this analysis is the need to clearly define time series at a similar rate between spike and local field data. [117,118] This could confound data interpretation when comparing spike coherence data to different sleep states such as REM and NREM which are dominated by different frequencies of local field activity as well as subsets of cell populations that fire differently during different states. [119,120] Spike coherence is also more sensitive to task variability, and recording from freely moving animals could cause confusion in the data. [121] Similarly, mean phase coherence (MPC) quantifies the extent of phase locking between time series of individual signals. [103] A problem with this is that data can once again be biased by the number of spikes. When recording from heterogeneous populations of cells, with unknown firing frequencies, this becomes problematic.

An additional analysis in this category is cross-correlation, which determines repetitions of the same spike-timing relationship between pairs of neurons. Cross-correlation defines how closely two signals are changing together and can be easily

applied to neuronal time series after convolving the event times with a Gaussian distribution. However, for cross-correlation there are two free parameters when analyzing data: the size of convolution of spike times and the time shift (or delay) between the spike trains. For our data, the time delay parameter alters output of this measure greatly. For example, if one uses a specific delay for which cross-correlation in maximized, the information 1) may change over time for a given pair of neurons and 2) is not applicable to other neuronal pairs in the network, meaning data will not be informative if the patterns change over time (which have been shown to happen in biological paradigms of learning) or if there are noisy channels.

Both measures for MPC and cross-correlation have a limitation that affects their usefulness for analyzing many pairwise relationships over long time periods. Namely, statistical significance for these metrics must be calculated using a bootstrapping method, with is computationally time consuming. [122] Significance is assessed by generated distributions of non-correlated data, often times with the introduction of a jitter. Jitter is a type of spike resampling used to analyze the time scale on which temporal correlations occur. [123] This involves repeated random sampling to obtain numerical results; with the essential idea being randomness is used to solve problems that might be deterministic in principle. Thereafter, computation of jitter-corrected cross correlograms is compared to spike trains from the biological data set. This is used to decide whether observed correlations at a given time scale are significant.[124] This method of repeated simulation of spike trains, is known as the Monte Carlo method.[124] One specific example of difficulty in determining statistical significance is that the bootstrapping (randomization of spike trains during simulation that makes no

assumption of firing rate) required for calculating cross-correlation significance is very slow, which is important when one is calculating changes in the pattern of functional connectivity over thousands of time windows. [125] Additionally, bootstrapping can conceal the fact that important assumptions are made about the independence of samples, perhaps that the distribution of cells is well known. [125] This cannot be assumed in heterogeneous populations of cells. For these reasons, cross-correlation, along with the other similarity metrics discussed above are not best adapted for observation of rapidly changing biological systems.

Average minimum distance (AMD) is another method of fitting a mathematical model to spike train data from pairs of neurons using statistics. AMD is useful in capturing coincident firing between neurons which helps determine functional groupings. [97] Pairs of neurons' spike train data **(Figure 3.1c)** can be used to compute the AMD between two spike trains N_C and N_D, the distance $\Delta t_{D/C}$ from each spike in N_C to the next closest spike in N_D. **(Figure 3.1d)** The differences in spike timing calculated in a pairwise manner across a network can help us estimate functional groupings".[49] Critically, statistical analytical analysis of AMD, which assumes a Poisson distribution of spikes, 1) can be done more quickly than with bootstrapping, and 2) means that AMD significance does not rely critically on the firing rates of the respective neurons interval of time.[118] This is important for our purposes because it has been shown that firing rates are increased following learning. [45] This assumption of distribution would be unbiased against these changes.

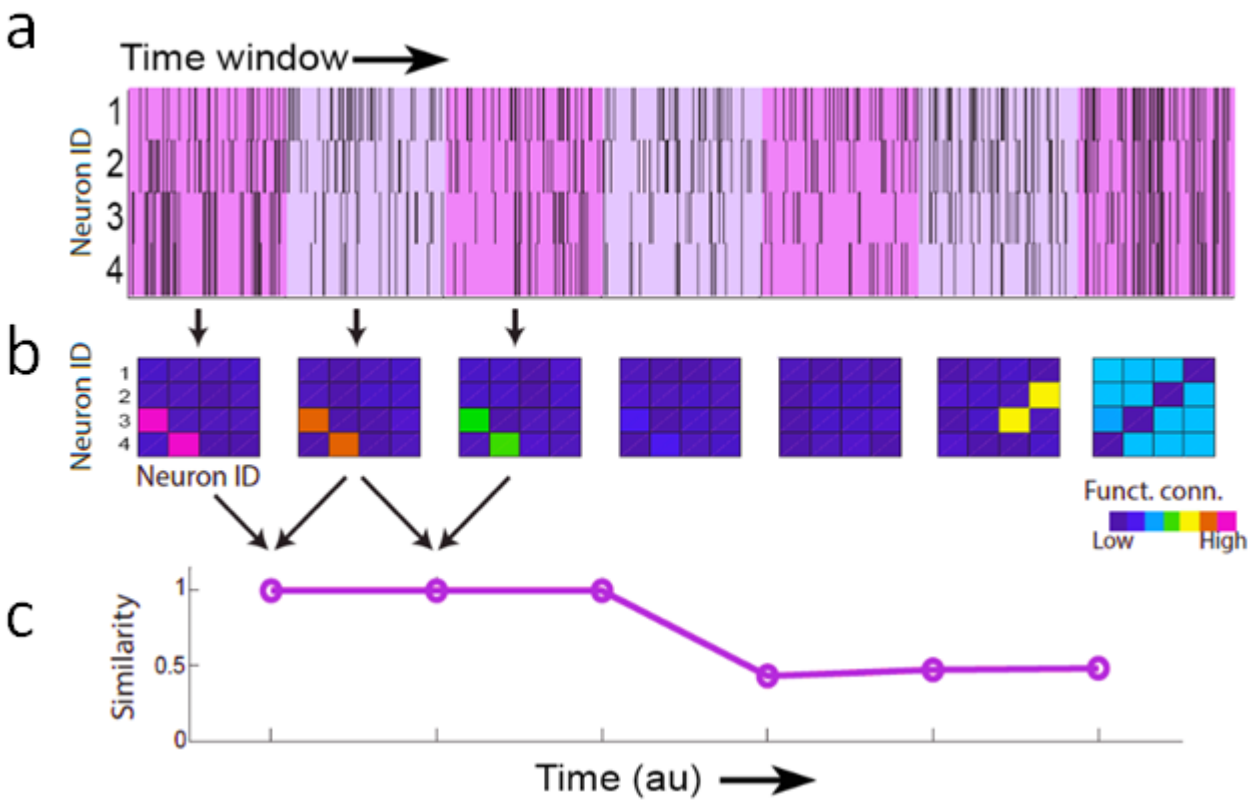

Figure 3.2: Functional network stability (FuNS) as a metric of functional connectivity dynamics. (a) An example of firing raster consisting of four neurons partitioned into seven time bins. (b) Functional connectivity matrices were constructed for every one minute interval of recording, based on spike rasters from all stably-recorded neurons estimated using the AMD metric. This represents the pattern of functional connectivity at any time point. Pairs with smaller AMD values are more likely to be functionally connected (shown in pink in the matrix) than those with larger AMD values (shown in blue in the matrix). **(c)** A comparison of matrices at adjacent time points yields a similarity value, which is plotted across the entirety of a recording

Analytical calculation of AMD significance (as opposed to bootstrapping) works best if the jitter introduced is smaller than ½ inter-spike interval (ISI). (**Figure 3.1e)** ISI distributions from experimental data are a common method to study neuronal changes given a *stationary* input, such as heterogeneity (or in biological systems a memory engram) where neurons being recorded are altered by this stimulus. AMD thus allows for respectable estimate of functional connectivity with the caveat that spike timings are well determined. Data also suggest that AMD-based metrics are not only more efficient from a computational standpoint than cross-correlation, it is also more sensitive and reliable for detecting changes in network dynamics in response to perturbations such as single-trial learning. [68]

3.3 Functional network stability (FuNS) as a novel metric to measure functional connectivity strength over time

The Zochowski lab uses the AMD metric to define functional groupings across a recorded population of neurons, using a method called the Functional Clustering Algorithm (FCA). [97] FCA does not depend on structural network information, like some connectivity metrics, but instead derives the functional information from the temporal interdependencies of network elements- the individual spike trains. **(Figure 3.2a)** This is specifically important when looking at changes in the network associated with new information encoding and storage, e.g. consolidation of a novel memory, where it is not exactly known where within the network the information will be stored. [3] The FCA dynamically groups pairs of spike trains based on a chosen similarity metric (here AMD), forming progressively more complex spike patterns. If connectivity is similarity of dynamics of nodes in a network, the advantage of FCA is no *a priori* knowledge is

needed of the number of functional groups already embedded in a network. [72,126] The FCA jitters the time of events in all spike trains, Si, and recalculates the AMD between spike trains. After jittering a large number of times (~1000-10000) an expected distribution of AMDs emerges for each pair of spike trains. The significance of each neuronal pair's AMD can be found by comparing to the jittered distribution, which is normalized with a t-test.[97]

AMD is used to calculate pairwise functional connectivity matrices for all stably-recorded neurons across a defined window of time **(Figure 3.2b)** These matrices can then compare between successive time intervals. The mean minute-to-minute similarity of these matrices is quantified as functional network stability (FuNS). **(Figure 3.2c)** We have used this metric to investigate how the consolidation of a memory consolidation affects overall network dynamics.

3.3.1 Computational measurements of network dynamics for statistical significance

The Zochowski lab has used computational modeling to clarify how newly-encoded information could affect FuNS across a network. These studies have made clear that FuNS is sensitive to changes in the strength of connections between neurons. Modeled networks are 1D structures composed of N=1000 excitatory integrate-and-fire neurons. The network has a local connectivity density of 5%, and the neurons for which stability is calculated are an average Euclidean distance of ~500 lattice units apart, which corresponds to an average network separation of ~2.7 number of connections**.** Introduced heterogeneities (analogous to memory engrams) are strengthened connections within 10% of the total population. Analysis of these modeled networks

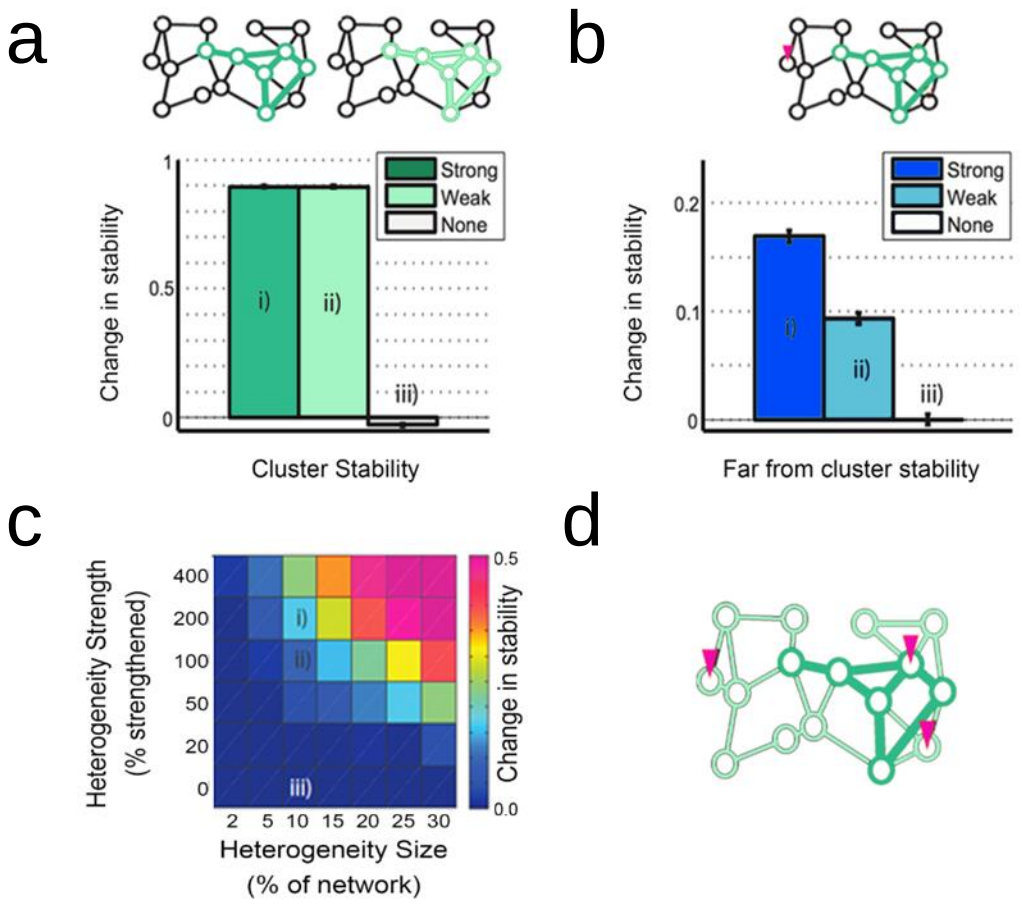

Figure 3.3: Comparison of functional stability within identical networks in the presence and absence of a localized heterogeneity. (a) A representative network of interconnected neurons, with strengthened green connections identifying members of a structural heterogeneity. Quantified is the change in functional stability due to introduction of heterogeneity of varying strength, calculated for neurons positioned **within** that heterogeneity. Bars denote (from the left) strong, weak and no structural heterogeneity, respectively. **(b)** Same as panel (a), calculated for 100 neurons positioned far outside the heterogeneity. Representative network of neurons shows recording neuron (pink arrow) in reference to heterogeneity **(c)** Change of functional stability as a function of heterogeneity size and strength calculated for representations of 100 neurons positioned at maximal distances from the heterogeneity. Roman numbering of the bars corresponds parametric positions in panels **a-b. (d)** A representative network of interconnected neurons, following introduction of heterogeneity, Based on panel **b**, recording from cells from outside the heterogeneity will still yield changes in stability. Global distribution of strength resulting from introduced structure.

have shown that there is a global stabilization, quantified as a persistence of functional connectivity over time, of network firing patterns upon introduction of a local heterogeneity. **(Figure 3.3)** This is critical information for applying any metric to memory consolidation and the establishment of heterogeneity in biological systems, because we cannot always be certain that spike data is being collected from cells involved in the memory. However, recent work with Daniel Maruyama in the Zochowski lab has shown comparisons of functional stability within identical networks in the presence and absence of a localized heterogeneity. **(Figure 3.3 a-b)** Changes in functional stability due to introduction of heterogeneity can be calculated for heterogeneities of different strengths as well as for data recorded from neurons outside of the heterogeneity. Therefore, we do not have to assume directional connectivity- which is necessary for the use of many other metrics of similarity. Rather, for application to biological systems, these data show that a single memory engram (heterogeneity) can provide a substrate for systems-wide memory consolidation that could promote a globally-distributed representation of new memories. **(Figure 3.3c)**

3.4 Changes in FuNS predict subsequent memory formation after fear learning in mice

To provide experimental support for the above metric in a biological system, we investigated whether FuNS changes can be detected following learning-induced network reorganization *in vivo*. We hypothesized that changes in network dynamics due to synaptic plasticity in hippocampal area CA1 following single-trial contextual fear conditioning (CFC) is a plausible biological analogue of the modeled storage of a new representation. [43,127] For this reason, we recorded the same population of CA1 neurons

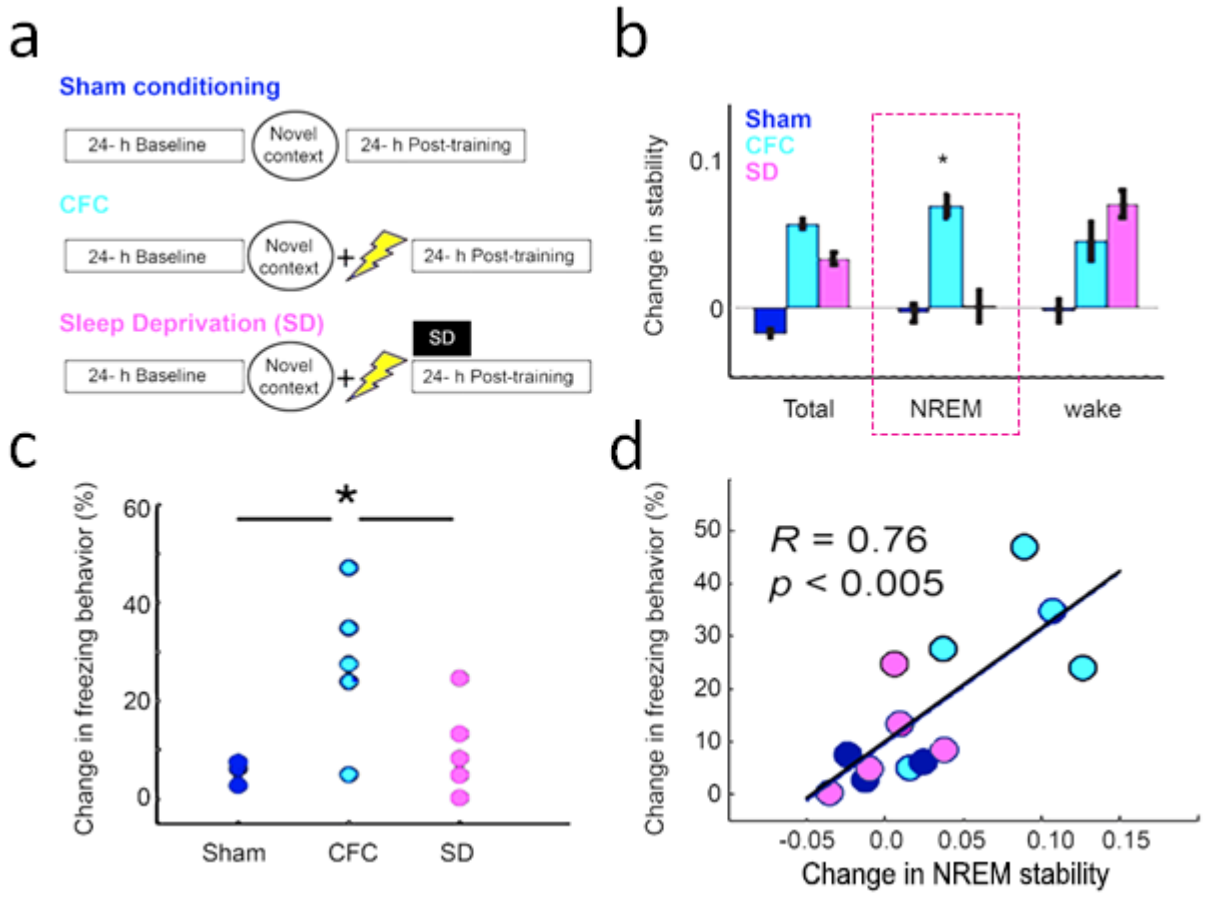

Figure 3.4: FuNS changes in the hippocampal network predict fear memory consolidation. (a) Experimental paradigm: 24h baseline followed by either Sham conditioning (novel environment context, no foot shock), CFC (contextual fear conditioning; novel environmental context + foot shock), and SD (CFC followed by a 6-hr period of sleep deprivation). **(b)** Average change in CA1 hippocampus FuNS (from 24-hr baseline) for the same conditions as described above. Values are averaged over the entire 24-hr post-training period (regardless of behavioral state), over post-training SWS alone, and over post-training wake alone. * indicates $p < 0.05$, Holm-Sidak post hoc test vs. Sham and Sleep Dep mice **(c)** Behavioral measurement of fear memory consolidation (% change in context-specific freezing) for mice in the three experimental groups. * indicates $p < 0.05$, Holm-Sidak post hoc test vs. Sham and Sleep Dep mice **(d)** Post-training changes in NREM FuNS (changes in dashed box from panel b) vs. observed changes in freezing behavior for individual mice; $R^2 = 0.58$, $p < 0.005$ Pearson correlation.

over a 24-h baseline and for 24 h following CFC to determine how functional network dynamics are affected by *de novo* memory formation. C57BL/6J mice underwent either CFC (n = 4 mice), sham conditioning (n = 4 mice), or CFC followed by 6 h of sleep deprivation (SD) (n = 5 mice). [44,88,128] **(Figure 3.4a)** We measured FuNS changes after each manipulation by quantifying pairwise AMD on a minute-by-minute basis over the entire pre- and post-training intervals. We observed an increase in FuNS over the 24-h following CFC, which was most pronounced when comparing FuNS in NREM sleep **(Figure 3.4b**). We hypothesize that this may be due to the fact that NREM corresponds to internal network dynamics, rather than the changing external drive to the network experienced during wakefulness. In contrast, no change in NREM FuNS was seen in Sham mice or following the period of experimental sleep deprivation in in SD mice. Group differences in SWS FuNS were reflected in the behavior of the mice 24 h post-training, when contextual fear memory (CFM) was assessed behaviorally. CFC mice showed an increase in context-specific freezing upon return to the conditioning environment, which was significantly greater than freezing in Sham and SD mice. **(Figure 3.4c)** Remarkably, NREM-specific FuNS increases for individual mice were predictive of their behavioral performance during subsequent memory assessment **(Figure 3.4d).** Thus the formation of a behaviorally-accessible memory trace *in vivo* is accompanied by increased FuNS in the CA1 network. We have shown with the above data that we can assess FuNS for different states and get an understanding that the strength of connections of cells following learning is increased and stable.

Stabilization of spike-timing relationships within CA1 may be a plausible strategy for preserving a memory trace (*i.e.*, an engram) of CFC during consolidation. The

memory trace would be weakened by replacing sleep with wakefulness (*i.e.*, with sleep deprivation) - which could provide a network-level mechanistic explanation for why sleep deprivation disrupts mnemonic function.

3.5 Discussion and next steps

Basic electrophysiological analyses (e.g. frequency and power changes) often only give data for a specific temporal window on a cell-by-cell basis, but how these biological changes within sleep states contribute to functional connectivity still has to be determined. Through collaborative work with investigators in the Department of Physics, we have developed computational metrics to analyze such data which will be indispensable to our understanding of temporal dynamics during consolidation related to 3 critical points:

I. Quantification of changes at the **cell level** by assessing similarity of firing patterns
II. At the **network level**, characterization of cell-by-cell functional connectivity relationships over time allowing analysis of stability
III. Analysis of **how entire networks change over time**, with the generation of functional similarity matrices across specified recording times.

These metrics will be applied throughout the remainder of this dissertation to shed light on network stabilization and sleep-associated network oscillations following learning. Specifically, that they may work together to regulate spike timing across neural networks throughout the brain, as a substrate for systems-level memory consolidation.

CHAPTER IV:

Parvalbumin-expressing interneurons coordinate hippocampal network dynamics required for memory consolidation

This chapter includes the manuscript: **Ognjanovski N**, Schaeffer S, Wu J, Mofakham S, Maruyama D, Zochowski M, Aton SJ. Parvalbumin-expressing interneurons promote memory consolidation by driving hippocampal network oscillations and stabilizing neuronal ensembles. *(2017) Nature Communications*

Abstract:

Activity in hippocampal area CA1 is essential for consolidating episodic memories, but it is unclear how CA1 activity patterns drive memory formation. We find that in the hours following single-trial contextual fear conditioning (CFC), fast-spiking (FS) interneurons (which typically express parvalbumin [PV]) show greater firing coherence with CA1 network oscillations. Post-CFC inhibition of PV+ interneurons blocks fear memory consolidation. This effect is associated with loss of two network changes associated with normal consolidation: 1) augmented sleep-associated delta (0.5-4 Hz), theta (4-12 Hz), and ripple (150-250 Hz) oscillations, and 2) stabilization of CA1 neurons' functional connectivity patterns. Rhythmic activation of PV+ interneurons

increases CA1 network coherence and leads to a sustained increase in the strength and stability of functional connections between neurons. Our results suggest that immediately following learning, PV+ interneurons drive CA1 oscillations and reactivation of CA1 ensembles, which directly promotes network plasticity and long-term memory formation.

4.1 Introduction

Recent findings have highlighted the importance of hippocampal activity patterns in episodic memory encoding and retrieval. A significant body of evidence suggests that coordinated activation of an engram-specific population of hippocampal neurons is sufficient for subsequent recall. [129–133] However, much less is known about hippocampal network dynamics involved in memory consolidation, and how these dynamics are coordinated following learning. While network activity in hippocampal area CA1 is essential for long-term memory consolidation, it is unclear 1) how newly-learned information affects the CA1 network, and 2) how CA1 activity is coordinated to promote long-term storage of this information. One hypothesis is that following learning, hippocampal oscillations (*e.g.*, those occurring in sleep) drive reactivation of specific neuronal ensembles; such reactivation could drive network plasticity. [16,43,71,120] Numerous studies have demonstrated sequential replay of network activity patterns associated with prior experience. [81,83] Selective offline reactivation of neuronal populations activated during a learning experience has also been widely reported. [134–138] Of the two phenomena, reactivation appears less constrained to specific behavioral paradigms (*e.g.*, hippocampal place cell activation while traversing a maze), and more importantly, occurs at a time (just following a new experience) when it could play a

pivotal role in consolidation. However, while behavioral state-dependent hippocampal oscillations (such as sharp wave ripples; SPWRs) may support sequential replay, the mechanisms mediating reactivation are still completely unknown. [139] Critically, it is still unclear whether hippocampal oscillations, replay, or reactivation are required for memory consolidation following novel learning.

Individual PV+ interneurons in CA1 innervate large numbers of neighboring pyramidal neurons. [62,140,141] Thus from a connectomic standpoint, they are well-positioned both to coordinate hippocampal oscillations and to pattern neuronal ensemble activity. To test the hypothesis that PV+ interneurons optimally pattern network activity in the context of memory formation, we characterized firing in the CA1 FS (typically PV+) interneuron population during contextual fear memory (CFM) consolidation. We find that these neurons (and neighboring pyramidal neurons) show selectively enhanced firing coherence with delta and theta oscillations in the hours immediately following single-trial CFC. We also assessed how experimental manipulation of CA1 PV+ interneuron activity affects memory consolidation. Under normal conditions, CFC leads to subsequent increases in CA1 delta, theta, and ripple oscillations during sleep.[45] Critically, these sleep-associated changes are maximal over the first 6 h following conditioning, when sleep plays a critical role in CFM consolidation, and the degree to which they are enhanced predicts the success of CFM consolidation. [142] We show that pharmacogenetic inhibition of CA1 PV+ interneurons disrupts CFM consolidation, and also blocks post-CFC enhancements in CA1 network oscillations. We also find that PV+ interneuron activity is required to stabilize functional connectivity patterns among CA1 neurons, which is a hallmark of normal CFM consolidation in the

hours following training. Finally, rhythmic optogenetic activation of PV+ interneurons is sufficient to generate coherent firing rhythms and stabilize communication patterns across the CA1 network. Greater network stability and stronger network connections remain in CA1 for hours after rhythmic PV+ interneuron stimulation ends, suggesting that this manipulation induces long-lasting synaptic changes. Based on these results, we conclude that PV+ interneurons play a critical, instructive role in coordinating CA1 network communication after a novel learning experience, which drives both long-term network plasticity and memory formation.

4.2 Methods

4.2.1 Mouse handling and surgical procedures

All animal husbandry and surgical/experimental procedures were approved by the University of Michigan IACUC. With the exception of conditioning and fear memory testing, mice were individually housed in standard caging with beneficial environmental enrichment (nesting material and novel foods) throughout all experimental procedures. Lights were maintained on a 12 h:12 h light: dark cycle (lights on at 8 AM), and food and water were provided *ad lib*. C57BL/6J mice (Jackson) were implanted with custom-built, driveable head stages with two bundles of stereotrodes for single unit/LFP recording and EMG wires for nuchal muscle electromyographic recording, as previously described. [45] The two stereotrode bundles were spaced approximately 1.0 mm apart within right-hemisphere CA1 (relative to Bregma: 1.75-2.75 mm posterior, 1.5-2.5 mm lateral, and 1.0 mm ventral). CA1 recording sites for these experiments are shown in **Supplemental Figure 4.2**.

At age 2-3 months, male *Pvalb-IRES-CRE* mice (*B6;129P2-Pvalb*$^{tm1(cre)Arbr}$*/J*; Jackson) received bilateral CA1 injections of adeno-associated virus (AAV) to express either the inhibitory receptor hM4Di (rAAV2/Ef1A-DIO-hM4Di-mCherry; UNC Vector Core: Lot # AV4708), or an mCherry reporter without hM4Di (control; rAAV2/Ef1A-DIO-mCherry; UNC Vector Core: Lot # AV4375FA) in a CRE-dependent manner. [142] For both vectors, a volume of 1 µl was injected bilaterally via a 33 gauge beveled syringe needle at a rate of 0.2 µl/min (from Bregma 2.0 mm posterior, 2.0 mm lateral). They were subsequently implanted with driveable headstages as described above. CA1 recording sites for these experiments are shown in **Supplemental Figure 4.4**.

4.2.2 Recording procedures

Mice were prepared for chronic stereotrode recording as described previously, either 1 week after implantation surgery (C57BL/6J) or 4 weeks after AAV transduction (*Pvalb-IRES-CRE*). [45] Mice in their home cage were placed into sound-attenuated chambers (Med Associates) for recording of CA1 activity during natural sleep/wake states and contextual fear conditioning (CFC; see below). Stereotrode bundles were slowly advanced into CA1 in 10–20 µm steps over a period of 3-7 days, until stable recordings were obtained. During this period, mice were habituated to daily handling and the recording apparatus (including tethering via lightweight recording cables [Plexon, Inc.]). All experiments began with a 24-h baseline recording period, starting at lights-on, and continued throughout subsequent, single-trial CFC, a 24-h post-training contextual fear memory (CFM) consolidation period, and subsequent CFM testing in the conditioning chamber. Neuronal spike and local field potential (LFP) signals were acquired by differentially filtering data from each electrode wire (bandpass 300 Hz-8

KHz and 0.5-300 Hz, respectively); these data were digitized and amplified using Plexon Omniplex hardware and software as described previously. [45]

4.2.3 Conditioning and pharmacogenetic inhibition

Following 24 h baseline recording (beginning within 1 h of lights-on), mice underwent single-trial CFC or sham conditioning. Mice were placed in a novel conditioning chamber with walls made of clear Plexiglas and a shock grid floor (Med Associates). CFC and sham conditioned C57BL/6J mice (*n* = 5 mice per group) were placed in the same environmental context for training (Context A, below). CFC mice were allowed to explore the conditioning chamber for 2.5 min before receiving a 2-s, 0.75 mA foot shock via the grid floor. After the foot shock, mice remained in the conditioning chamber for an additional 28 s. Sham mice received no foot shock during 3 min of exploration. *Pvalb-IRES-CRE* mice underwent CFC in either Context A or Context B as described. Each mouse was then immediately given a 0.04 mL *i.p.* injection of either 0.3 mg/kg clozapine-*N*-oxide (CNO; Santa Cruz Biotechnology; *n* = 6 mice) dissolved in DMSO, or an injection of DMSO alone (vehicle; *n* = 6 mice).

Following CFC or sham conditioning, all mice were then left undisturbed in their home cage for the next 24 h, after which they were returned to the conditioning chamber for 5 min to assess CFM. Contextual freezing was quantified as a change in the percent of time spent in freezing behavior from pre-shock baseline during CFC or during sham conditioning. *Post hoc* scoring of videos for freezing behavior was conducted by an observer blind to both the animals' viral expression and drug treatment. Behavior was scored as freezing in the following conditions: crouched

posture with an absence of all body movement save respiration (including an absence of head and whisker movement). [40,41]

For Context A, the chamber was cylindrical in shape and had vertical stripes over one half of the vertical surface. For Context B, the chamber was square in shape and had a horizontal grating pattern on 3 of the 4 walls. Chamber walls and floor were cleaned thoroughly with 70% ethanol both prior to and immediately following conditioning.

4.2.4 Immunohistochemistry

At the end of each experimental recording, mice were anesthetized with isoflurane and all electrode sites were lesioned (2 mA, 3 s per wire) prior to perfusion and euthanasia. To verify CA1 electrode placement and confirm proper AAV-mediated expression relative to recording electrodes, the brain was post-fixed and sectioned at 50 µm. To confirm AAV-mediated transgene expression to PV+ interneurons (*e.g.*, **Figure 4.2a**), brain sections containing dorsal CA1 were immunostained with goat anti-parvalbumin (1:1000; Abcam; ab11427). Brain slices were mounted using DAPI Fluoromount-G (Southern Biotech). The mCherry tag on the virus will allow visual confirmation of proper viral injection into CA1. Only mice with PV+ interneurons in CA1 that had co-localization of virus in at least 70% of cells were included in behavioral analysis. Of the 6 mice per treatment group, only 2 were removed from treatment group Control-CNO; 1 for improper electrode placement and the second from failure to express viral transduction in enough cells. All animals expressing hM4Di had sufficient coverage and proper electrode placement in CA1.

To confirm CNO-mediated inhibition of PV+ interneurons, *Pvalb-IRES-CRE* mice (*n* = 5) expressing rAAV2/Ef1A-DIO-hM4Di-mCherry in right CA1 and rAAV2/Ef1A-DIO-mCherry in left CA1 underwent single-trial CFC at lights on. Immediately following CFC, each mouse was administered CNO, after which they were allowed *ad lib* sleep in their home cage. 90 minutes later, each mouse was deeply anesthetized with isofluorane, perfused with ice cold 0.1M phosphate buffered saline (PBS), and perfused with 4% paraformaldehyde in PBS (PFA-PBS). 50 µm coronal brain sections were obtained for histochemistry using antibodies for c-Fos (1:6250; Millipore; PC05). Images were collected for all brain slices containing virally-transduced hippocampal regions. Quantification of c-Fos immunoreactivity in virally-transduced PV+ interneurons was conducted by a scorer blind to treatment conditions, following previously published methods [42]. Briefly, for each brain slice, the number of CA1 neurons expressing mCherry (i.e. those virally-transduced neurons with CRE-mediated transgene expression) was first counted. CNO-induced changes in PV+ interneuron activity were assessed by quantifying the percentage of mCherry-expressing neurons which were also c-Fos immunopositive (# of cells c-Fos positive/ # of mCherry-positive cells). Comparisons were made between right (hM4Di) and left (control) hemispheres in the same mouse. Neurons with cell bodies that were out of the plane of focus were not included in quantification.

4.2.5 Single-neuron discrimination and firing analysis

Single-neuron data were discriminated offline using standard principle-component based procedures (Offline Sorter; Plexon). Individual neurons were discriminated on the basis of spike waveform, relative spike amplitude on the two

stereotrode recording wires, relative positioning of spike waveform clusters in three-dimensional principal component space, and neuronal subclass (*e.g.*, FS vs. principal; **Supplemental Figure 4.1a-b**). Single-neuron isolation was verified using standard techniques - *i.e.*, elimination of clusters with interspike interval (ISI)-based absolute refractory period violations. [43] For assessing spike cluster quality, spike clusters on channels with multiple stably-recorded single units were compared with one another, and with identified noise, in principal component space (**Supplemental Figure 4.1c**). Waveform cluster separation was first validated using MANOVA on the first 3 principal components ($p < 0.05$ for all sorted clusters), and further characterized using the Davies-Bouldin (DB) validity index (a metric with inter-cluster distance as the denominator, thus lower values indicating better cluster separation). [44] The mean (± SEM) DB value for all sorted waveform clusters (across all groups) was 0.36 ± 0.02 (for spike clusters vs. spike clusters) and 0.46 ± 0.02 (for spike clusters vs. noise), which compares favorably with DB values from single-unit data used in other studies (distributions of discrimination values shown in **Supplemental Figure 4.1c**). [45,46]

Only those neurons that 1) met the criteria described above and 2) were reliably discriminated and continuously recorded throughout each experiment (*i.e*., those stably recorded across both 24-h baseline and 24-h post-CFC recording) were included in firing rate analyses from behaving mice (n =10 FS and 34 principal neurons for CFC C57BL/6J mice, n = 5 FS and 41 principal neurons for sham C57BL/6J mice; n = 27 neurons for Control+CNO (from 4 animals), 35 neurons for hM4Di+CNO (from 3 animals), and 21 neurons for hM4Di+vehicle (from 3 animals) in *Pvalb-IRES-CRE* mice. Given the design of our multi-electrode recording arrays (2 bundles of tetrodes) animals

that did not have at least 75% of channels with stable neurons at baseline (at least 9 neurons of a possible 12 channels) were removed. Two animals from hM4-expressing group were removed because one whole bundle yielded no data (either from board breakage or malfunction or snapped wires), with an additional mouse removed from this group because only 4 neurons out of a minimum of 12 were recorded for the entirety of the 48-h recording time. This was possibly due to drop off of several cells when mouse underwent CFC. Quick, aggressive movement/jumping around the conditioning chamber may have jostled the implant, resulting in loss of many of the neurons that were present during baseline recording. For the Control group, 2 mice were removed from data analysis. One was removed for gross loss of neurons during a large portion (~3 hours) of baseline recording, which was (given video evidence) possibly due to the mouse spilling its water cup on the implant. A second mouse was removed because one side of the multielectrode array was post-hoc shown to have zero conductance across all channels on that side (possibly due to acetone erosion of glue attaching head cable adapter to board).

Learning-induced coherence changes were calculated by directly comparing state-specific firing coherence from 0.5-20 Hz across the first 6 h of baseline recording and the first 6 h following CFC or sham conditioning. Post-CFC firing rate changes were calculated over 6-h windows for each neuron as a percent change from baseline, as described previously. [45]

4.2.6 Sleep/wake behavior and LFP analyses

Intrahippocampal LFP and nuchal EMG signals were used to categorize each 10-s interval of recording as REM, NREM, or wake (**Supplemental Figure 4.3a**) using custom software. REM was identified based on highly regular theta-frequency activity in the LFP and low EMG activity, NREM was characterized by relatively high-amplitude, low frequency LFP oscillations, and wake was characterized by high-frequency, low-amplitude LFP activity and relatively high EMG activity. The proportion of time spent in REM, NREM, and wake (and mean bout duration for each state) was calculated during the baseline and post-CFC recording periods for each mouse using standard conventions.

Raw LFP power (0-300 Hz, in 0.4 Hz bands) was calculated on each channel where stable neuronal spike data was obtained. Spectral power was quantified from raw LFP traces within each 6-h time window at baseline and post-CFC. Changes in power were calculated within each frequency bin as ([power post-CFC - power at baseline]/power at baseline). These values were summed across frequency bands for recording site at delta (0.5–4 Hz), theta (4–12 Hz), and gamma (25–50 Hz) for subsequent analysis. Ripples were quantified within NREM sleep in 2-h windows, using previously described methods. [41] Briefly, LFPs were band-pass filtered (150-300 Hz) and ripple events were automatically detected using a threshold of 6 or more consecutive cycles of an oscillation with a voltage ± 2.0 SD from baseline signal mean. To compare ripple occurrence between baseline and post-CFC recording periods, ripples were detected across recording periods using the same (baseline) voltage threshold. Spectral power was calculated within detected ripple intervals at baseline and

post-CFC; changes in power were calculated as described above for comparisons of ripple amplitude between groups.

Spectrograms of 0-12 Hz PSD activity were generated in MATLAB. PSD data for representative LFPs were calculated in 1-s windows, and PSDs were convolved over 30 seconds at 1 Hz. PSDs were normalized over the entirety of the selected temporal window and expressed as V^2/Hz.

4.2.7 Functional connectivity analysis

Functional connectivity in CA1 was calculated using spike trains {S_1, S_2… S_n} for *n* stably recorded CA1 neurons. The functional relationship FC_{ij} was calculated for each pair of neurons (*e.g.*, *i*-th and *j*-th neurons) by first calculating the average temporal proximity of spike trains S_i and S_j The average distance from spike train S_i to S_j is given by the average minimum distance (AMD)[97]. $AMD_{ij} = \frac{1}{N_i}\sum_k \Delta t_k^i$, here N_i is the number of events in S_i and Δt_k^i is the temporal distance between event *k* in S_i to the nearest event in S_j. This value was compared with the expected sampling distance of the train S_j, μ_j, and the difference between the two was then normalized to the expected variation in sampling distance of the train S_j, σ_j. μ_j and σ_j, were calculated as follows, by integrating over the sampling minimum distance distribution of S_j. The expected mean sampling distance and standard deviation were calculated from interspike intervals (ISIs) in S_j of length *L*. These values were quantified as the first two moments of minimal distance given by $\mu^L = \langle MD^L \rangle = (1/4)L$ and $\langle (MD^L)^2 \rangle = (1/12)L^2$. The probability of sampling an interval of length *L* for a spike train of length *T* is (*L*/*T*). Thus we combined the intervals

to give $\mu_j =< MD_j >= \sum_{\{L\}} p_L \mu^L = \frac{1}{T}\sum_{\{L\}} \frac{L^2}{4}$, and $\left\langle \left(MD_j\right)^2 \right\rangle = \frac{1}{T}\sum_{\{L\}} \frac{L^3}{12}$. The expected standard deviation is given by $\sigma_j^2 = <(MD_j)^2> - <MD_j>^2$. Thus the functional connectivity between neurons *i* and *j* was calculated as: $FC_{ij} = \sqrt{N_i}\,\frac{\mu_j - AMD_{ij}}{\sigma_j}$. This value represents the significance of mean temporal proximity of S_i to S_j after taking into account the spiking distributions of S_j.

The performance of AMD is compared with cross-correlation-based methodology in **Supplemental Figure 4.9**. The two methods were first used on two simulated spike trains. The first 30-spike spike train was generated randomly over a 1-s time interval. The second train was created by introducing a variable temporal jitter (1-100 ms) to the first spike train. Cross-correlation was based on convolution of the two trains, using Gaussians of variable width (2.36 ms ≤ half-width ≤ 35.4 ms). Cross-correlation significance was calculated at 0 time delay, using bootstrapping based on 100 randomized (shuffled ISI) spike trains, and standard deviation of significance was estimated over 100 repetitions of the randomized spike train. For comparison, AMD significance was calculated both analytically (as described above) and using the same bootstrapping technique.

4.2.8 Functional similarity and stability analysis

The functional connectivity of the entire recorded CA1 population for a given mouse was calculated over successive 1-min time segments (this is schematized as the functional connectivity matrix in **Figure 4.6**). Adjacent time segments' connectivity patterns were then compared using cosine similarity, $C_{AB} = \cos\theta_{AB} = \frac{<A,B>}{\sqrt{<A,A>*<B,B>}}$, as

a measure of the overlap between the two values. A cosine similarity value of 1 denotes no change in the network and a value of 0 indicates that the two networks are completely unrelated. Cosine similarity was calculated across the entire series of adjacent time windows, over the entire 24 h of baseline and the entire 24 h of post-CFC recording. Average cosine similarity values (for adjacent time windows in a given behavioral state, *e.g*., NREM or wake) constituted the functional stability metric for that state. Due to the relative infrequency and short duration of REM epochs (which typically lasted less than 1 min each) there were an insufficient number of successive recording epochs to reliably calculate network stability changes specifically within REM. Post-CFC changes in CA1 network stability were calculated separately for NREM and wake as (mean stability baseline - mean stability post-CFC) / mean stability baseline × 100. Functional Similarity matrices (FSMs; **Fig. 7**) were calculated using the algorithm described above, however instead of comparing only consecutive 1-min time windows we made a pairwise comparison of all the existing windows. The x and y axes denote the recording times on which the windows are centered.

4.2.9 Optogenetic stimulation of PV+ interneurons

Two groups of mice were used to assess the effects of rhythmic stimulation of PV+ interneurons. For experiments shown in **Supplemental Figures 4.13** and **4.15,** *Pvalb-IRES-CRE* mice were crossed to either *B6;129S-Gt(ROSA)26Sor*$^{tm32(CAG-COP4*H134R/EYFP)Hze}$*/J* or *B6.Cg-Gt(ROSA)26Sor*$^{tm6(CAG-ZsGreen1)Hze}$*/J* transgenic mice (Jackson) to express ChR2 (*PV:ChR2*) or eGFP (*PV:GFP*), respectively, in a CRE-dependent manner in PV+ interneurons. At age 2–5 months, male *PV:ChR2* (*n* = 7) or *PV:GFP* (*n* = 6) mice were anesthesized with isofluorane (0.5-0.8%) and 1 mg/kg

chlorprothixene (Sigma). Mice were head-fixed and a 1mm × 1mm matrix multielectrode (250 µm electrode spacing; FHC) was slowly advanced into CA1 until stable recordings (with consistent spike waveforms continuously present for at least 30 mins prior to baseline recording) were obtained. An optical fiber was placed adjacent to the recording array for delivery of 473 nm laser light (CrystaLaser). Power output at the fiber tip was estimated at 3-10 mW for all experiments.

For the first set of recordings (**Supplemental Figure 4.12a**), CA1 neurons were recorded over a 15-min baseline period, after which PV+ interneurons were stimulated over multiple successive 15-min periods with a range of frequencies (2-18 Hz, 40 ms pulses). The various stimulation frequencies were presented in a random interleaved manner, during which neuronal activity continued to be recorded. Following the final stimulus period, neurons were recorded for an additional 15 min to measure changes in network activity from baseline. Only those neurons recorded throughout the entire experiment (baseline + optogenetic stimulation + post-stimulation) were included in analyses of optogenetically induced spike-field coherence and network stability changes.

For the second set of recordings (**Supplemental Figure 4.12b**), neurons were recorded for a longer (30-min) baseline period, a 30-min stimulation period (7 Hz; 40 ms light pulses), and a longer post-stimulus interval lasting 2 h. Only those neurons recorded throughout the entire experiment (baseline + optogenetic stimulation + post-stimulation) were included in analyses of optogenetically induced spike-field coherence and network stability changes.

To ensure that effects of optogenetic manipulation were not due to expression of ChR2 outside of CA1 in *PV:ChR2* mice, male *Pvalb-IRES-CRE* mice (aged 2-3 months, *n* = 7) received bilateral CA1 injections of AAV2/9.EF1a.DIO.hChR2(H134R)-EYFP.WPRE.hGH (Penn Vector Core). 4-6 weeks after AAV transduction, these mice underwent the same optogenetic manipulations described above; data from these experiments are shown in **Figure 4.8** and **Supplemental Figure 4.14**. To test whether rhythmic stimulation of PV+ interneurons could induce CA1 rhythms and long-term changes in the CA1 network in the absence of anesthesia, two additional groups of AAV-transduced mice (ChR2- and GFP-expressing, *n* = 3/group, aged 2-3 months) were implanted with stereotrode recording arrays as described above, with optical fibers targeting CA1. Once stable neuronal recordings were achieved, these mice were recorded for two h under awake, behaving baseline conditions, across a 2-h period of 7-Hz stimulation, and over a 2-h post-stimulus interval (**Supplemental Figure 4.12c**). Data from these experiments are shown in **Supplemental Fig. 16.**

Following all optogenetic experiments, mice were perfused and brains were processed for histological assessment as described above. AAV-mediated gene expression in CA1, optic fiber position, and electrode position were validated prior to data analysis.

4.2.10 Data analysis for optogenetic recordings

Single neuron discrimination and sorting was conducted as described above for stereotrode recordings, except that relative spike amplitude across channels was not used as a criterion for discrimination. For all spike-field coherence analyses, LFP traces

for each neuron's corresponding electrode recording site were filtered across a narrow band (stimulation frequency ± 0.2 Hz). 500-ms segments of this filtered LFP trace (centered on each spike) were averaged, and the amplitude (maximum - minimum voltage) of each mean trace was calculated as spike-field coherence metric.

To calculate functional network stability for each recorded neuron (**Figure 4.8d**, **Supplemental Figure 4.15d-e)**, we first generated a functional connectivity matrix of all stably-recorded CA1 neurons across successive 1-min time bins. Each row of the matrix represents the functional connectivity vector of a specific neuron with respect to all other neurons. Stability values for each neuron were then calculated using cosine similarity between adjacent functional connectivity vectors across the whole series of time bins. Individual neuronal stability was obtained as described for whole-network stability (above) by averaging cosine similarity values across each recording period.

To quantify how the strength of functional connectivity changed between neurons before vs. after a period of stimulation (under both anesthetized and non-anesthetized conditions), we calculated the differences between corresponding elements of the functional connectivity matrix, using the AMD metric described above. To quantify the long-term effects of optogenetic stimulation on connection strength, we quantified pairwise connectivity for the last 15 min of baseline recording, and the last 15 min of a 2-h post-stimulation recovery period. We then subtracted post-stimulation values from baseline. Distributions of these functional connectivity changes were then compared for experiments using ChR2- vs. GFP-expressing mice (**Figure 4.8g**, **Supplemental Figures 4.15h** and **4.16d**).

4.3 Results

4.3.1 CA1 neurons' firing coherence increases after learning

To characterize the dynamic response of CA1 neurons to newly-learned information, we continuously recorded the firing of FS interneurons and non-FS (presumptive principal) neurons in wild-type mice during CFM consolidation, using chronically implanted stereotrode arrays (**Supplemental Figures 4.1** and **4.2**). Following a 24-h baseline recording period (during which CA1 neuronal and local field potential [LFP] activity was recorded continuously), C57BL/6J mice underwent single-trial CFC or sham conditioning. Recording continued over the next 24 h to assess changes in neuronal and network activity associated with CFM consolidation (**Figure 4.1a-b**). FS interneurons (identified based on characteristically narrow spike waveform) showed dramatically increased spike-field coherence in the first 6 hours following CFC, but not following sham conditioning (**Figure4.1c**). [45,149] Similarly, neighboring principal neurons showed greater spike-field coherence following CFC, but not sham conditioning (**Figure 4.1d**). These changes were evident for both delta- and theta-frequency oscillatory activity in CA1, across behavioral states (**Figure 4.2a**), and were not due to changes in post-CFC sleep architecture (**Supplemental Figure 4.3**). These data suggest that rhythmic synchrony of neuronal firing in the CA1 network is augmented during active memory consolidation. Neuronal firing was also altered during SPWR events following CFC (**Figure 4.2b-c**). While no change in spike-field coherence was detected during ripple oscillations, following CFC there was an increase in both the overall frequency of SPWR events (**Figure 4.2b**) and FS interneuron firing rates during SPWRs (**Figure 4.2c**).

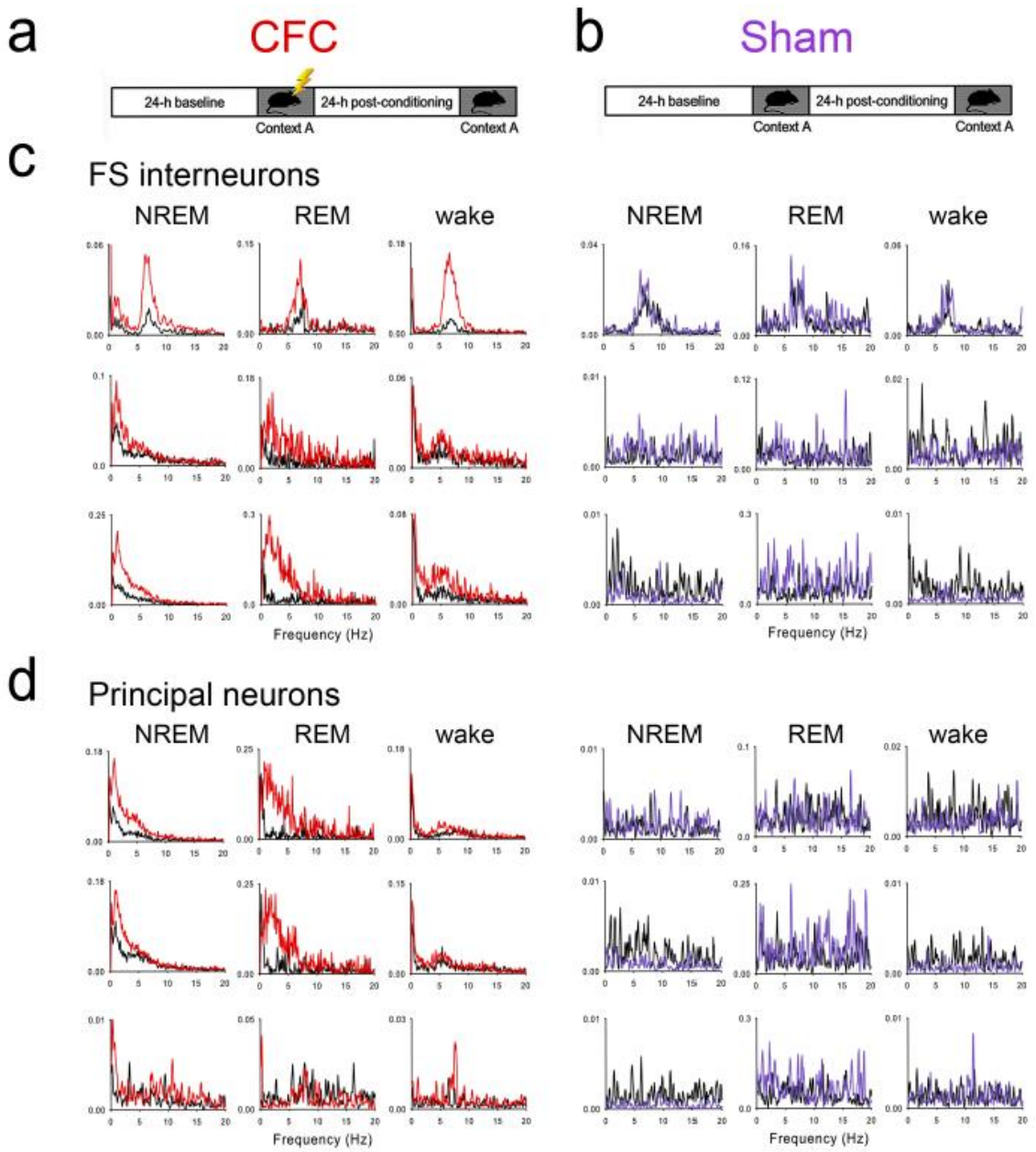

Figure 4.1: Coherence changes in CA1 neurons during CFM consolidation. (**a-b**) Experimental paradigm. Male C57BL/6J mice were recorded for a 24-h baseline period in their home cage, starting at lights-on, after which they either underwent single-trial CFC in a novel recording chamber (**a**) or sham training (**b**) (*n* = 5 mice per group). Afterward, all mice were returned to their home cage for an additional 24 h of recording. Context-specific freezing was assessed as a measure of CFM consolidation 24 hours later. (**c-d**) Coherent firing is shown for 3 representative FS interneurons (**c**) and 3 representative principal neurons from the same site (**d**) recorded in CA1 over the first 6 h of baseline (black) or the first 6 h following either CFC or sham conditioning (red or purple, respectively). Coherent firing is shown separately for periods of NREM, REM and wake.

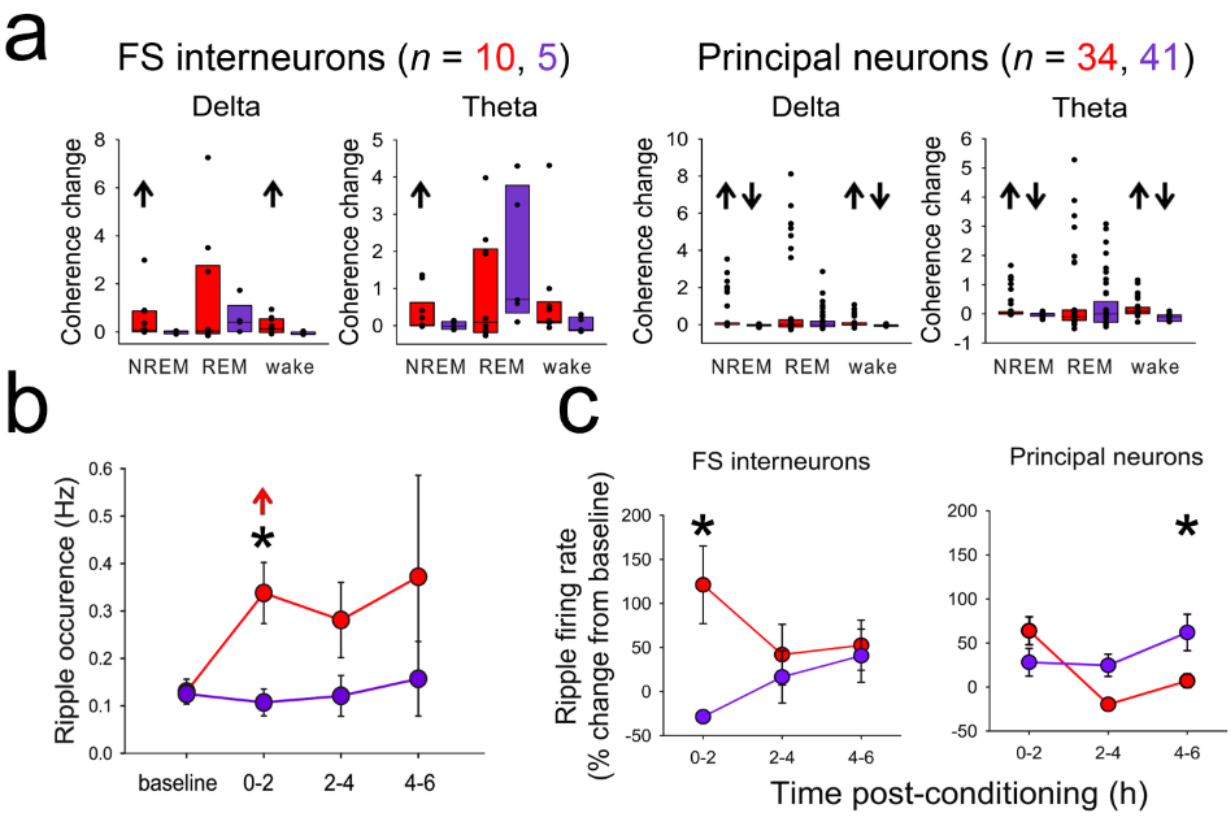

Figure 4.2: CFC induces coherence changes in CA1 neurons for both delta- and theta-frequency oscillatory across behavioral states, as well as increases in NREM SPWR events. (**e**) Quantification of post-CFC changes in delta and theta coherence (from baseline) for FS interneurons and principal neurons. Box plots indicate 25th, 50th, and 75th percentile values. ↑↓ indicates relative increases or decreases of $p < 0.05$ for post-CFC or post-Sham vs. baseline, Wilcoxon signed rank test. (**f**) Mean (± SEM) frequency of SPWR events for CFC and Sham mice during the first 6 h of baseline recording, and following CFC or sham conditioning. ↑ indicates relative increase of $p < 0.05$ for post-CFC vs. baseline, * indicates $p < 0.05$ post-CFC vs. post-Sham, Holm-Sidak *post hoc* test. (**g**) Mean (± SEM) firing rate changes (from baseline values) during SPWR events. * indicates $p < 0.05$ post-CFC vs. post-Sham, Holm-Sidak *post hoc* test.

Based on these findings, we carried out a series of experiments to test two hypotheses: 1) that CA1 FS interneurons (which are typically PV+) augment network rhythms following CFC, and 2) that PV+ interneuron-mediated rhythms play an essential role in memory consolidation.

4.3.2 Inhibition of CA1 PV+ interneurons blocks CFM consolidation

To test these hypotheses, we used an AAV vector to express the inhibitory receptor hM4Di-mCherry in a CRE recombinase-dependent manner in area CA1 of *Pvalb-IRES-CRE* transgenic mice (**Figure 4.3a**). This allowed transient pharmacogenetic inhibition of CA1 PV+ interneurons upon systemic administration of the hM4Di ligand clozapine-N-oxide (CNO). [142] We confirmed inhibition by CNO *in vivo* by characterizing c-Fos expression in these neurons 90 minutes after single-trial CFC (followed immediately by CNO administration). For these studies we expressed hM4Di in right-hemisphere CA1 and a control (mCherry) vector in left-hemisphere CA1 in each mouse (**Figure 4.3b**), to compare the number of c-Fos-immunopositive PV+ interneurons with vs. without pharmacogenetic inhibition. Under these conditions, the proportion of c-Fos+, hM4Di-expressing neurons was significantly lower than the proportion of c-Fos+, mCherry-expressing neurons (**Figure 4.3 c-d**), consistent with CNO-mediated inhibition of PV+ interneurons after CFC.

To assess the behavioral and hippocampal network effects of PV+ interneuron inhibition, mice expressing either hM4Di or mCherry bilaterally in CA1 were implanted with CA1 stereotrode arrays (**Supplemental Figure 4.4**). Following a 24-h baseline recording period (during which baseline neuronal and local field potential [LFP] activity

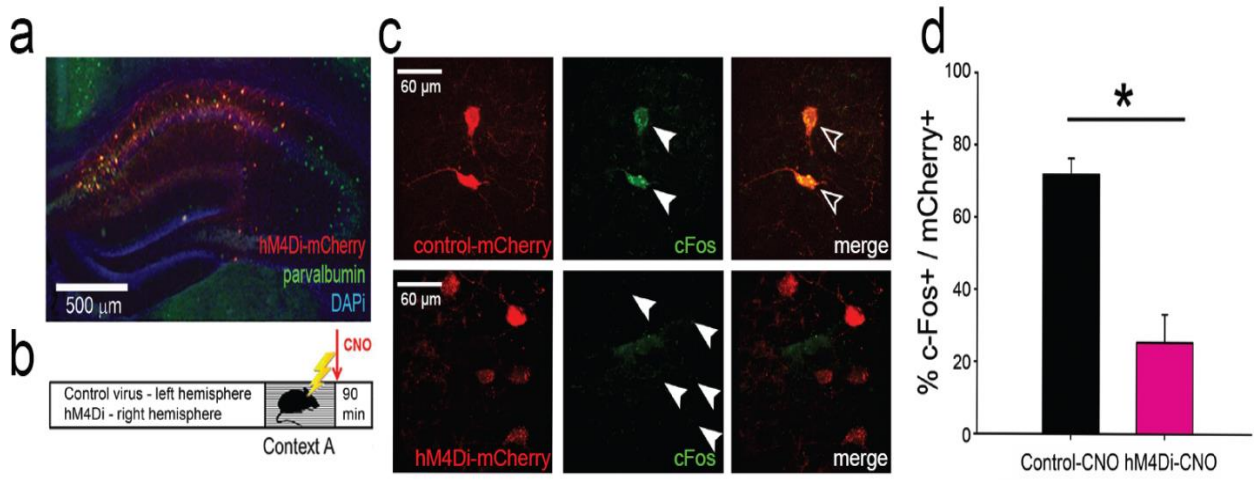

Figure 4.3: Pharmacogenetic inhibition of PV+ FS interneurons. (**a**) Representative image for expression of AAV-hM4Di-mCherry in CA1 PV+ interneurons. Scale bar = 500 µm. (**b**) Experimental paradigm: *Pvalb-IRES-CRE* mice (*n* = 5) expressing hM4Di-mCherry in right-hemisphere CA1 and control (mCherry) virus in left-hemisphere CA1 underwent single-trial CFC were immediately administered CNO (0.3 mg/kg, *i.p.*) and were returned to their home cage for 90 min prior to sacrifice. (**c**) CNO-mediated inhibition of PV+ interneurons was confirmed by comparing the proportion PV+ interneurons which were c-Fos-immunopositive 90 min post-CFC between right (hM4Di-mCherry) and left (control) hemisphere. ***Left panel****:* mCherry expression in left and right hemispheres (top and bottom, respectively). Scale bar = 60 µm. ***Center panel****:* c-Fos staining in cell bodies (green); locations of mCherry-expressing cell bodies identified by solid arrowheads. ***Right panel****:* merged images showing c-Fos and mCherry expression (empty arrowheads indicate cells expressing both c-Fos and mCherry). (**d**) Fewer mCherry-labeled neurons expressed c-Fos in the hM4Di-expressing right hemisphere compared with the left (control) hemisphere (values indicated mean ± SEM / hemisphere). * indicates $p < 0.001$, Student's *t*-test, error bars are SEM.

was recorded), mice underwent single-trial CFC followed by CNO administration (**Figure 4.4a**). CFM was assessed (as context-specific freezing) 24 h later, when mice were returned to the same environmental context. In hM4Di-expressing mice, CNO administration immediately following CFC disrupted CFM consolidation (**Figure 4.4b**). Effects of PV+ interneuron inhibition on memory were not due to changes in post-CFC sleep architecture (which was similar between treatment groups; **Supplemental Figure 4.6**). [128,150] Nor were these effects due to induction of hippocampal seizures (*i.e*., ictal spiking was absent from CA1 LFPs and behavior was unchanged following CNO administration) or gross dysregulation of neuronal firing rates in CA1 (**Supplemental Figure 4.8**). To test whether CFM deficits were driven by hM4Di expression alone, the same hM4Di-expressing mice underwent single-trial CFC two weeks later in a second, dissimilar environmental context and were subsequently administered a vehicle (DMSO). Under these conditions, CFM consolidation in hM4Di-expressing mice was comparable to that of mCherry-expressing controls (**Figure 4.4b**). Taken together, these data show that CA1 PV+ interneurons play an essential role in CFM consolidation.

4.3.3 PV+ interneuron-driven oscillations predict memory recall

To determine how PV+ interneurons coordinate CA1 network activity during memory consolidation, we first characterized changes in CA1 LFP activity over the first 6 h following CFC. LFP power spectra during rapid eye movement (REM) sleep and non-REM (NREM) sleep are shown for a representative hM4Di-expressing mouse in

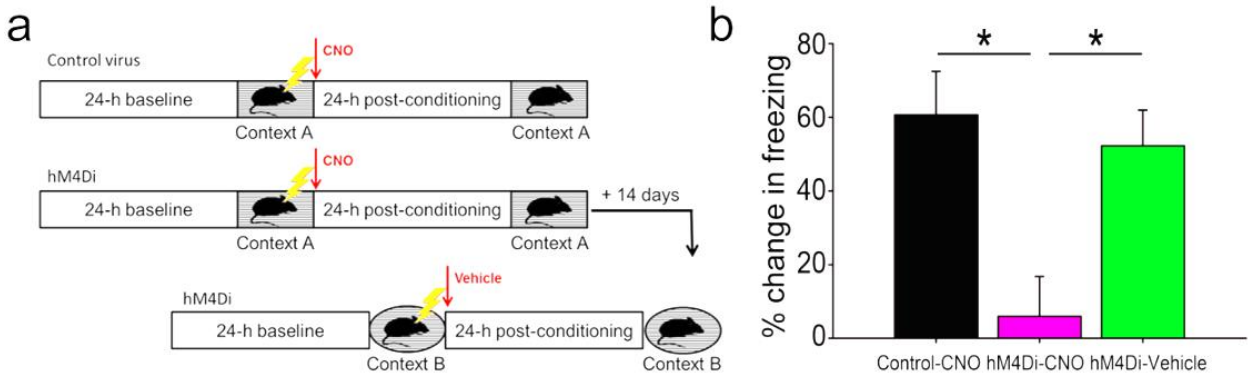

Figure 4.4: Pharmacogenetic inhibition of CA1 PV+ interneurons blocks CFM consolidation. (**a**) Experimental paradigm: Mice expressed either hM4Di or mCherry (n=5 for each group) bilaterally in CA1. Following a 24-h baseline recording period in their home cage, mice were placed into a novel recording chamber (Context A) for single-trial CFC. They were subsequently administered CNO and returned to their home cage. Context-specific freezing was assessed as a measure of CFM consolidation 24 hours later. Two weeks later, hM4Di-expressing mice again underwent single-trial CFC - this time in a second, dissimilar context (Context B), after which they were administered vehicle (DMSO). (**b**) CFM in Context A was significantly reduced in mice with post-CFC inhibition of PV+ interneurons. These same mice showed normal CFM in Context B when PV+ interneurons were not inhibited. * indicates $p = 0.006$ one-way ANOVA, $p < 0.05$ Holm-Sidak *post hoc* test for hM4Di-CNO ($n = 6$) vs. Control-CNO ($n = 4$) and vs. hM4Di-vehicle ($n = 6$). Control-CNO vs. hM4Di-vehicle *N.S.* All error bars are SEM.

PV+ interneuron inhibition (CNO) and control (vehicle) conditions (**Figure 4.5a-b**; see also **Supplemental Figure 4.5a**). Under control conditions, CA1 spectral power in delta (0.5-4 Hz) and theta (4-12 Hz) frequency bands increased dramatically during post-CFC REM and NREM (but not wake; **Supplemental Figure 4.5**). These changes in spectral power were evident in data averaged across states, although there was some evidence that they waxed and waned across bouts of sleep (**Figure 4.5g**). Delta and theta increases were transient (generally returning to baseline levels after approximately 6 h; **Supplemental Figure 4.5b**), and were blocked by CNO administration (**Figure 4.5c** and **e**, respectively; see also **Supplemental Figure 4.7**). Critically, the degree to which NREM delta and theta activity increased in the first 6 h following CFC predicted individual animal's subsequent behavioral performance (*i.e.*, context-specific freezing measured 24 h post-CFC; **Figure 4.5d** and **f**, respectively).

Because PV+ interneurons are implicated in generation of CA1 sharp wave ripple oscillations (SPWRs), and NREM SPWRs are hypothesized to play a role in memory consolidation, we also assessed the effects of PV+ interneuron inhibition on SPWRs in the hours following CFC. [26–28] Under control conditions, both the amplitude and frequency of ripple (150-250 Hz) oscillations increased significantly over the first 2-4 hours of post-CFC NREM sleep; these changes were also blocked by PV+ interneuron inhibition (**Figure 4.6**). Together, these data demonstrate that PV+ interneurons normally coordinate multiple sleep-associated CA1 network oscillations in the hours following learning, and suggest that these oscillations in turn promote CFM.

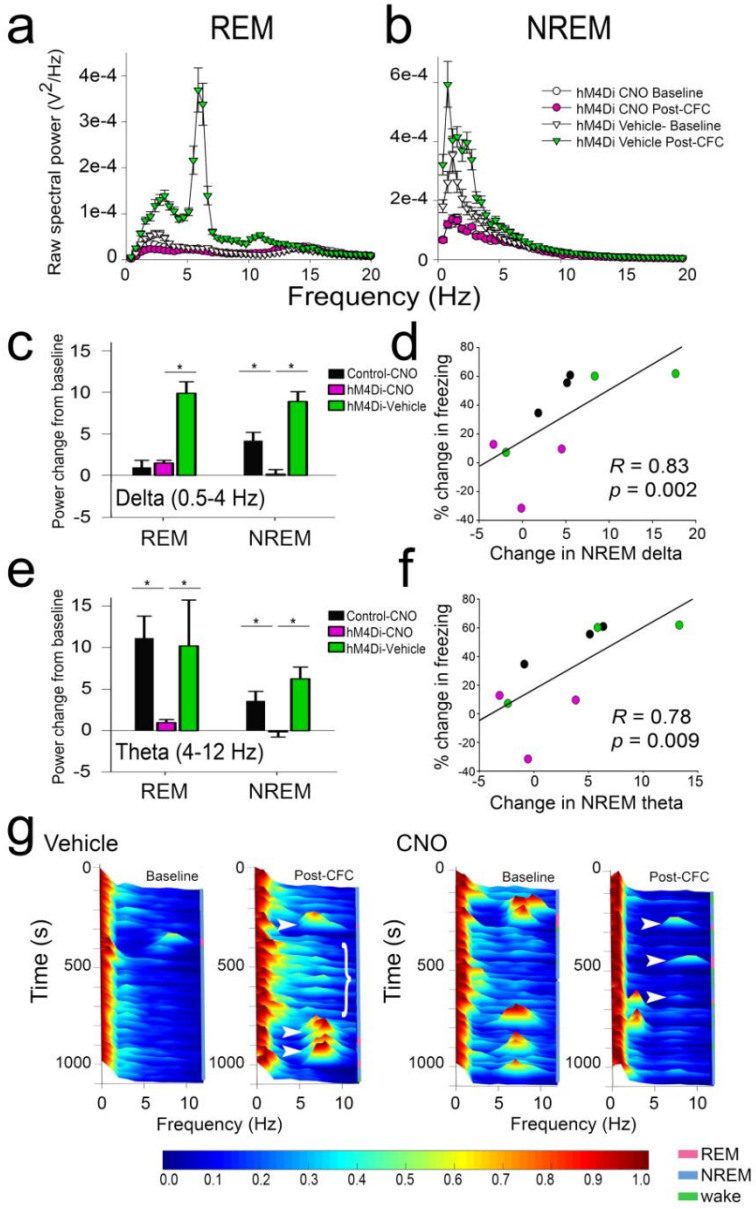

Figure 4.5: Inhibition of PV+ interneurons disrupts augmentation of CA1 delta and theta oscillations, which are associated with successful CFM consolidation. (**a,b**) Raw CA1 LFP spectral power in REM and NREM sleep from a representative hM4Di-expressing mouse over the first 6 h post-CFC, following administration of CNO (pink circles) vs. vehicle (green triangles) for a representative animal. (**c,e**) Post-CFC increases in delta and theta spectral power (from baseline) were present in the first 6 h of post-conditioning sleep in the two control conditions; these increases were blocked by PV+ interneuron inhibition. * indicates $p < 0.01$, Holm-Sidak *post hoc* test. (hM4-CNO, $n = 74$; hM4-vehicle, $n = 74$; Control-vehicle; $n = 58$). (**d,f**) Increases in NREM delta and theta power over the first 6 h post-CFC were correlated with subsequent CFM consolidation (values indicate mean LFP changes per mouse; Spearman rank order). (**g**) Representative LFP spectrograms showing spectral power in delta and theta bands across 1000 s of recording time (matched for time of day) during baseline and in the hours immediately following CFC. In vehicle-treated mice, following CFC there was greater power in delta and theta bands in NREM (bracket) and dramatically increased theta power during REM bouts (filled arrowheads). In CNO-treated mice, there was a suppression of theta in REM bouts (filled arrowheads) as well as a general suppression of 2-12 Hz activity across all states.

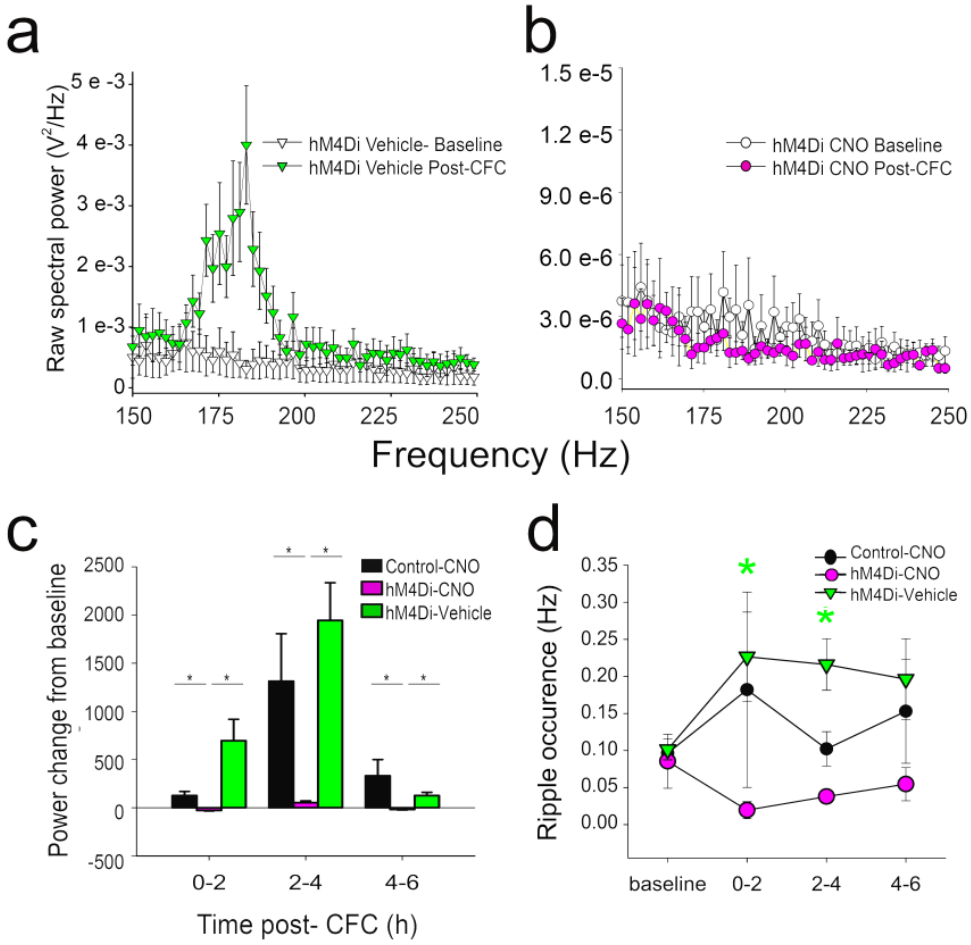

Figure 4.6: Inhibition of PV+ interneurons disrupts augmentation of CA1 ripple oscillations during CFM consolidation. (**a,b**) Ripple amplitude increased immediately following CFC + vehicle, but not CFC + CNO. Mean ± SEM shown for local field potential values for all animals across a given treatment (hM4-CNO, *n* = 74; hM4-vehicle, *n* = 74). (**c**) Post-CFC increases in ripple power from baseline were present in the first 4 h of post-conditioning sleep in the two control conditions; these increases were blocked by PV+ interneuron inhibition. * indicates $p < 0.01$, Holm-Sidak *post hoc* test. (**d**) Post-CFC NREM ripple frequency increases were blocked by PV+ interneuron inhibition. * indicates $p < 0.05$, Holm-Sidak *post hoc* test, vehicle vs. CNO and vs. baseline. All values indicate mean ± SEM.

4.3.4 PV+ interneurons coordinate ensembles during consolidation

Delta, theta, and ripple oscillations could play a critical role in regulating spike timing between neurons, a process which is likely essential for memory consolidation. [22,71,84] To determine whether PV+ interneurons also play a role in coordinating CA1 neuronal ensemble activity in the context of CFM consolidation, we characterized neuronal functional connectivity patterns before and after CFC. To do this, we divided spike trains recorded from CA1 neurons into 1-min time bins, and compared spike train relationships among neurons within each time bin using a previously-developed metric referred to as average minimum temporal distance (AMD). [97] AMD characterizes functional connectivity relationships between pairs of neurons, based on the temporal proximity of their respective spike trains (**Figure 4.7a**; see also **Supplemental Figure 4.9**).

Using AMD, we generated pairwise functional connectivity matrices for all stably-recorded CA1 neurons. These matrices were then compared between successive time intervals (**Figure 4.7b**). Based upon mean minute-to-minute similarity of these matrices, we were able to quantify stability of the CA1 network across baseline and post-CFC recording periods. A representative baseline similarity trace is shown in **Figure 4.7c** for a mouse expressing hM4Di-mCherry. Changes in CA1 network stability measured across 24 h after CFC (*i.e.*, from 24-h baseline) were compared between treatment groups. In vehicle-treated mice, CA1 network stability was significantly enhanced following CFC - a change which was present in both NREM sleep and wake. Increases in stability were blocked by PV+ interneuron inhibition (**Figure 4.7d**). NREM stability following CFC was correlated with the occurrence of NREM ripples (particularly in the

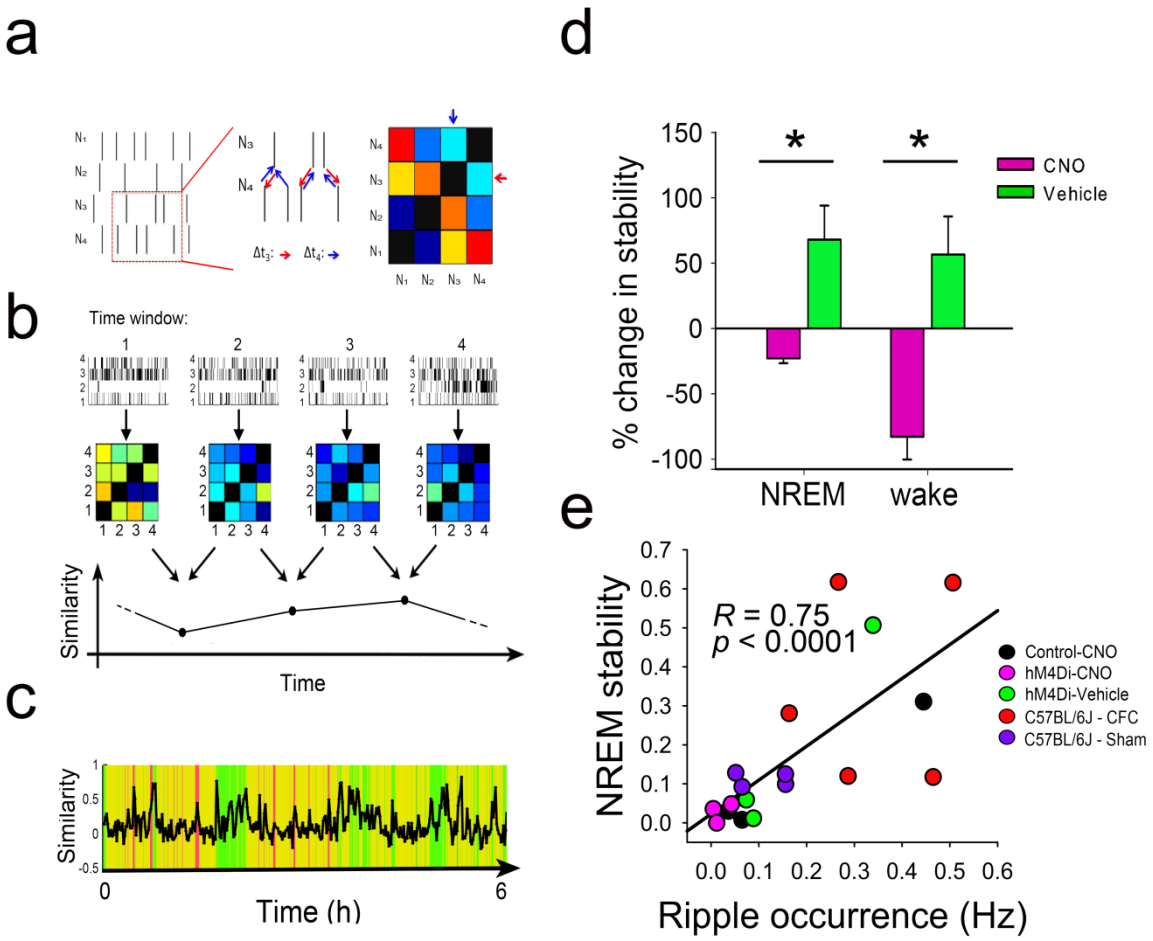

Figure 4.7: Inhibition of PV+ interneurons disrupts learning-induced stabilization of CA1 network dynamics. (**a**) Average minimum temporal distance (AMD) is calculated between spikes of two neurons. An example of AMD calculations for neurons '3' and '4'. The closest spikes of neuron '4' to each given spike of neuron '3' (red arrows) and vice versa (blue arrows). Pairwise AMD values were calculated for every 1-min interval, based on spike trains of stably recorded neurons. From these values, a functional connectivity matrix is generated, which represents the pattern of functional connectivity at any time point. Pairs with smaller AMD values are more likely to be functionally connected (shown in red in the matrix) than those with larger AMD values (shown in blue in the matrix). (**b**) Functional connectivity matrices were constructed for every one minute interval of recording, based on spike rasters from all stably-recorded neurons (n = 5-16 neurons/mouse, 3 mice/condition). A comparison of matrices at adjacent time points yields a similarity value, which is plotted across the entirety of a recording period. (**c**) Similarity values are shown over the first 6 h of baseline recording in a representative animal. Yellow indicates NREM sleep, green: wake, pink: REM sleep. (**d**) In the 24 h following CFC, mean (± SEM shown) minute-to-minute CA1 network stability increased during both NREM and wake (REM stability could not be calculated due to the low number of REM epochs ≥ 2 min in duration). CNO inhibition of PV+ interneurons decreased stability across this same time period. * indicates $p < 0.05$, Wilcoxen rank-sum test. (**e**) Across individual mice, post-CFC (or post-Sham) NREM stability was predicted by NREM ripple frequency in the first 2 h following training (Spearman rank order).

first 2 h following training; **Figure 4.7e**), but was not predicted by NREM theta or delta changes (*N.S.*, Spearman rank order, data not shown). Destabilization of functional connectivity patterns by post-CFC PV+ interneuron inhibition was not due to gross dysregulation of CA1 neuronal activity, as firing rates were not significantly altered by CNO treatment. (**Supplemental Figure 4.8**) Together this suggests that PV+ interneurons play a critical role in stabilizing communication patterns throughout the CA1 network in the hours following CFC**.**

4.3.5 PV+ interneurons coordinate ensemble reactivation over time

To visualize how CA1 network communication patterns change in the hours following CFC, we generated a functional similarity matrix (FSM; schematized in **Figure 4.8a**) for each recording. The FSM illustrates the degree of similarity between a network's functional connectivity pattern at a given time point and at all other time points across a recording. FSMs are shown for NREM epochs a representative hM4Di-expressing mouse at baseline and for the first 6 h after CFC following either vehicle or CNO administration, respectively (**Figure 4.8b**). Distributions of similarity values were quantified and compared across baseline and post-CFC recording periods (**Figure 4.8c**). In vehicle-treated mice, there was more frequent and consistent repetition of specific network functional connectivity patterns throughout the first 6 h of post-CFC NREM, shown as a rightward shift in the similarity distribution after CFC (**Figure 4.8c-d**; see also **Supplemental Figure 4.10**). As was true for delta and theta LFP power changes, stable repetition of network patterns waxed and waned (and in some cases, appeared to do so in concert with LFP power changes; see **Supplemental Figure 4.11**). Such changes in connectivity patterns across time were not seen when PV+

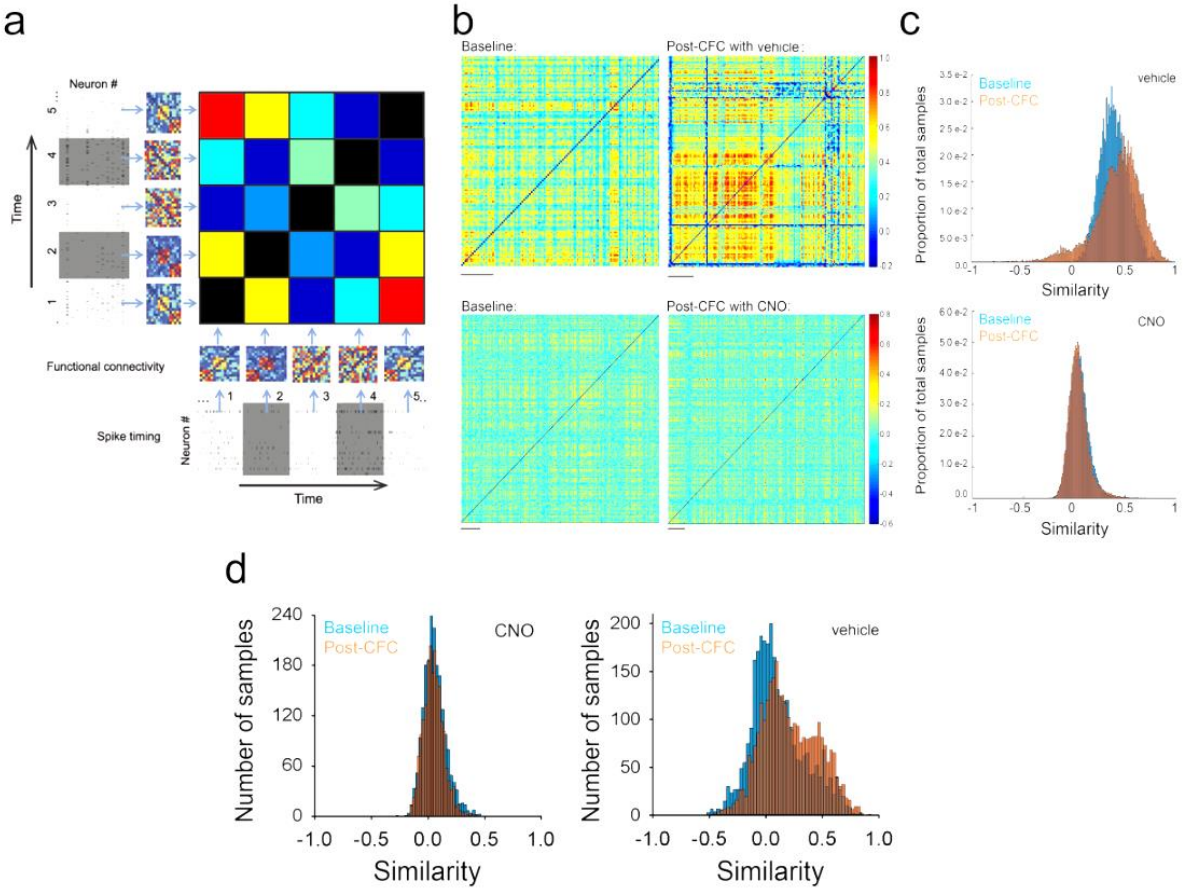

Figure 4.8: PV+ interneurons promote consistent reactivation of CA1 neural ensembles following learning. (**a**) Generation of a functional similarity matrix (FSM). The FSM displays the similarity of functional connectivity patterns (*i.e*., matrices from **Figure 4.6b**) across all time intervals. (**b**) NREM CA1 network FSMs from a representative hM4Di-expressing mouse at baseline, and over the first 6 h post-CFC (vehicle and CNO conditions). Color in the body denotes the degree of similarity between NREM functional connectivity patterns at any given time point in the recording, and NREM patterns at all other time points. Scale bars = 20 mins of recording time. (**c**) Distributions of minute-to-minute similarity values (at baseline, and following CFC) for the data shown in 4.**7b**. (**d**) Distributions of NREM sleep similarity values from all stably-recorded mice at baseline, and following CFC (n = 3/condition). For both **c** and **d**, similarity distributions were significantly shifted to higher values following CFC in vehicle-treated mice, but not CNO-treated mice ($p < 0.001$, Mann-Whitney rank sum test).

interneurons were inhibited. These findings show that in addition to promoting network oscillations after learning, PV+ interneurons promote consistent reactivation of CA1 neural ensembles over time.

4.3.6 PV+ interneuron-driven rhythms promote network stability

We next tested whether rhythmic PV+ interneuron activity is sufficient to augment CA1 oscillations and stabilize CA1 ensembles. To do this we recorded network dynamics among CA1 neurons before, during, and after rhythmic optogenetic stimulation of PV+ interneurons in anesthetized animals, which, for testing sufficiency is a much less labor intensive recording paradigm (**Supplemental Figure 4.12**). In transgenic mice expressing Channelrhodopsin 2 (ChR2) in PV+ interneurons (*PV:ChR2*), stimulation across a range of frequencies led to rhythmic activation of FS interneurons, and rhythmic inhibition of neighboring principal neurons (**Supplemental Figure 4.13a**). Stimulation also led to frequency-specific, rhythmic activity in the CA1 LFP and enhanced neuronal spike-field coherence at the stimulation frequency (**Supplemental Figure 4.13a**; **Supplemental Figure 4.15a**). In contrast, stimulation above (18 Hz) or below (2Hz) this range had relatively modest effects on spike-field coherence. Because PV-expressing interneurons outside CA1 can contribute to CA1 network oscillations, we repeated these experiments in AAV-transduced *Pvalb-IRES-CRE* transgenic mice with CA1-targeted expression of ChR2. [153] In these mice, rhythmic PV+ interneuron activation led to similar increases in CA1 rhythmic firing and LFP rhythmicity (**Figure 4.9a-b**; **Supplemental Figure 4.14**). This was true both under anesthetized conditions (**Figure 4.9a-b**) and in awake, behaving mice (**Supplemental**

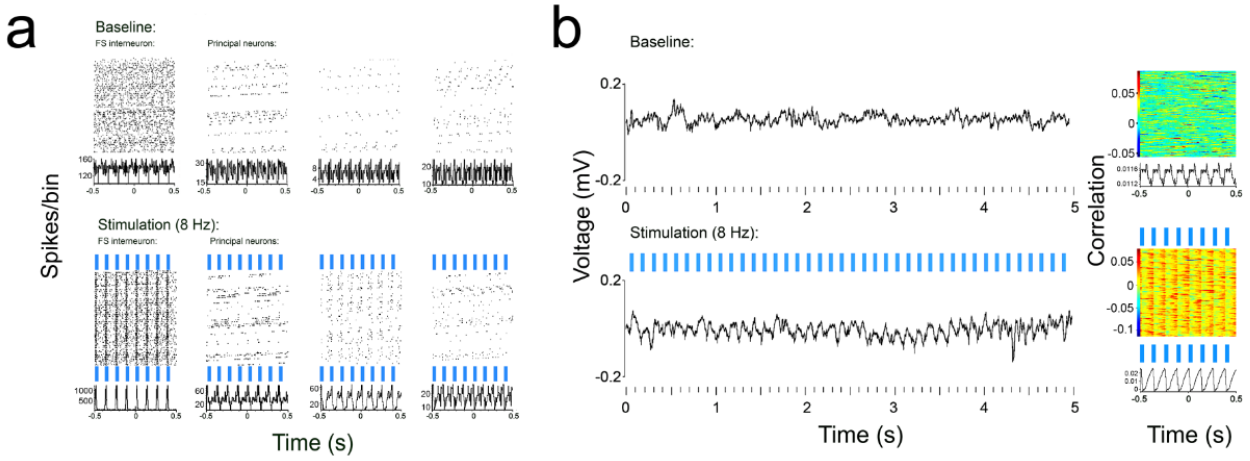

Figure 4.9: Rhythmic optogenetic stimulation of PV+ interneurons is sufficient to drive network activity patterns (**a**) Perievent firing rasters (***top panels***) and perievent firing histograms (***bottom panels***) for a representative CA1 FS interneuron and 3 neighboring principal neurons recorded from a *Pvalb-IRES-CRE* mouse expressing ChR2. (**b**) A representative 5-s LFP trace (***left***) and perievent LFP raster (***right***) for one of the recording sites from (**a**) in baseline and stimulation conditions.

Figure 4.16). Again, the strongest effects on spike-field coherence were seen for stimulation frequencies between 4 and 10 Hz (**Figure 4.10a**).

To test how optogenetically-induced coherent firing affected stability of communication patterns between CA1 neurons, we quantified stability of functional connectivity between each neuron and all of its neighbors (see **Methods** for details) at baseline, during stimulation at various frequencies, and post-stimulation. Stimulation of PV+ interneurons across 2-10 Hz significantly increased network stability, relative to baseline (with the largest increases between 4 and 10 Hz; **Supplemental Figure 4.15d**). Across the 4-10 Hz frequency range, the degree to which stimulation increased coherence predicted the change in stability of neurons' functional connectivity patterns (**Figure 4.10b**; **Supplemental Figure 3.15e**). Intriguingly, stability of network connectivity remained high relative to baseline even after the stimulation period ("post"; **Supplemental Figure 4.15d**). This suggests that rhythmic synchronization of firing in CA1 has an effect on the network which can outlast the period of PV+ interneuron stimulation.

To test the longer-term effects of PV+ interneuron-induced network coherence, we carried out two additional sets of experiments (in anesthetized and awake mice, respectively) where stimulation at 7 Hz (*i.e.*, the middle of the 4-10 Hz range) was followed by least 2 h of post-stimulation recording (**Supplemental Figure 4.12b-c**). This stimulation frequency evoked a robust increase in spike-field coherence in *PV:ChR2* mice, but not in control mice expressing GFP in PV+ interneurons (*PV:GFP*; **Figure 4.10c**; **Supplemental Figure 4.13b**; **Supplemental Figure 4.15f**). Stimulation of PV+

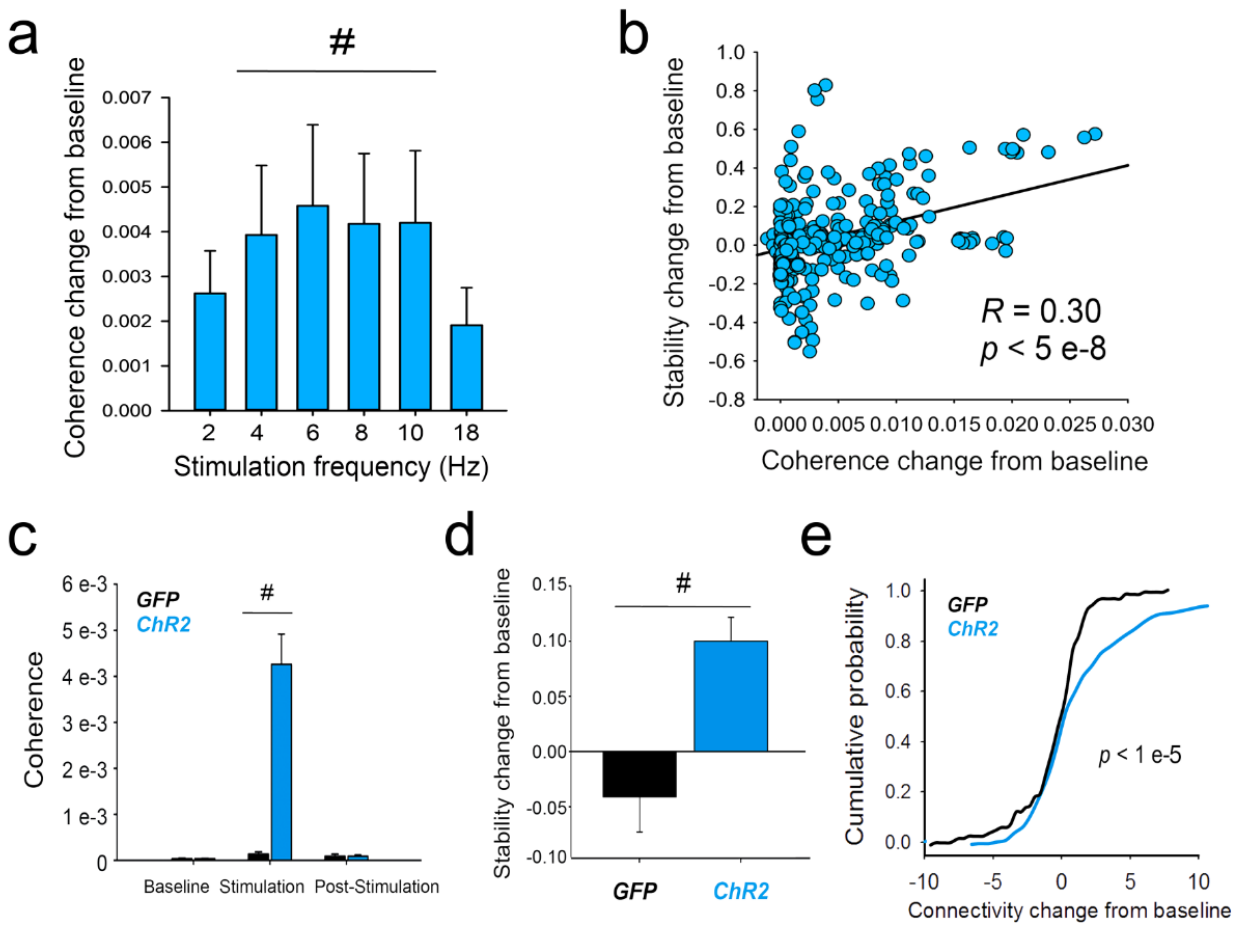

Figure 4.10: Rhythmic optogenetic stimulation of PV+ interneurons increases CA1 network coherence, stability, and connection strength. (**c**) Changes in spike-field coherence (from baseline) induced by various frequencies of rhythmic PV+ interneuron stimulation in virus-expressing neurons. Significant increases (from baseline) were present at stimulation frequencies between 4 and 10 Hz. # indicates $p < 0.05$, Wilcoxon signed rank test. (**d**) Across 4-10 Hz stimulation frequencies, changes in spike-field coherence predicted changes in stability of functional connectivity for individual neurons (Spearmann rank order, $n = 320$ neurons). (**e**) Comparison of CA1 spike-field coherence across a 30-min baseline period, 30 min of 7 Hz stimulation, and 2 h or post-stimulation recovery, in mice with CA1 expression of ChR2 (blue) or GFP (black). (**f**) Over the 2 h following 7 Hz stimulation, CA1 neuronal functional connectivity in mice expressing ChR2 showed an increase in stability relative to baseline. For **c-d**, # indicates $p < 0.05$, Wilcoxon signed rank test. (**g**) Neuronal functional connectivity strength also showed an increase in ChR2-transduced mice following 7 Hz stimulation p value indicates results of Kolmogorov-Smirnov test.

interneurons at 7 Hz induced a significant increase in CA1 network stability that lasted through the entire post-stimulation period (**Figure 4.10d**; **Supplemental Figure 4.15g**; see also **Supplemental Figure 4.16c**). This manipulation also induced a long-lasting increase in the strength of network connections (quantified as the average mean temporal distance between neuronal pairs' spike trains; see **Methods** for more details; **Figure 4.9g**; **Supplemental Figure 4.15h**). Not only could a long-term change in network connection strength be induced in anesthetized animals; it was also seen in awake, behaving animals for up to 2 h after cessation of 7-Hz stimulation (**Supplemental Figure 4.16d**). Taken together, these data suggest that rhythmic coordination of CA1 network activity by PV+ interneurons (at frequencies corresponding to those where increased network rhythmicity is seen following learning) has long-lasting effects on both the stability and strength of network connections.

4.4 Discussion

Our current findings demonstrate the essential mechanistic role that PV+ interneurons play in hippocampally-mediated memory consolidation. We find that CA1 FS interneurons show natural changes in their firing dynamics during active memory consolidation in the hours following single-trial CFC. We also find that when inhibiting a majority of CA1 PV+ interneuron activity, 1) CFM consolidation is completely blocked, 2) normal post-CFC enhancements in delta, theta, and ripple oscillations are lost, and 3) normal post-CFC stabilization of network communication patters is lost. Rhythmic activity in PV+ interneurons is also sufficient to drive coherent firing in neighboring CA1 neurons and to stabilize firing relationships among them, leading to long-lasting changes in network communication patterns and the strength of network connections.

Thus the role of CA1 PV+ interneurons in CFM consolidation is not only essential, it may also be instructive - promoting the changes to neuronal ensemble-level dynamics seen in the hours following learning.

While relatively few in number (~2.6% of the CA1 neuronal population), PV+ interneurons each innervate large numbers of pyramidal cells. [62] Thus, from an anatomical standpoint, they are uniquely well-suited to coordinate ensemble activity and spike timing within neuronal ensembles. PV+ interneurons were recently shown to play a critical role in driving theta and ripple oscillations in *ex vivo* hippocampal slices. [141,154] We have previously shown that the amplitude of CA1 theta and delta oscillations naturally increases following single-trial CFC in C57BL/6J mice. However, whether (and how) these network oscillations promote memory consolidation has remained a matter of speculation. [45] Here we show that 1) PV+ interneurons are necessary for learning 2) drive enhancements in theta, delta, and ripple oscillations in the hours following learning and 3) these oscillations can have long-lasting effects on the strength of network connections and the stability of CA1 ensemble activity.

Reactivation and sequential replay have been widely reported in CA1 after spatial learning, yet little is known about what drives these processes, or what their functional significance might be. [71,81,134,135] Here we employ a new set of metrics, which can be used to detect network changes after single-trial learning events such as CFC, and do not rely on specific features such as sequential place cell activation. For these reasons, they may be more broadly applicable for studies of memory consolidation when compared with other metrics. By quantifying changes in functional connectivity between CA1 neurons in the hours following single-trial CFC (when *de novo* memory

consolidation is clearly occurring), our data add to what is known about reactivation and replay in several ways. First, we show that consolidation-related changes in CA1 network dynamics can be measured over a longer time window than previously reported for either sequential replay or ensemble reactivation (*i.e*., over several hours following learning, vs. tens of minutes). [42] This timescale more closely matches what is known about CFM consolidation, in which memories remain susceptible to disruption for several hours following learning. [6,24,25,37] Second, we find that stabilization of functional connectivity patterns is associated with reliable reactivation of CA1 ensemble activity patterns in the hours after learning. Third, we show that disrupting PV+ interneurons' activity disrupts stabilization of the CA1 network and the consistent reactivation of CA1 neural ensembles over time. Finally, we show that the rhythmic activation of PV+ interneurons (which is naturally augmented following learning) is sufficient to stabilize CA1 network dynamics over behaviorally-relevant timescales (*i.e.*, hours).

Our data suggest that rhythmic activity in PV+ interneurons is capable of promoting long-term *functional* plasticity in the CA1 network. Whether, and how, PV+ interneuron-driven dynamics affect *structural* plasticity in CA1 remains an open question. Recent studies suggest that these neurons themselves undergo synaptic remodeling as a function of memory formation. [29,155] Intriguingly, disruption of sleep in the hours following learning has also been shown to impair structural plasticity in CA1 pyramidal neurons' dendritic spines. [38] One possibility is that the sleep-associated coordination of activity among CA1 neurons, over a timescale of hours, drives such structural changes by regularizing spike-timing relationships (*i.e*., via spike timing-dependent plasticity).

In summary, our present data demonstrate that PV+ interneuron-mediated network oscillations are associated with successful memory consolidation. We show for the first time that these oscillations can: 1) drive reliable ensemble reactivation, 2) stabilize patterns of neuronal communication, and 3) induce long-lasting changes in the strength of functional connectivity relationships between CA1 neurons. We conclude that these neurons may provide instructive offline reinforcement of newly-learned information by coordinating neuronal activity patterns across the CA1 network.

4.5 Supplemental Figures

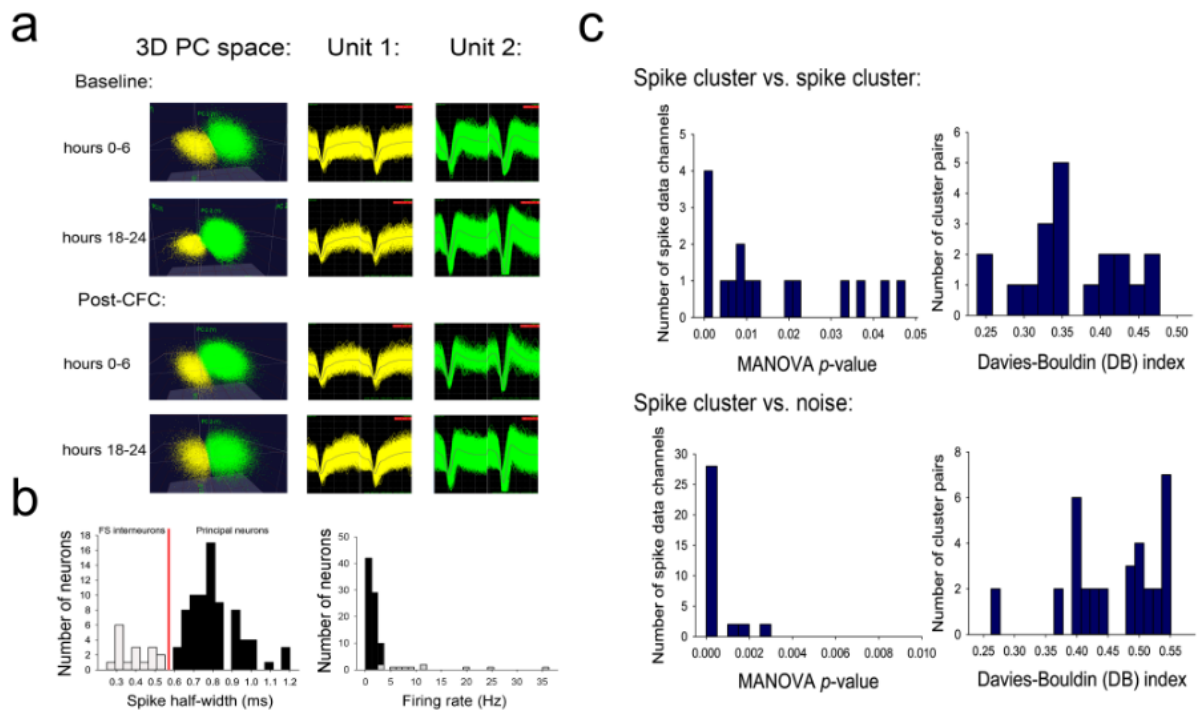

Supplemental Figure 4.1: Spike sorting for recordings from freely-behaving mice. (**a**) An example of spike cluster separation vs. time across baseline and post-CFC recording period. (**b**) Distribution of spike half-width (in ms; *left*) and mean waking firing rates (*right*) for all stably-recorded neurons with data shown in **Fig. 1**. Red line indicates threshold value for classification as FS interneurons (light gray; half-width ≤ 0.55 ms) or principal neurons (black; half-widths > 0.55 ms). Mean half-widths (± SEM) for FS interneurons and principal neurons were 0.39 ± 0.03 and 0.81 ± 0.02 ms, respectively (comparable to previously published measurements for CA1 FS interneurons and pyramidal neurons). [157,158] Mean firing rates (± SEM) for FS interneurons (light gray) and principal neurons (black) were 9.9 ± 2.6 and 1.2 ± 0.1 Hz, respectively. Both spike half-width distributions and firing rate distributions were significantly different between the two cell populations ($p < 0.001$, Mann-Whitney U test). (**c**) Spike cluster quality metrics for individual spike clusters vs. one another (*top*) and vs. noise (*bottom*). *Left:* Distributions of MANOVA *p*-values for principal component-based spike cluster separation, for all channels with multiple stably-recorded neurons. *Right:* Distributions of Davies-Bouldin (DB) validity indices for cluster pairs on channels with multiple stably-recorded neurons.

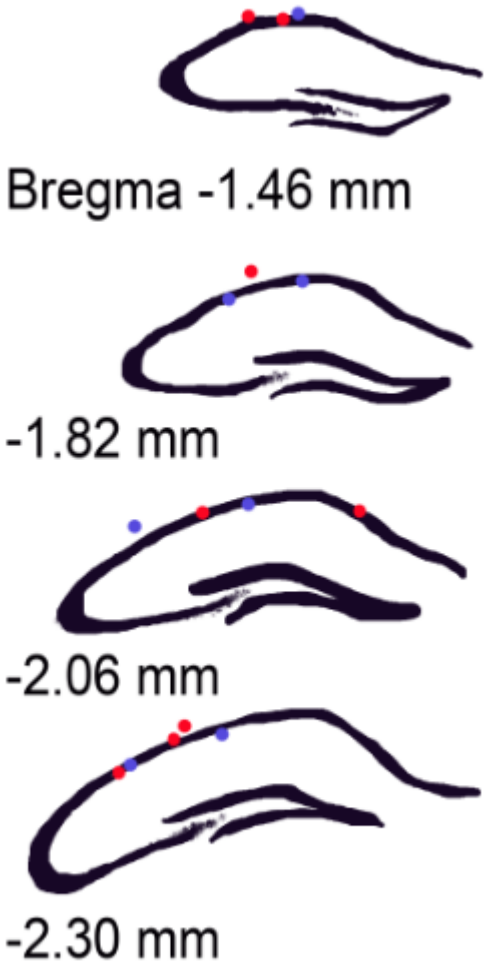

Supplemental Figure 4.2: Recording sites for C57BL/6J mice. Positions of electrode bundles for single-unit and LFP recordings for C57BL/6J mice used in CFC (*n* = 4 mice; red dots) and sham (*n* = 4 mice; purple dots) experiments.

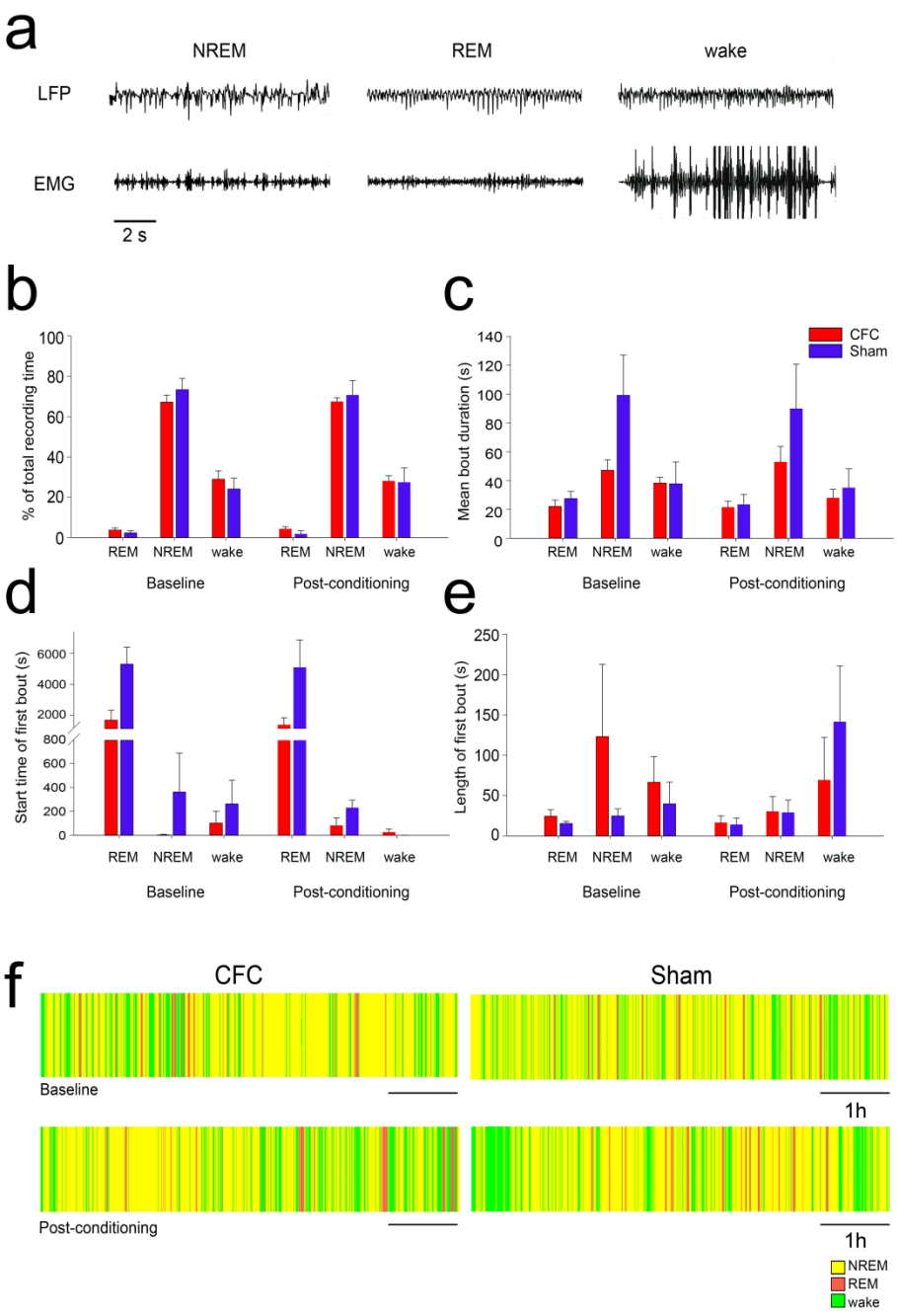

Supplemental Figure 4.3: Sleep architecture in C57BL/6J mice. Representative LFP and EMG traces in (**a**) show typical activity during NREM, REM, and wake. There was no significant effect of treatment on (**b**) percent of time spent in REM, NREM, and wake, (**c**) mean duration of REM, NREM, and wake bouts, (**d**) time to onset of the first bout of REM, NREM, and wake, or (**e**) the length of the first bout of REM, NREM, and wake. All error bars are SEM. (**f**) Hypnograms showing sleep state transitions over the first 6 h of either baseline (***top***) or post-conditioning (***bottom***) recording, in representative CFC (***left***) and Sham (***right***) mice.

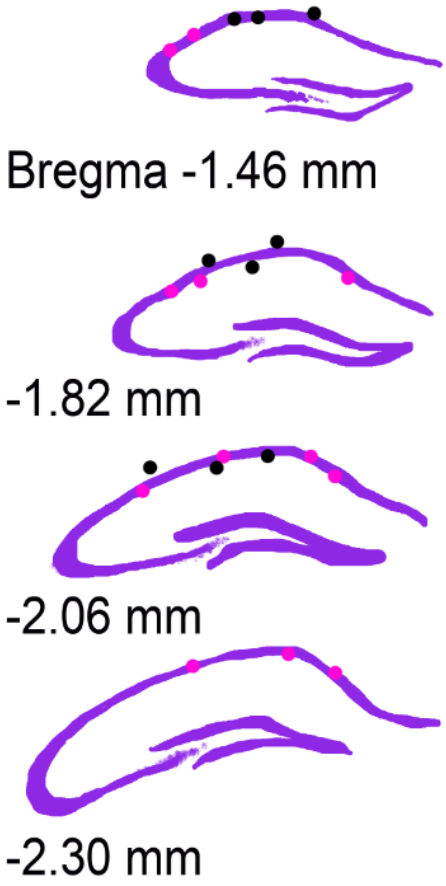

Supplemental Figure 4.4: Electrode placement in hM4Di- and mCherry-expressing mice. Positions of electrode bundles for single-unit and LFP recordings for *Pvalb-IRES-CRE* mice expressing either control virus (mCherry; *n* = 4 mice; black dots) or hM4Di-mCherry (*n* = 6 mice; pink dots).

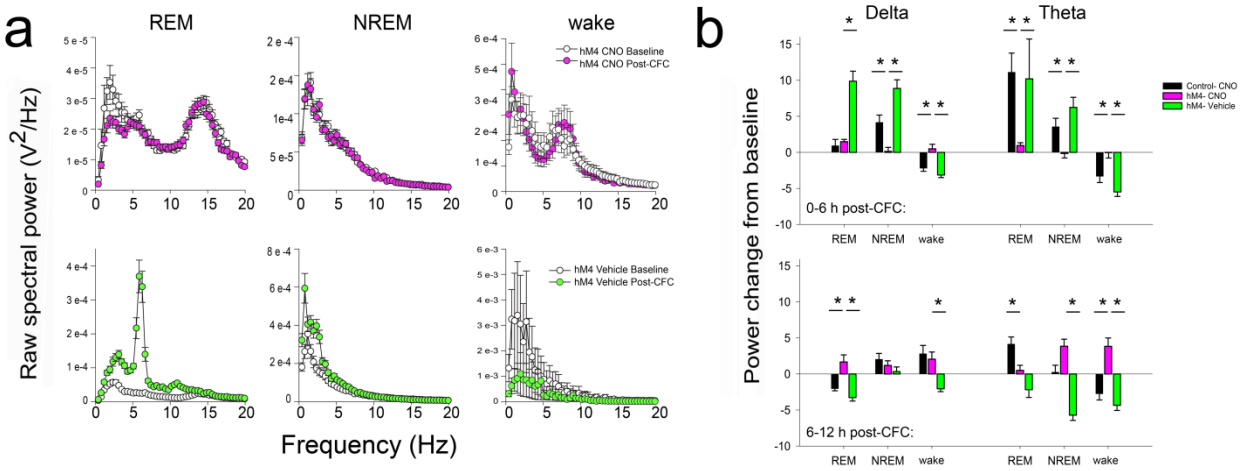

Supplemental Figure 4.5: LFP spectral changes across REM, NREM, and wake across hours 0-6 and 6-12 post-CFC. (**a**) Raw CA1 LFP spectral power in REM, NREM, and wake from the same hM4Di-expressing mouse shown in **Fig. 4** over the first 6 h post-CFC. Data are shown separately for baseline and following post-CFC administration of CNO (white and pink circles, respectively, top), and for a second baseline two weeks later and following post-CFC administration of vehicle (white and green circles, respectively, bottom). Post-CFC increases in delta and theta spectral power (from baseline) were present in hours 0-6 of REM and NREM sleep (but not wake) in the two control conditions. These increases were largely absent in hours 6-12 post-CFC. * indicates $p < 0.05$, Holm-Sidak *post hoc* test. Mean ± SEM shown for all local field potential values across a given treatment.

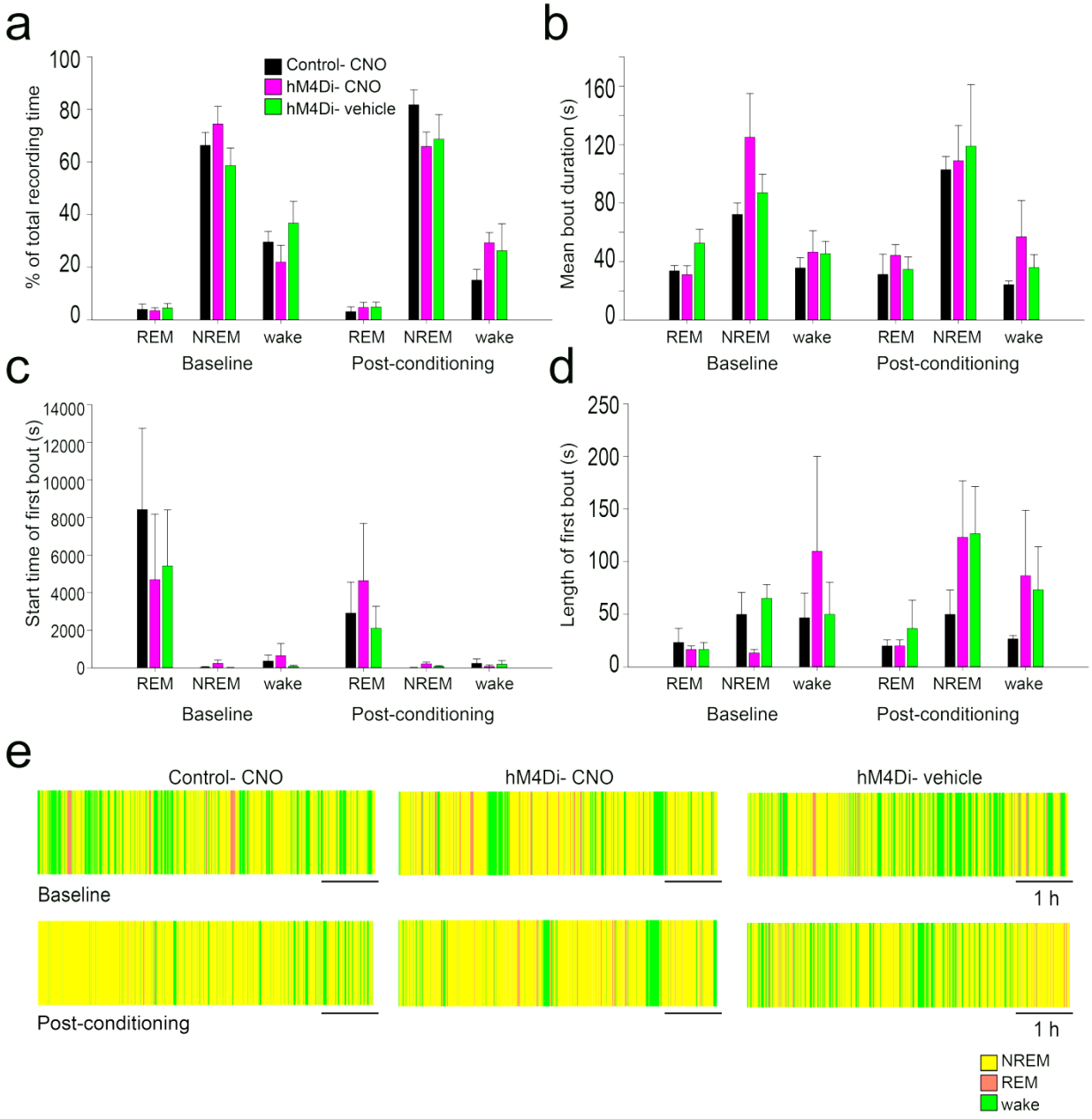

Supplemental Figure 4.6: Sleep architecture during pharmacogenetic experiments. There was no significant effect of treatment on either (**a**) percent of time spent in REM, NREM, and wake, (**b**) the mean duration of REM, NREM, and wake bouts, (**c**) time to onset of the initial bout of REM, NREM, and wake or (**d**) the length of initial bout of REM, NREM, and wake. All error bars are SEM. (**e**) Representative hypnograms for hours 0-6 at either baseline (***top***) or post-conditioning (***bottom***) for Control-CNO (***left***), hM4Di-CNO (***center***), and hM4Di- vehicle (***right***) animals.

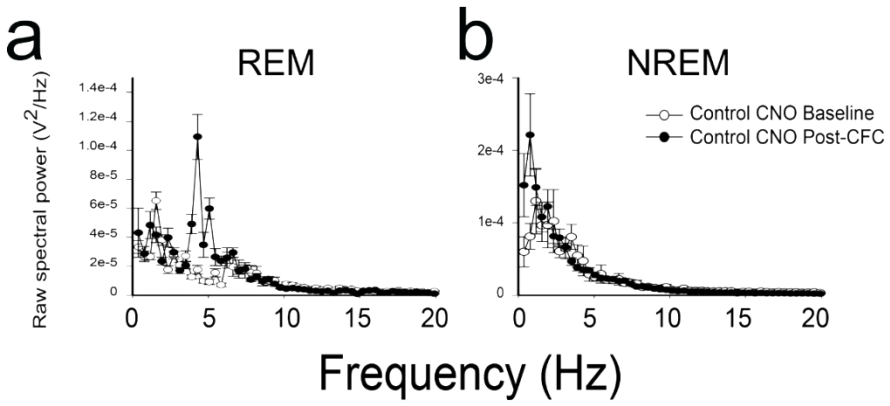

Supplemental Figure 4.7: CA1 LFP spectral power for mCherry-expressing mice. Raw CA1 LFP spectral power during the first 6 hours of recording at baseline (white circles) and post-CFC (black circles) for a representative *Pvalb-IRES-CRE* mouse expressing control (mCherry) virus during (**a**) REM and (**b**) NREM sleep (Mean ± SEM shown for local field potential values for all animals within treatment group hM4-vehicle, *n* = 74).

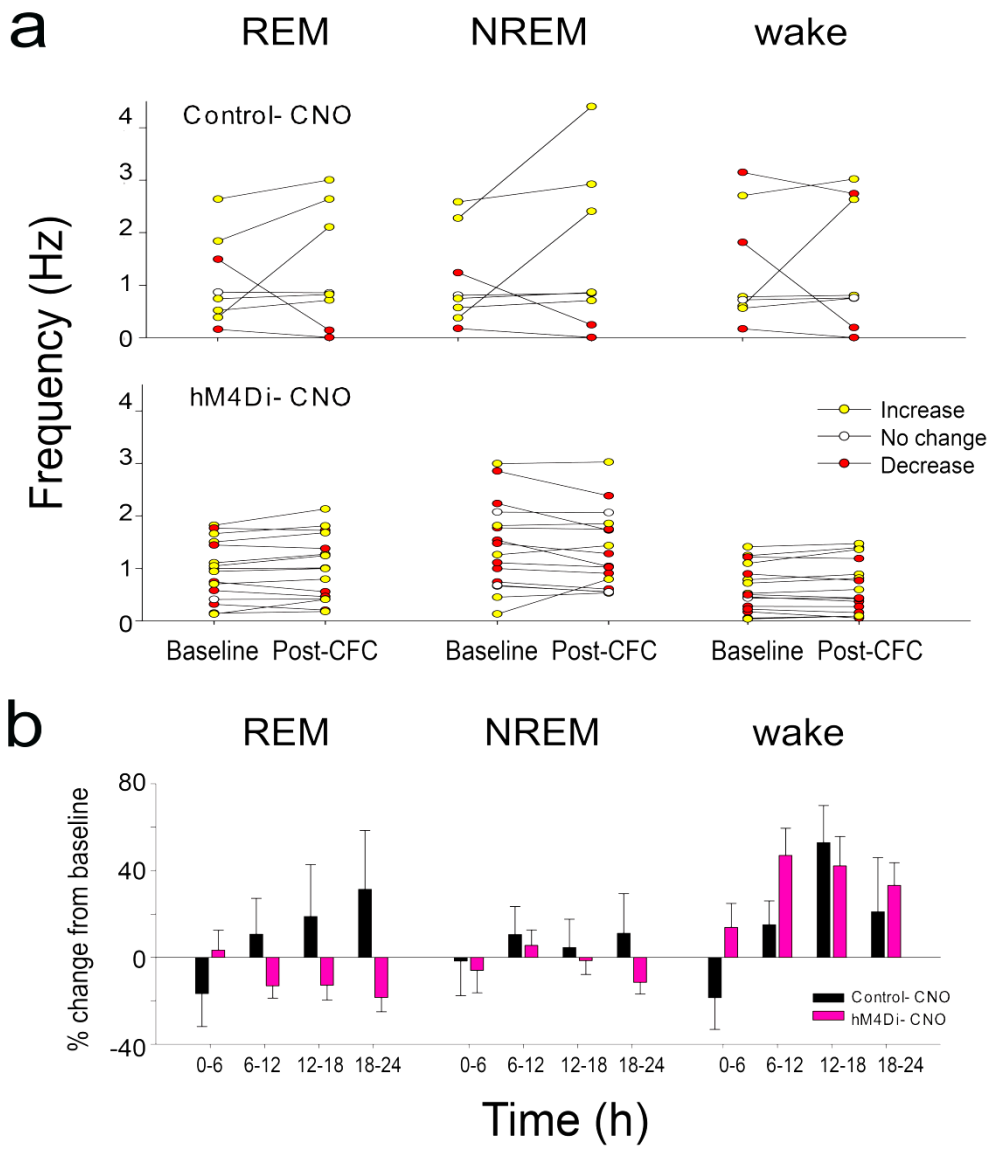

Supplemental Figure 4.8: CA1 firing rate changes following pharmacogenetic inhibition of PV+ interneurons. (**a**) Firing rate changes (in the first 6 h following CFC and CNO treatment) for all neurons stably recorded from a representative mouse in each treatment group (n = 8, Control- CNO; n = 15, hM4Di-CNO) . Increases and decreases in mean firing rate of ≥ 5% from the same period at baseline are shown in yellow and red, respectively. (**b**) In hM4Di-expressing mice, CNO did not significantly affect mean firing rates in the first 6 h following administration. In mCherry-expressing control mice, a gradual increase in REM firing rates was observed over the 24 hours following CFC. This change was blocked by post-CFC administration of CNO to hM4Di-expressing mice (virus x time interaction $p < 0.05$, two-way RM ANOVA). Post-CFC firing rates during NREM sleep and wake were unaffected following CNO administration (NREM - *N.S.*, two-way RM ANOVA; wake - main effect of time: $p < 0.001$; virus x time interaction *N.S.*, two-way RM ANOVA). Mean ± SEM shown for individual cell firing rate for all animals within treatment group. n = 27, Control-CNO; n = 35, hM4Di-CNO.

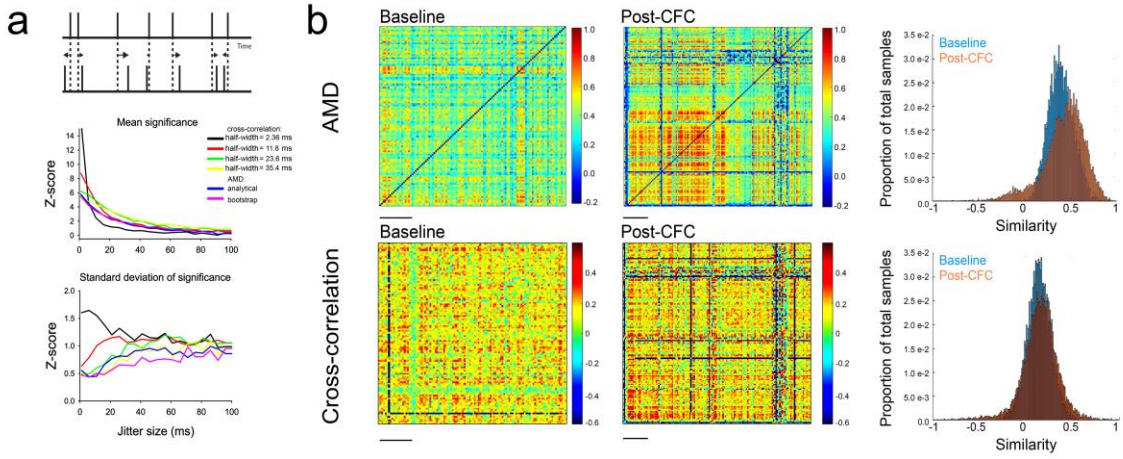

Supplemental Figure 4.9: Comparison of AMD-based and cross-correlation-based metrics for functional connectivity and stability analyses. (**a**) AMD and cross-correlation measures were compared for quantifying functional connectivity of two simulated spike trains. ***Top:*** The first 1-s, 30-spike train was generated randomly. The second train was generated by introducing jitter to the times of spikes from the first train. The amount of jitter was varied systematically between 1 and 100 ms, to determine how this variable (which should decrease with stronger functional connectivity) affects the two measures. ***Middle:*** Comparison of significance of functional connectivity measures for the two spike trains, across a range of jitter sizes. Cross-correlation significance between the two trains was calculated at 0 lag based on bootstrapping with 100 randomized spike trains, and Gaussian convolution of various half-widths. For comparison, AMD significance was calculated both analytically and using a similar bootstrapping technique (see **Methods**). ***Bottom:*** Standard deviation of functional connectivity significance values was estimated over 100 repetitions using randomized spike trains. Across a range of jitter sizes, AMD metrics provide a more reliable estimate of significance. (**b**) Comparison of AMD and cross-correlation for quantifying network stability using *in vivo* data. AMD-based FSMs (***top***; data reproduced from **Figure 4.7**) and cross-correlation-based FSMs (***bottom***) for the same network data recorded at baseline, and over the first 6 h post-CFC. Scale bar = 20 mins of recording time. Distributions of minute-to-minute similarity values showed a greater degree of change after CFC when AMD was used to calculate functional connectivity.

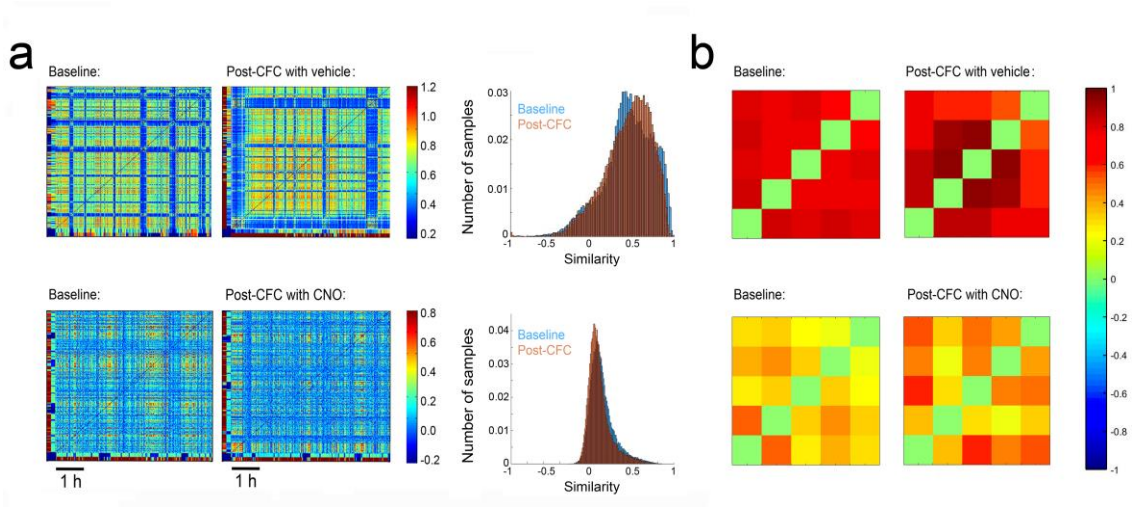

Supplemental Figure 4.10: FSMs for a representative mouse calculated across all behavioral states, and across only the longest intervals of NREM sleep. (**a**) ***Left:*** CA1 network FSMs across all behavioral states, for the same mouse shown in **Fig. 7** at baseline, and over the first 6 h post-CFC (vehicle and CNO conditions). Color bars along the outer edge of axes represents the behavioral state of the animal (blue - wake, red - NREM or REM, mixed sleep and wake are represented by color blends, *e.g.,* yellow) and inner axis color bars indicate the relative firing frequency (blue - low, red - high). ***Right:*** Distributions of minute-to-minute similarity values (at baseline, and following CFC) for the data shown in the FSMs. (**b**) CA1 network FSMs across the 5 longest bouts of NREM sleep in the 24 h following CFC.

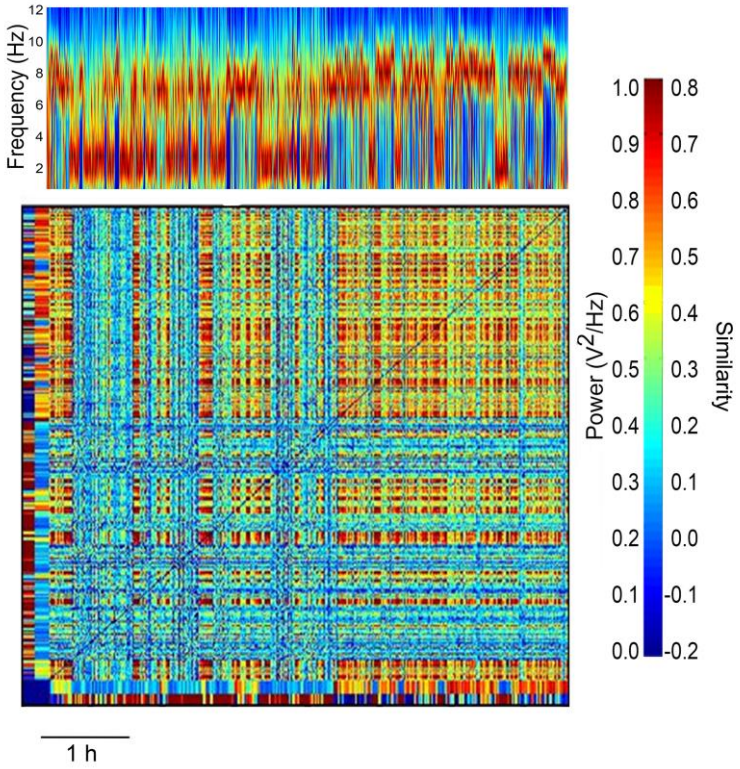

Supplemental Figure 4.11: Relationship between LFP spectral power and functional connectivity patterns in a representative mouse at baseline. Example of temporal relationships between CA1 LFP power (***top***) and FSM structure (***bottom***) over the same 6-h time period. Color in the body of the FSM denotes the degree of similarity between functional connectivity patterns at any given time point in the recording, and patterns at all other time points. Color bars along the outer edge of axes represents the behavioral state of the animal (blue - wake, red - NREM or REM, mixed sleep and wake are represented by color blends, *e.g.,* yellow) and inner axis color bars indicate the relative firing frequency (blue - low, red - high).

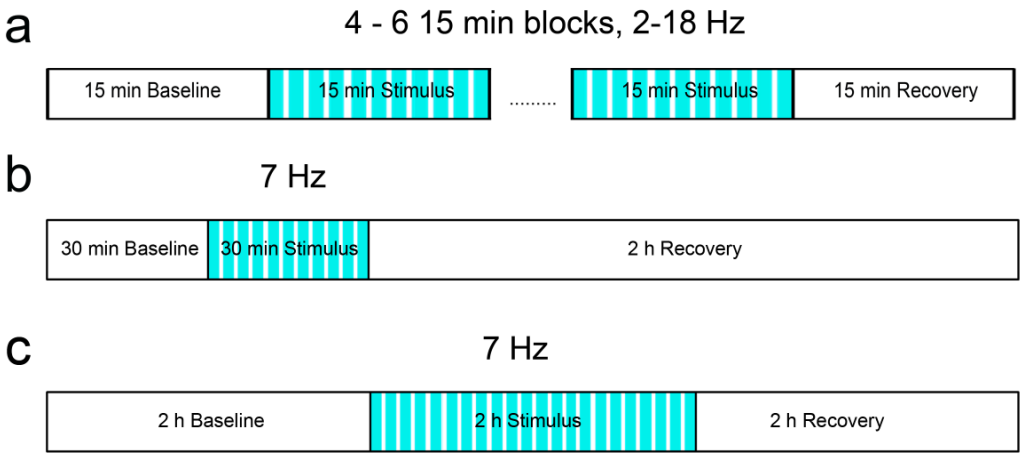

Supplemental Figure 4.12: Recording paradigms for optogenetic experiments. (**a**) PV+ interneurons in CA1 were stimulated at a range of frequencies in a random order (2-18 Hz, 40 ms pulses, 15 min for each frequency) for experiments described in **Fig. 8a-e**, and **Supplemental Fig.15a-b**. (**b**) CA1 neurons were recorded over a longer duration (30 min before and 2 h after 7 Hz stimulation) for experiments described in **Fig. 8f-h**, and **Supplemental Fig.15c-e**. (**c**) For experiments using non-anesthetized mice (**Supplemental Fig. 16**), CA1 neurons were recorded over a 2-h baseline, a 2-h period of 7 Hz stimulation, and a 2-h post-stimulation period.

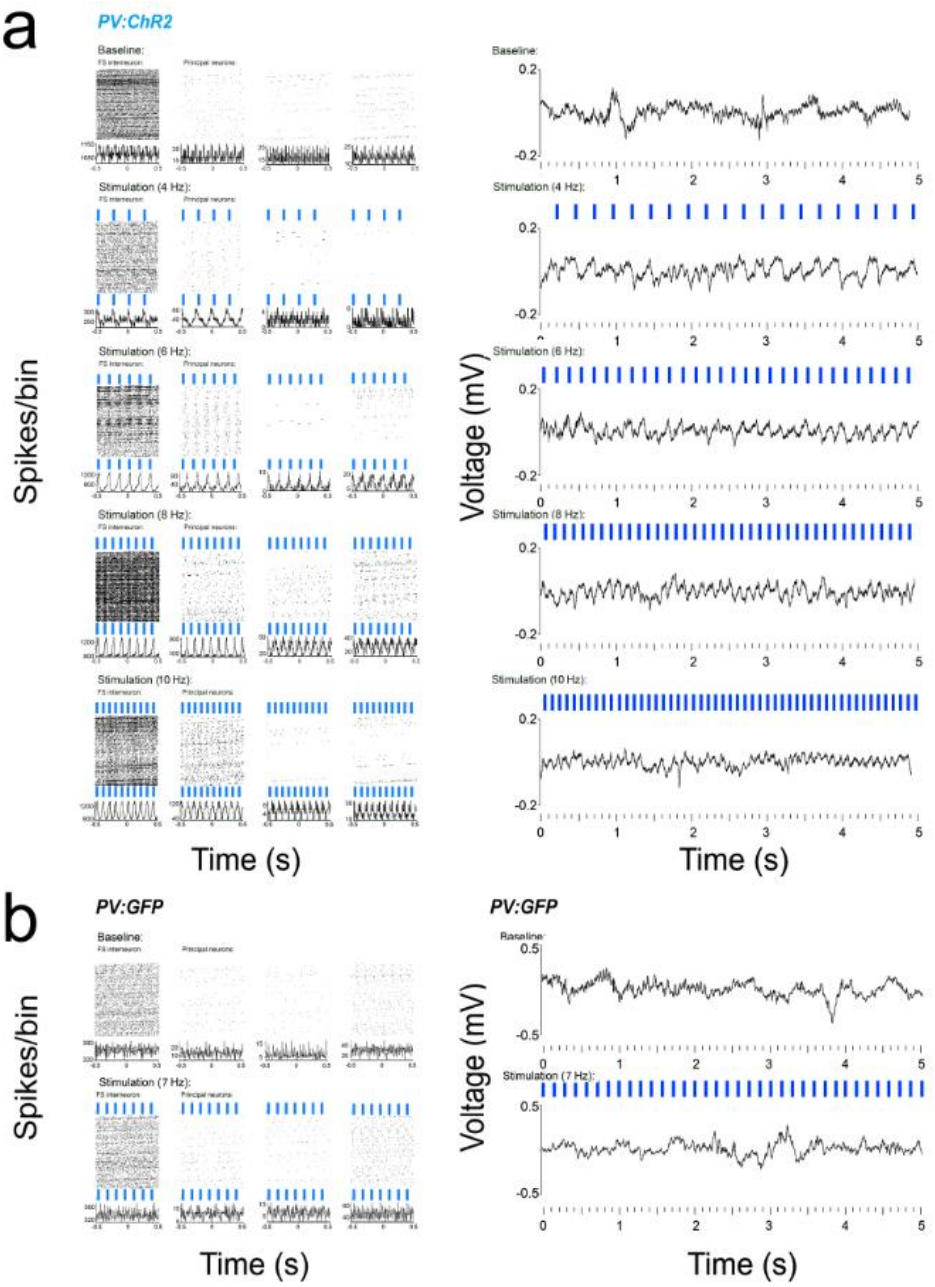

Supplemental Figure 4.13: Responses of CA1 neurons and LFPs across a range of optogenetic stimulation frequencies. (**a**) ***Left****:* Perievent firing rasters (top panels) and perievent firing histograms (bottom panels) for a representative CA1 FS interneuron and 3 neighboring principal neurons recorded from a *PV:ChR2* mouse, before and during rhythmic (4-10 Hz) stimulation of PV+ interneurons. ***Right****:* A representative 5-s LFP trace for one of the recording sites from in baseline and stimulation conditions. (**b**) ***Left****:* Perievent firing rasters (top panels) and perievent firing histograms (bottom panels) for a representative CA1 FS interneuron and 3 neighboring principal neurons recorded from a *PV:GFP* mouse, before and during rhythmic (7 Hz) stimulation of PV+ interneurons. ***Right****:* A representative 5-s LFP trace for one of the recording sites from in baseline and stimulation conditions.

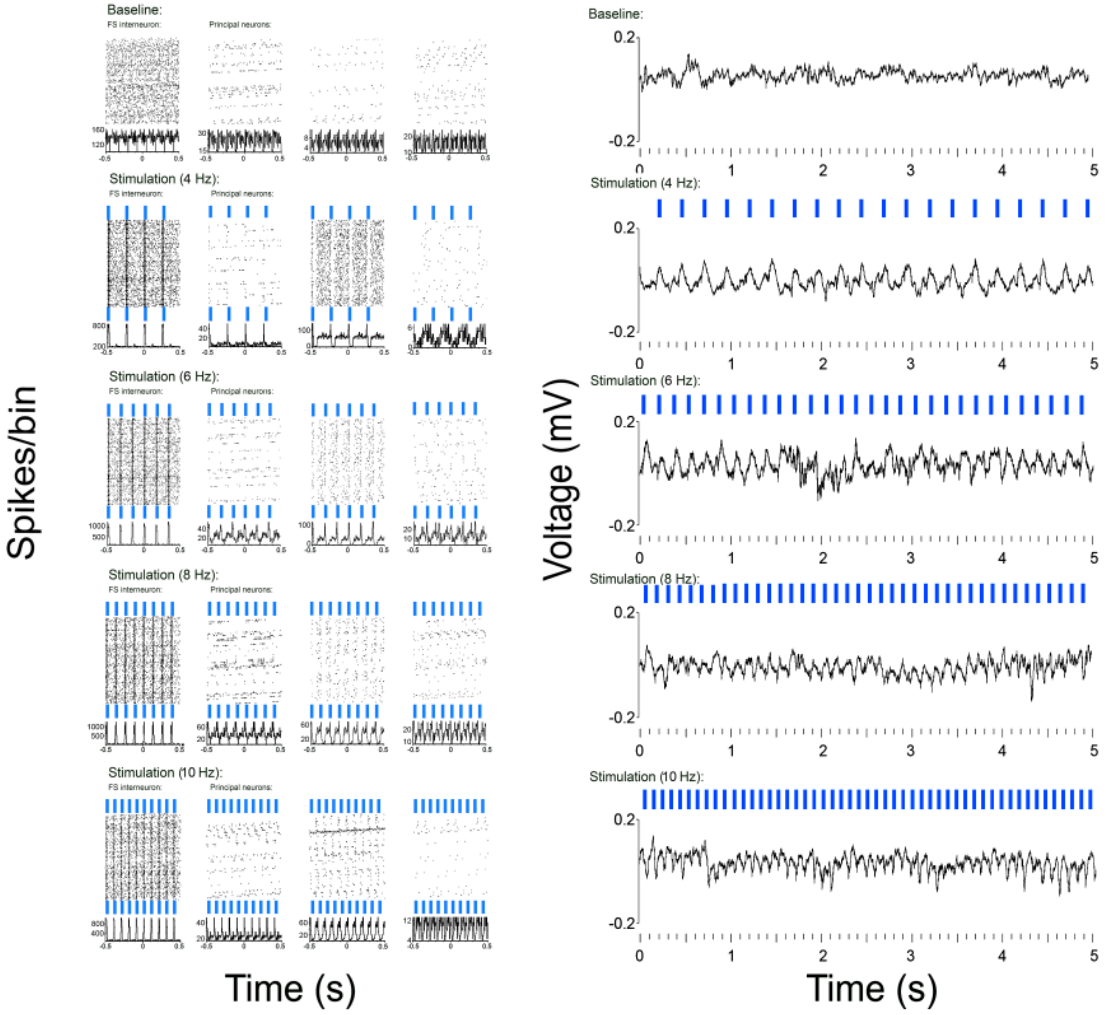

Supplemental Figure 4.14: Responses of CA1 neurons and LFPs across a range of optogenetic stimulation frequencies following viral transduction of PV+ interneurons with ChR2. ***Left****:* Perievent firing rasters (top panels) and perievent firing histograms (bottom panels) for a representative CA1 FS interneuron and 3 neighboring principal neurons recorded from a virally-transduced mouse, before and during rhythmic (4-10 Hz) stimulation of PV+ interneurons. ***Right****:* A representative 5-s LFP trace for one of the recording sites from in baseline and stimulation conditions.

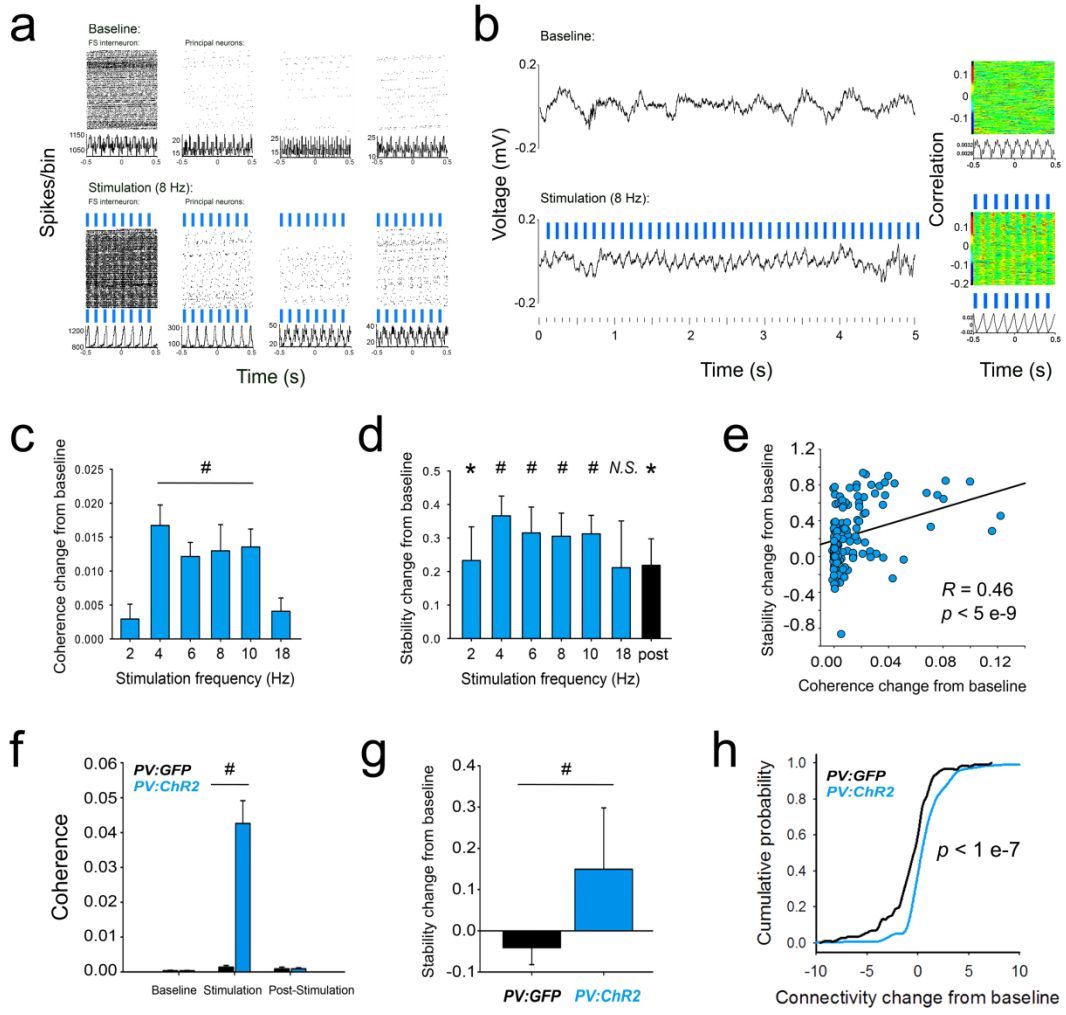

Supplemental Figure 4.15: Rhythmic optogenetic stimulation of PV+ interneurons increases CA1 network coherence, stability, and connection strength. (**a**) Perievent firing rasters (***top panels***) and perievent firing histograms (***bottom panels***) for a representative CA1 FS interneuron and 3 neighboring principal neurons recorded from a *PV:ChR2* transgenic mouse. Firing is shown over 250 s of recording before and during rhythmic (8 Hz) 473 nm light stimulation of PV+ interneurons. (**b**) A representative 5-s LFP trace (***left***) and perievent LFP raster (***right***) from (**a**) in baseline and stimulation conditions. (**c**) Changes in spike-field coherence (from baseline) induced by various frequencies of rhythmic PV+ interneuron stimulation. (**d**) Changes in neuronal functional connectivity stability (from baseline) induced by various frequencies of rhythmic PV+ interneuron stimulation. (**e**) Across 4-10 Hz stimulation frequencies, changes in spike-field coherence predicted changes in stability of functional connectivity for individual neurons (Spearmann rank order, n = 153 neurons). (**f**) Comparison of CA1 spike-field coherence across a 30-min baseline period, 30 min of 7 Hz stimulation, and 2 h or post-stimulation recovery, in *PV:ChR2* (blue) and *PV:GFP* (black) mice. (**g**) Following 7 Hz stimulation, CA1 neuronal functional connectivity in *PV:ChR2* mice showed an increase in stability relative to baseline. For **c-g**, * indicates $p < 0.05$ and # indicates $p < 0.001$, Wilcoxon signed rank test. (**h**) Neuronal functional connectivity strength also showed an increase in *PV:ChR2* mice relative to baseline. A similar change that was not seen in *PV:GFP* mice. p value indicates results of Kolmogorov-Smirnov test.

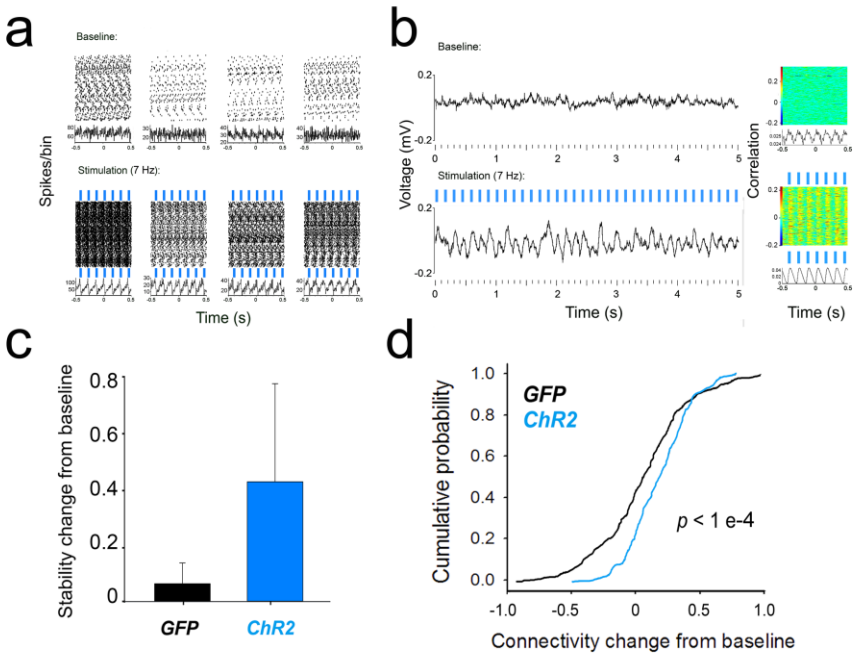

Supplemental Figure 4.16: Rhythmic optogenetic stimulation of ChR-2 expressing PV+ interneurons synchronizes firing and LFP rhythms in CA1 under non-anesthetized conditions. (**a**) Perievent firing rasters (***top panels***) and perievent firing histograms (***bottom panels***) for 4 representative CA1 principal neurons recorded from an awake, freely-behaving ChR2-transduced mouse. Firing is shown over 400 s of recording before and during rhythmic (7 Hz) 473 nm light stimulation of PV+ interneurons. (**b**) A representative 5-s LFP trace (***left***) and perievent LFP raster (***right***) for one of the recording sites from (**a**) in baseline and stimulation conditions. (**c**) Following a 2-h period of 7-Hz stimulation, CA1 neuronal functional connectivity in mice transduced with ChR2 showed a tendency for increased stability relative to baseline, which was not seen in GFP expressing mice (n = 3 mice/group, *N.S.*, Wilcoxon signed rank test. (**d**) Neuronal functional connectivity strength showed an increase in ChR2-transduced mice following 7 Hz stimulation, which was not seen in GFP-transduced mice. p value indicates results of Kolmogorov-Smirnov test, for n = 36 neurons (172 pairwise comparisons) recorded from ChR2-expressing mice, n = 32 neurons (144 pairwise comparisons) recorded from GFP-expressing mice.

CHAPTER V:

Parvalbumin-expressing interneurons are critical for NREM sleep oscillations that play a causal role in memory consolidation

5.1 Introduction

Sleep is thought to play a critical role in promoting various forms of learning and memory, and is also thought to regulate plasticity in brain circuits *in vivo*.[85,88,150] However, the mechanisms underlying this relationship are poorly understood. Sleep controls many aspects of brain physiology, including neuronal and network activity, neurotransmitter and neuromodulator release, interstitial flow and ionic composition, gene transcription, and protein translation. [16,25,27,38,40,48,86–88,92,159,160] Numerous studies have pointed to sleep-associated network oscillations as a potential driver of synaptic plasticity during memory consolidation. For example, hippocampal oscillations occurring in either rapid eye movement (REM) and non-REM (NREM) sleep have been proposed to play a role in contextual and spatial memory formation, possibly due to the role of these oscillations in patterning ensemble activity. [33,81,153] A significant body of evidence has led to the hypothesis that offline-reactivation of specific populations of hippocampal

neurons, coordinated by network oscillations, could drive long term memory formation.[80,129,134,136]

Recently, studies have targeted specific oscillations as a mechanism for sleep-dependent memory consolidation. For example, disrupting hippocampal input from the medial septum during post-learning REM sleep (leading to disrupted theta [4-12 Hz] activity) was shown to disrupt memory formation. [153] This is not surprising, as theta-frequency stimulation of these inputs after learning improves memory consolidation, and theta burst stimulation of inputs to CA1 can cause LTP of synaptic transmission.[40,161] We have previously shown that parvalbumin-expressing (PV+) interneurons coordinate naturally-occurring increases in CA1 oscillations (including delta (0.5-4Hz), theta, and ripples (150-200 Hz) in both NREM and REM sleep following single-trial contextual fear conditioning . [45,68]Critically, ripple oscillations have also been implicated in memory consolidation; targeted disruption of these oscillations (via direct stimulation of the hippocampus) following training sessions slows the pace of learning. [33]. However, because these oscillations occur together across periods of sleep, and because behavioral sleep deprivation (SD) disrupts all sleep oscillations, we are still far from understanding which aspects of sleep are sufficient for sleep's benefits for memory consolidation. [17,84,162] Moreover, relatively little is known about how hippocampal network dynamics in the hours immediately following learning drive the longer-term processes of consolidation (which can last days to weeks). Here we employ state-targeted optogenetic inhibition of CA1 PV+ interneuron activity in CA1 following CFC, to determine in whether REM or NREM-associated network oscillations are required for consolidation of contextual fear memory (CFM). We also test whether rhythmic

activation of the hippocampal network is sufficient to overcome CFM consolidation deficits caused by SD. Finally, we characterize how state-associated hippocampal rhythms in the hours immediately following CFC drive subsequent changes in CA1 network dynamics that may drive memory formation.

5.2 Methods

5.2.1 Mouse handling and surgical procedures

All animal husbandry and surgical/experimental procedures were approved by the University of Michigan IACUC. With the exception of conditioning and fear memory testing, mice were individually housed in standard caging with beneficial environmental enrichment (nesting material and novel foods) throughout all experimental procedures. Lights were maintained on a 12 h:12 h light: dark cycle (lights on at 8 AM), and food and water were provided *ad lib*. C57BL/6J mice (Jackson) were implanted with custom-built, driveable head stages with two bundles of stereotrodes for single unit/local field potential (LFP) recording and EMG wires for nuchal muscle electromyographic recording, as previously described. [45] The two stereotrode bundles were spaced approximately 1.0 mm apart within right-hemisphere CA1 (relative to Bregma: 1.75-2.75 mm posterior, 1.5-2.5 mm lateral, and 1.0 mm ventral). CA1 recording sites for these experiments are shown in **Supplemental Figure 5.1**.

Two groups of mice were used to assess the effects of optogenetic manipulation of PV+ interneurons. For experiments shown in **Figures 5.2** - **5.5,** *Pvalb-IRES-CRE* mice were crossed to either B6.Cg-*Gt(ROSA)26Sor*$^{tm40.1(CAG\text{-}aop3/EGFP)Hze}$/J, *B6;129S-Gt(ROSA)26Sor*$^{tm32(CAG\text{-}COP4*H134R/EYFP)Hze}$*/J,* or *B6.Cg-Gt(ROSA)26Sor*$^{tm6(CAG\text{-}}$

ZsGreen1)Hze/J transgenic mice (Jackson) to express Arch (*PV:Arch*), ChR2 (*PV:ChR2*) or eGFP (*PV:GFP*), respectively, in a CRE-dependent manner in PV+ interneurons. At age 2–5 months, male *PV:Arch* (n=14) *PV:ChR2* (*n* = 7) and *PV:GFP* (*n* = 13) mice were) were implanted with custom-built, driveable head stages as described above. [45] The two stereotrode bundles were spaced approximately 4.0 mm apart with a bundle in both right and left hemisphere CA1 (relative to Bregma: 1.75-2.75 mm posterior, 1.5-2.5 mm lateral, and 1.0 mm ventral). An optical fiber was placed adjacent to each bundle in the recording array for delivery of laser light. CA1 recording sites for these experiments are shown in **Supplementary Figures 5.4** a**nd 5.11**

5.2.2 Recording procedures

Mice were prepared for chronic stereotrode recording 1 week after implantation surgery as previously described. [45] Briefly, electrodes were lowered into the hippocampus in 30 μm steps until stable recordings were achieved, with the same waveforms continuously present on recording channels for at least 24 h, after which baseline recording began (starting at lights-on). Neuronal spike and LFP signals were acquired by differentially filtering data from each electrode wire (bandpass 300 Hz-8 KHz and 0.5-300 Hz, respectively); these data were digitized and amplified using Plexon Omniplex hardware and software as described previously. [45]

5.2.3 Contextual fear conditioning (CFC) and sleep deprivation (SD)

Following 24-h baseline recording (and within 1 h of lights-on), mice underwent single-trial CFC as previously described. [45] For these experiments, mice were either

allowed *ad lib* sleep (CFC, *n* = 5), or were sleep deprived by gentle handling, for the first six hours following training (a manipulation which is sufficient to disrupt contextual fear memory consolidation; Sleep Dep, *n* = 5). [44,128] All mice were allowed *ad lib* sleep for the remainder of the recording. At lights on, 24-h following training, mice were returned to the conditioning chamber for a 5-min assessment of contextual fear memory (CFM). This was calculated as the change in context-specific freezing between testing and training trials (i.e., % time spent freezing at test - % time spent freezing at baseline [pre-shock]). *Post hoc* scoring of videos for freezing behavior was conducted by an observer blind to treatment. Behavior was scored as freezing in the following conditions: crouched posture with an absence of all body movement save respiration (including an absence of head and whisker movement).

5.2.4 Optogenetic inhibition of PV+ interneurons

For experiments shown in **Figure 5.2 & 5.6,** *PV:Arch* and *PV:GFP* transgenic mice underwent post-CFC, state-targeted light delivery to the dorsal hippocampus. Following baseline recording, underwent CFC as described above. During the first six hours following CFC, mice received 532nm laser (Laserglow) light delivery for inhibition of PV+ CA1 interneurons during bouts of NREM, REM, or wake. For state targeting, data from LFPs, EMGs, and live video recording were used to determine the animal's state in real time. Experimenter observed live recordings and used a trigger to turn on laser when mouse entered target state. Percent of target state covered is shown in **Supplemental Figure 5.5c** and total percentage of state covered did not affect behavioral response. **(Supplemental Figure 5.5e)** Additional analysis calculating changes within laser on and off state are currently underway and data will be presented

as such in manuscript preparation. After this period of inhibition was over, mice were allowed to sleep *ad lib* for the next 18 h until CFC testing. *Post hoc* analysis of laser targeting efficiency was calculated as the percent of laser that was properly targeted to the given state, and the percent of the given state that received laser coverage. (**Supplemental Figure 5.5)** Power output at the fiber tip was estimated at 3-10 mW for all experiments.

5.2.5 Optogenetic stimulation of PV+ interneurons

Two groups of mice were used to assess the effects of rhythmic stimulation of PV+ interneurons. For experiments shown in **Figure 5.3-5.6,** *PV:ChR2* or *PV:GFP* transgenic mice were recorded from and underwent CFC as described above. CA1 neurons were recorded over a 24-h baseline period. After CFC at lights-one, these mice underwent 6 h of SD by gentle handling, while PV+ interneurons were rhythmically stimulated by delivery of 10 ms pulses of 473nm (Crystal Laser) laser light at 7 Hz. During this time, and for the next 18 h of *ad lib* sleep prior to CFM testing, neuronal activity continued to be recorded.

Following all optogenetic experiments, mice were perfused and brains were processed for histological assessment as described above. Optic fiber and electrode position were validated prior to data analysis.

5.2.6 Single-neuron discrimination and firing analysis

Single-neuron data were discriminated offline using standard principle-component based procedures (Offline Sorter; Plexon). Individual neurons were discriminated on the basis of spike waveform, relative spike amplitude on the two

stereotrode recording wires, relative positioning of spike waveform clusters in three-dimensional principal component space, and neuronal subclass as previously described. [68] Only those neurons that were reliably discriminated and continuously recorded throughout each experiment (*i.e.*, those stably recorded across both 24-h baseline and 24-h post-CFC recording) were included in firing rate analyses from behaving mice. Post-CFC firing rate changes were calculated over 6-h windows for each neuron in NREM, REM, and wake as a percent change from baseline, as described previously. [45]

5.2.7 Sleep/wake behavior and LFP analyses

Intrahippocampal LFP and nuchal EMG signals were used to categorize each 10-s interval of recording as REM, NREM, or wake using custom software as previously described. [45] The proportion of time spent in REM, NREM, and wake (and mean bout duration for each state) was calculated during the baseline and post-CFC recording periods for each mouse using standard conventions.

Raw LFP power (0-300 Hz, in 0.4 Hz bands) was calculated on each channel where stable neuronal spike data was obtained and spectral power was quantified from raw LFP traces as previously described. These values were summed across frequency bands for recording site at delta (0.5–4 Hz) and theta (4–12 Hz). Ripples were quantified within NREM sleep in both 2-h and 6-h windows. Briefly, LFPs were band-pass filtered (150-250 Hz) and ripple events were automatically detected using a threshold of 6 or more consecutive cycles of an oscillation with a voltage $\pm 2.0 < x < 3.5$ SD from baseline signal mean. Using these criteria, baseline ripple frequency during

NREM sleep was 0.1-0.5 Hz, consistent with previous reports.[21,33,151] To compare ripple occurrence between baseline and post-CFC recording periods, ripples were detected across both recording intervals using the same voltage threshold. Spectral power was calculated within detected ripple intervals at baseline and post-CFC; changes in power were calculated as described above for comparisons of ripple amplitude between groups.

Spectrograms of 0-12 Hz PSD activity were generated in MATLAB. PSD data for representative LFPs were calculated in 1-s windows, and PSDs were convolved over 30 seconds at 1 Hz. PSDs were normalized over the entirety of the selected temporal window and expressed as V^2/Hz.

5.2.8 Functional connectivity and functional network stability (FuNS) analysis

Functional connectivity in CA1 was calculated for all experiments using spike trains {$S_1, S_2, \ldots, S_n$} for n stably recorded CA1 neurons as previously described. Using the average mean distance (AMD) between spikes in respective neurons in a given neuron pair. [68,97] Pairwise functional connectivity across the network was quantified as a functional connectivity matrix. [68] Matrices were generated for adjacent 1-min time windows across baseline and post-CFC recording periods, both across and within NREM, REM, and wake states, the similarity between connectivity matrices in adjacent windows were compared across the entire recording – mean similarity values were quantified as a metric of Functional Network Stability (FuNS).

To quantify how the strength of functional connectivity changed between neurons before vs. after a period of state-specific inhibition or rhythmic stimulation, we calculated

the differences between corresponding elements of the functional connectivity matrix, using an AMD metric described previously. [68] We then quantified the effects of optogenetic manipulations on connection strength for each pair of neurons as a change from baseline.

5.3 Results

5.3.1 Post-CFC sleep is necessary for stability increases facilitating consolidation

To better understand the network dynamics associated with post-learning sleep, we first recorded CA1 network activity from C57L/6J mice after CFC which was followed by either sleep or 6 h of SD **(Figure 5.1a**). Sleep deprived animals predictably have a significant disruption of contextual fear memory (CFM) consolidation, assessed behaviorally 24 h after CFC **(Figure 5.1b and Supplemental Figure 5.2)** Consolidation in sleeping animals was associated with increases in firing rate immediately following CFC and for at least 12 h afterward; these increases were not seen in SD animals, even after recovery sleep. **(Figure 5.1c)** We then measured how functional network stability (FuNS) changes after post-CFC sleep or SD. We did this by quantifying pairwise spike timing relationships on a minute-by-minute basis over the entire pre- and post-training intervals. We observed an increase in FuNS (relative to baseline) across the 24-h period between CFC and CFM assessment, which was most pronounced when comparing network dynamics in NREM. **(Figure 5.1d)** As previously described (Chapter 3) NREM-specific FuNS increases for individual mice predicted their behavioral performance during CFM assessment **(Figure 5.1e)**

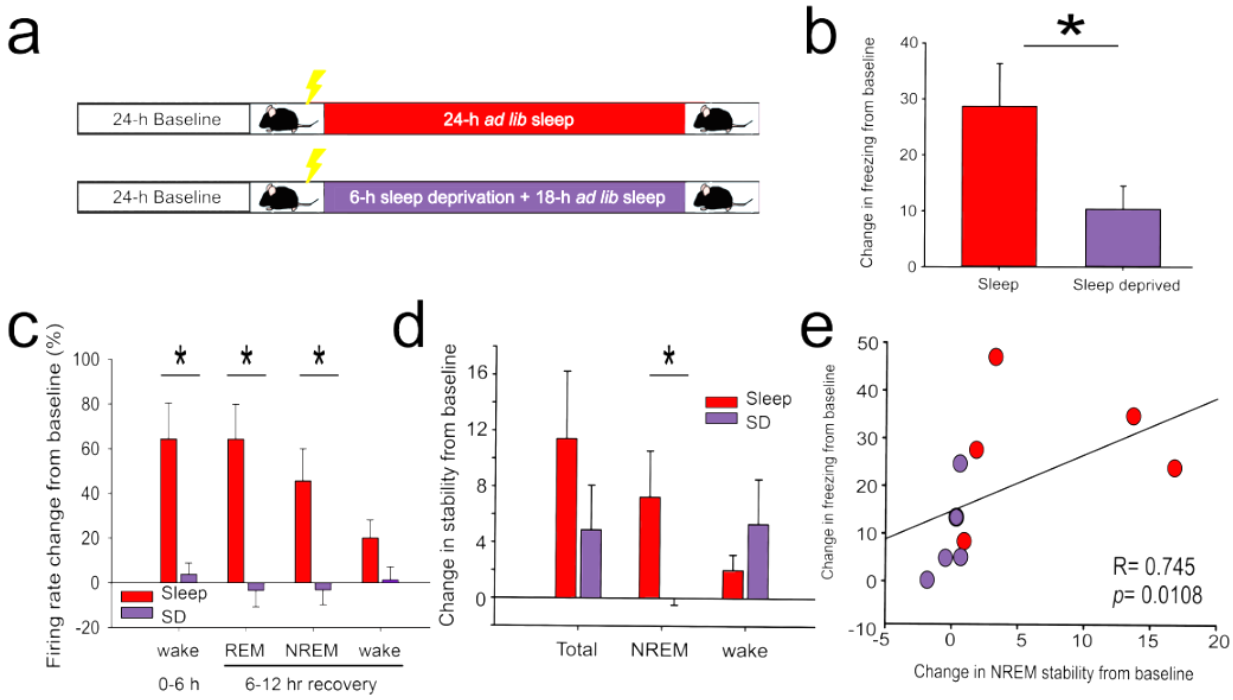

Figure 5.1: Post-CFC sleep is necessary for stability increases facilitating consolidation. (a) Experimental paradigm; Following a 24-h baseline recording in their home cage, C57B/J6 mice were placed into novel chamber for single-trial CFC. Following training, a subset of mice (n=5) were returned to their home cage and allowed to *ad lib* sleep for 24-h. Another set (n=5) was gently handled inducing sleep deprivation (SD)for 6 h-h post-CFC and then allowed to ad lib sleep for 18-h. **(b)** Context-specific freezing was assessed after 24-h. CFM is reduced in SD animals. * indicates p=0.045, student's t-test. **(c)** Post-CFC firing rates for individual neurons were expressed as a % change from corresponding period in baseline. * indicates p<0.004 Holm-Sidak *post hoc* test for baseline vs. post-CFC comparisons. **(d)** Changes in mean network stability (from baseline to post-CFC) show loss of stability in SD animals during recovery NREM sleep, but not during wakefulness or when averaged across all states. * indicates p=0.05 Holm-Sidak *post hoc* test. **(e)** Post-training changes in SWS FuNS vs. observed changes in freezing behavior for individual mice; R2= 0.58, p < 0.005 Pearson correlation.

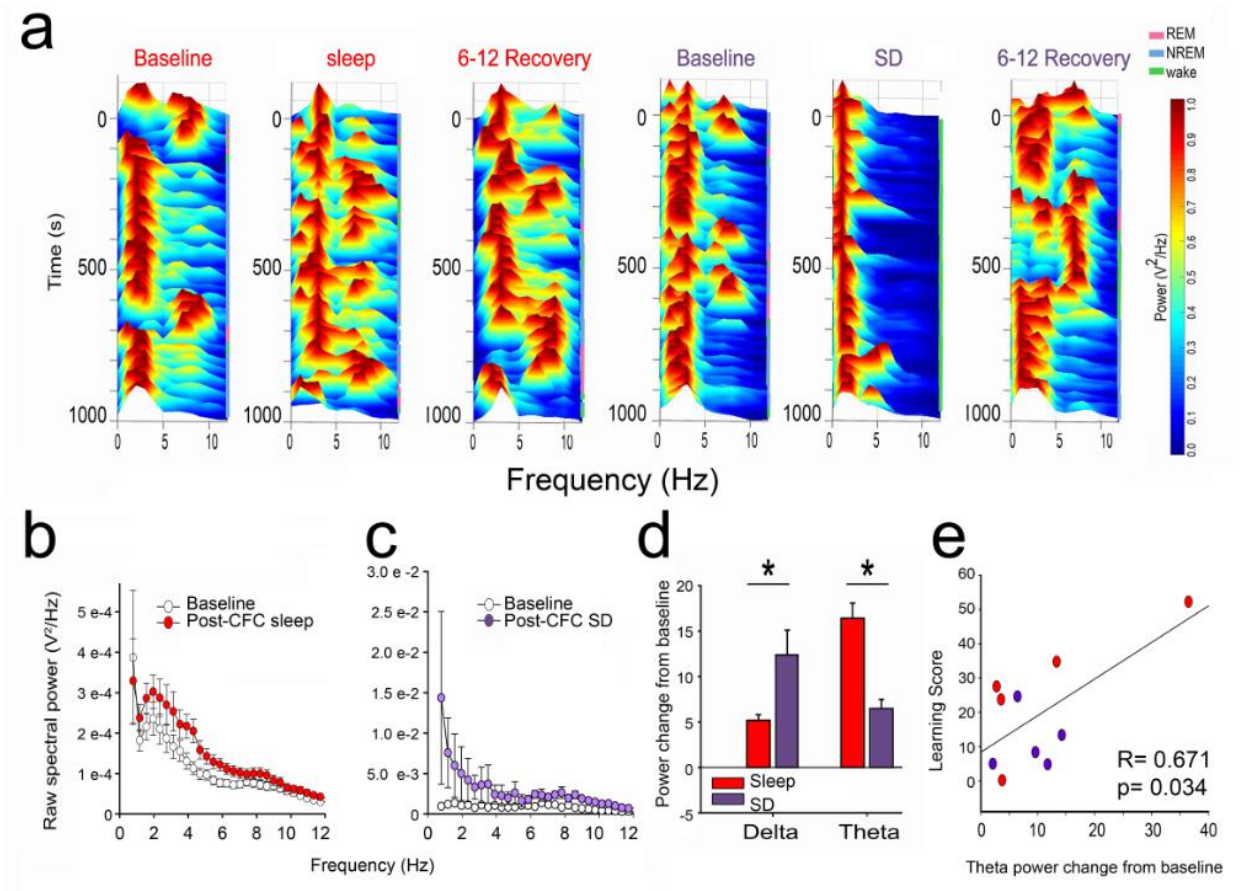

Figure 5.2: Post-CFC theta increases are predictive of consolidation. (a) Representative LFP spectralgrams showing power in delta and theta bands across 1000 seconds of baseline, 0-6 h post-CFC (sleep or SD), and hours 6-12 post-CFC (recovery) time (matched for time of day). Sleeping controls showed increased spectral power during NREM and REM states (colored denotation on right) in delta and theta, respectively which was not observed in SD animals, but were recovered in 6-12 h sleep. **(b-c)** Raw CA1 LFP spectral power across 0-6 h baseline (white circles) and post-CFC (red and purple) for a representative mouse for each treatment **(d)** Post-CFC increases in theta spectral power are seen in sleeping animals, but suppressed in SD. * indicates p,0.001 Holm-Sidak *post hoc* test **(e)** Post-CFC increases in theta are correlated with subsequent CFM consolidation, p= Spearman rank order.

Consolidation of CFM was also associated with changes in CA1 network oscillations. During post-CFC sleep, there were significant increases in delta and theta oscillation during NREM and REM sleep. The latter (increased theta) was disrupted by SD. **(Figure 5.2a-d)** The former (increased delta power) during SD is consistent with homeostatic changes that have previously been reported. [119] Theta power over the first 6 h (across all states) predicted an individual animal's behavioral performance 24 h after CFC **(Figure 5.2e)** Critically, SD led to reduced CA1 oscillations in the 6 h after deprivation ended (i.e., hours 6-12 post-CFC), suggesting that events occurring during sleep in the first 6 h post-CFC may have long-lasting effects on the CA1 network. **(Supplemental Figure 5.3)**

5.3.2 NREM sleep-targeted inhibition of PV+ interneurons disrupts NREM oscillatory activity, REM theta oscillations, and CFM consolidation

We have previously found that PV+ interneurons mediate post-CFC increases in delta, theta, and SPWR frequency activity. To assess the role of state-specific PV+ interneuron activity in CFM consolidation, we inhibited the dorsal CA1 PV+ population optogenetically, during bouts of NREM, REM, or wake. Light was targeted to CA1 bilaterally in mice expressing Archaerhodopsin or GFP in PV+ interneurons (*PV:Arch* and control respectively) in the first 6 h post-CFC. **(Figure 5.3a-b and Supplemental Figure 5.4)** We found that disruption of PV+ interneuron activity during NREM, but not REM or wake, interfered with CFM consolidation. **(Figure 5.3c)** This effect was not mediated by changes in sleep architecture, which was the same across treatment. To determine how state-targeted inhibition of PV+ interneurons affected CA1 network activity, we first characterized changes in CA1 LFP activity in the first 6 h following CFC.

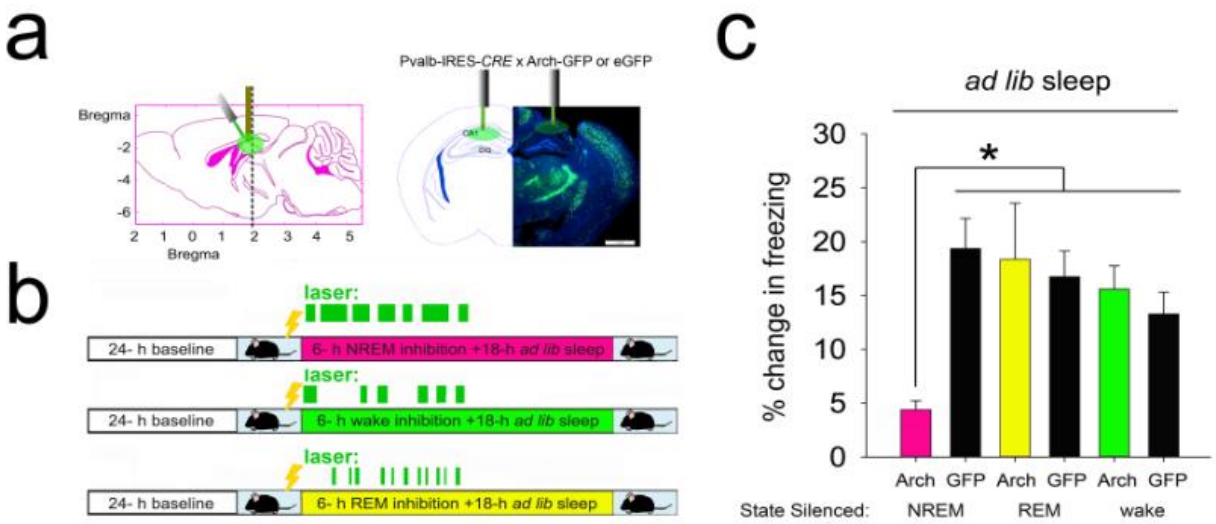

Figure 5.3: PV+ interneuron activity during NREM sleep, but not wake or REM, is critical for CFM. **(a)** Experimental design: Sagittal view (left) of stereotrode and optic fiber placement. Coronal view with PV:eGFP labeled neurons. **(b)** Experimental paradigm: *PV::Arch* or *PV::Control* mice following 24-h of baseline underwent CFC in a novel context. Following training, animals were optogenetically inhibited during NREM sleep, REM sleep, and wakefulness. For 6-h and were then allowed to ad lib sleep. CFM was asses 24 hours after CFC. **(c)** PV+ interneuron activity is necessary during NREM sleep, but not REM or wakefulness. * indicates p=0.008 Holm-Sidak *post hoc* test.

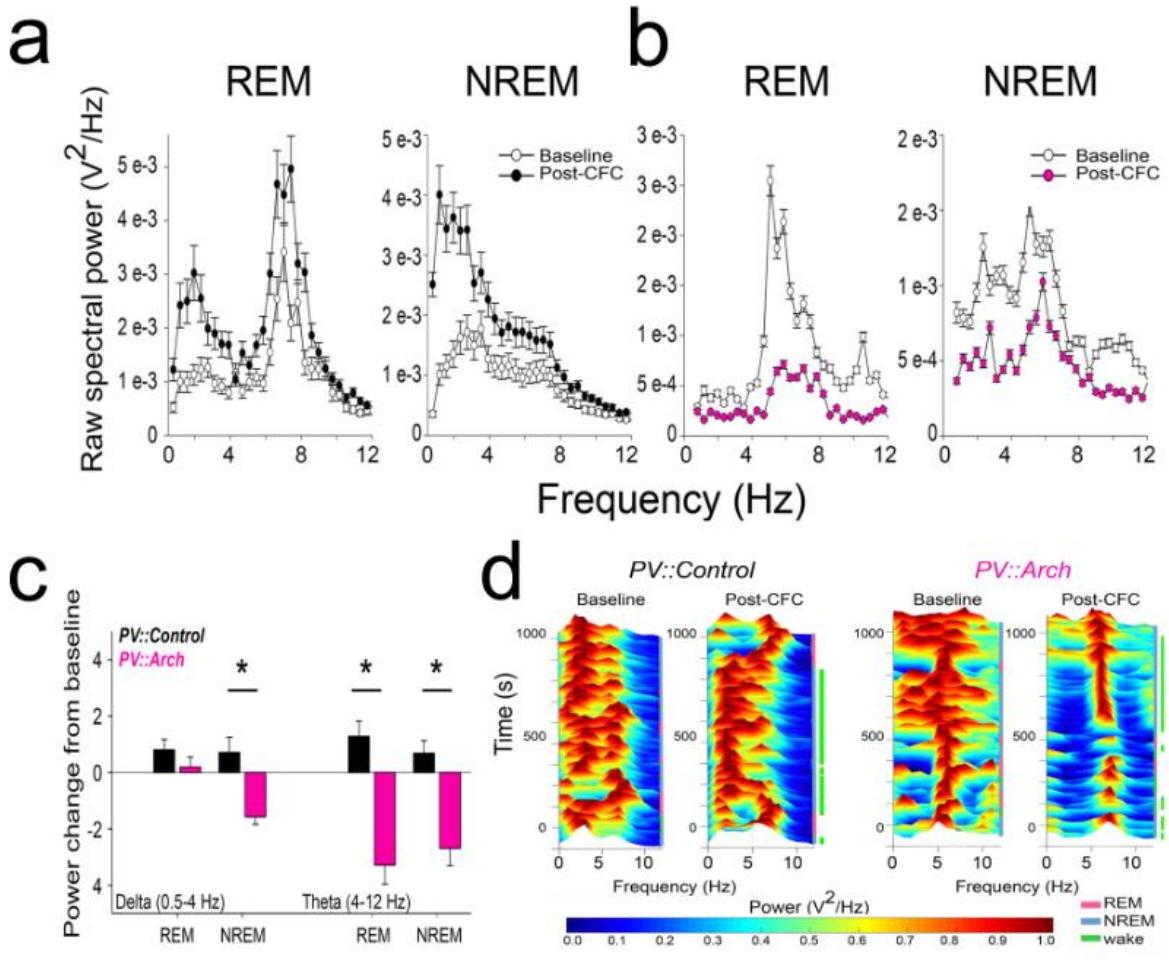

Figure 5.4: PV+ interneurons during NREM sleep are critical for delta and theta oscillatory increases following learning. (a) Raw CA1 LFP spectral power across 0-6 h baseline (white circles) and post-CFC (black) for representative control animal and **(b)** Arch-expressing animal (white at baseline, pink for post-CFC during REM and NREM sleep. (Mean ± SEM shown for all LFPs for each animal n=20 for control, n=26 for Arch) **(c)** Post-CFC increases in theta power in control animals during REM and NREM were suppressed in animals expressing Arch. Additionally, delta power during NREM sleep was decreased in Arch animals. * indicates P<0.001, Pairwise multi-comparison Holm-Sidak *post hoc* test. (Mean ± SEM shown for all LFPs for each treatment n=103 for control, n=130 for Arch) **(d)** Representative LFP spectralgrams showing spectra power in delta and theta bands across 1000 seconds during 0-6 h recording time at baseline and post-CFC (matched for time of day). Control mice showed increased spectral power during NREM and REM states (colored denotation on right) in delta and theta, respectively. There was a striking suppression of delta power and modest theta decreases in Arch-expressing animals.

NREM and REM LFP power spectra are shown for representative *PV:Arch* and control mice in **Figure 5.4a-b** (see also **Supplemental Figure 5.6a-c**). In control mice, CA1 spectral power in delta and theta frequency bands increased dramatically during post-CFC NREM and REM **(Figure 5.4c,** see additionally; **Supplemental Figure 5.6 and 5.8**). These changes in spectral power were evident in data averaged across states (although they tended to wax and wane across bouts of sleep, specifically during NREM sleep; **Figure 5.4d**), and persisted until later in the day. **(Supplemental Figure 5.7)** These increases in network oscillations were blocked both during, and after, NREM-targeted inhibition of PV+ interneurons (**Figure 5.4c,** see additionally; **Supplemental Figure 5.7)**. control mice also exhibited increases in firing rate that lasted for several hours after CFC; no such increases were seen in *PV:Arch* with NREM-targeted inhibition. This suggests that PV+ interneurons amplify NREM sleep-associated CA1 network oscillations, leading to long-lasting changes in the network.

Sharp-wave ripples (SPWRs) during post-learning NREM sleep have been hypothesized to promote memory consolidation.[34,39,163] Because PV+ interneurons are implicated in generation of CA1 SPWRs, we assessed the effects of NREM-targeted PV+ interneuron inhibition on SPWRs in the hours following CFC [26–28]. In control mice, the power of ripple oscillations (but not occurrence of ripples, see **Supplemental Figure 5.9**) increased significantly over the first 6 hours of post-CFC NREM sleep. **(Figure 5.5a-c)** This change in power (and changes in delta power) in NREM correlated with changes in theta oscillations during subsequent REM sleep **(Figure 5.5d-f)**. Both increases in ripples, and the association with REM theta were blocked by NREM-targeted PV+ interneuron inhibition (**Figure 5.5a-c, g-i**). Together, these data

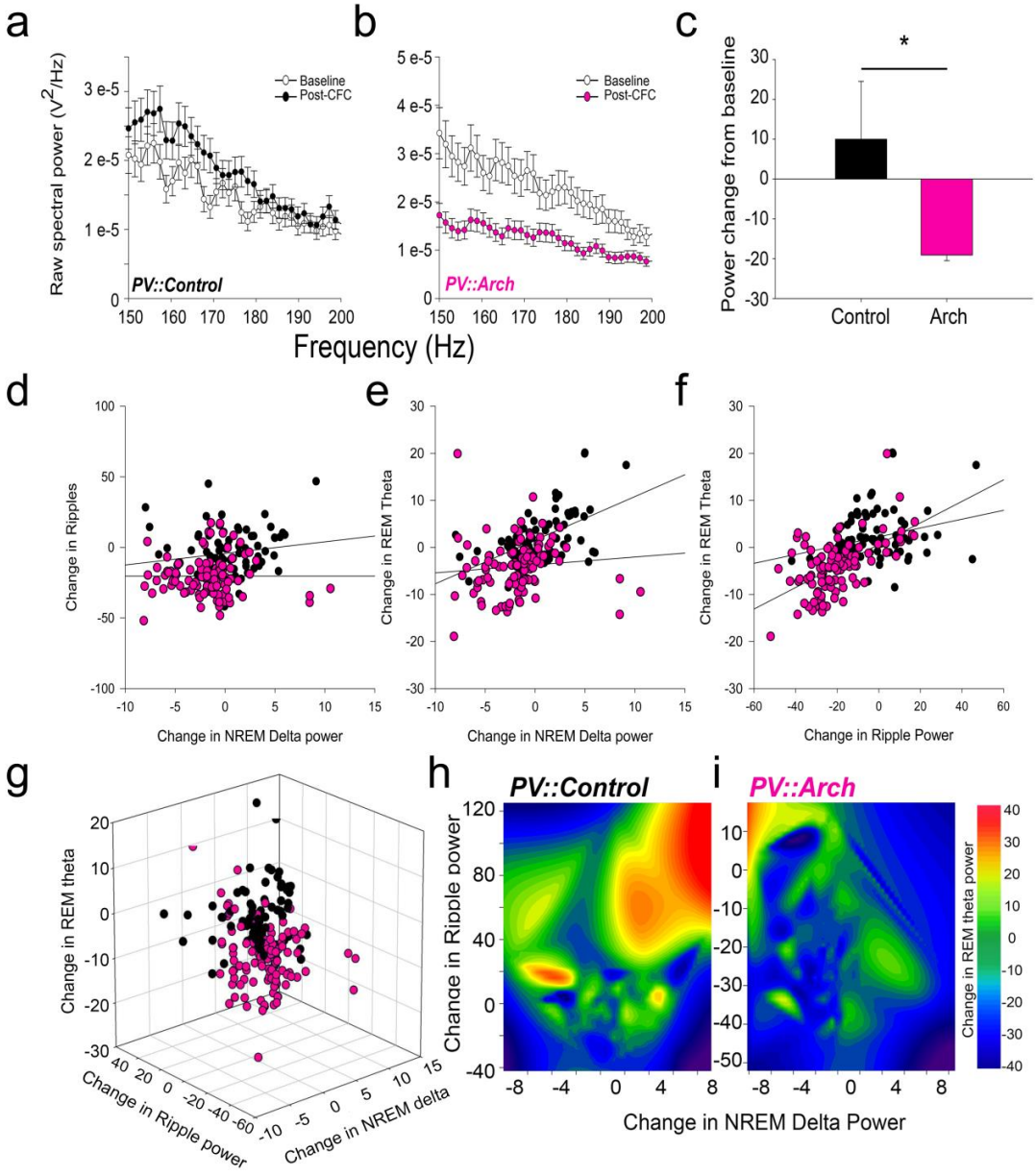

Figure 5.5: Inhibition of PV+ interneurons during NREM sleep disrupts augmentation of CA1 SPWR oscillations during CFM consolidation. Raw spectral power for ripple frequency for **(a)** a representative control mouse (n= 28 neurons) and (**b**) representative mouse expressing Arch (n= 28 neurons) at baseline (white circles, and post-CFC black and pink circles for control and Arch, respectively) Mean ± SEM shown for local field potential values within treatment group. **(c)** Ripple amplitude increased immediately following CFC in control animals, but not animals expressing Arch. Mean ± SEM shown for local field potential values for each animal across a given treatment. * indicates $p < 0.024$, student's paired t-test. (**d-f**) Power changes from baseline were quantified for NREM delta, NREM ripples, and REM theta during hours 0-6 post-CFC and comparisons were made. **(g)** 3D scatter plot of all relationships shown in (d-f). Control animals (black) have increased associations between NREM oscillations and REM theta. **(h-i)** Filled contour maps for control and Arch animals showing the relationships for each animal for data shown in (g)**.**

demonstrate that PV+ interneurons normally coordinate multiple sleep-associated CA1 network oscillations in the hours following learning, and suggest that these oscillations in turn promote CFM.

5.3.3 Stimulation of PV+ interneurons at a theta frequency is sufficient to rescue CFM in the absence of sleep

Since augmented theta frequency activity in CA1 predicted CFM consolidation, and since theta has been linked to memory formation in other paradigms we next tested whether theta rhythms driven by PV+ interneurons could rescue CFM in sleep deprived mice. [153] Mice expressing Channelrhodopsin or GFP in PV+ interneurons (*PV:ChR2* or control) underwent rhythmic (7 Hz) light delivery to bilateral CA1 across a 6-h period of post-CFC SD. **(Figure 5.6a**, see also **Supplemental Figure 5.11)** Raw LFP power spectra for baseline and post-CFC periods are shown for a representative control mouse allowed *ad lib* sleep, and for *control* and *PV:ChR2* mice during SD. **(Figure 5.5b-d)** In *PV:ChR2* mice, there is a noticeable peak of spectral power at 7 Hz during stimulation recording with a slight subharmonic frequency band at ~4 Hz. **(Figure 5.6d)** control animals showed loss of all spectral power in delta and theta frequencies during SD, while sleeping control had naturally occurring increases in these frequency bands. **(see also Supplemental Figure 5.13-5.14)** Strikingly, rhythmic stimulation of CA1 PV+ interneurons is sufficient to completely rescue CFM from deficits caused by SD. **(Figure 5.6e)** Memory rescue was not attributable to changes in sleep architecture in *PV:ChR2* mice during the post-stimulus recording period, which was identical following SD regardless of stimulation. **(Supplemental Figure 5.12)**

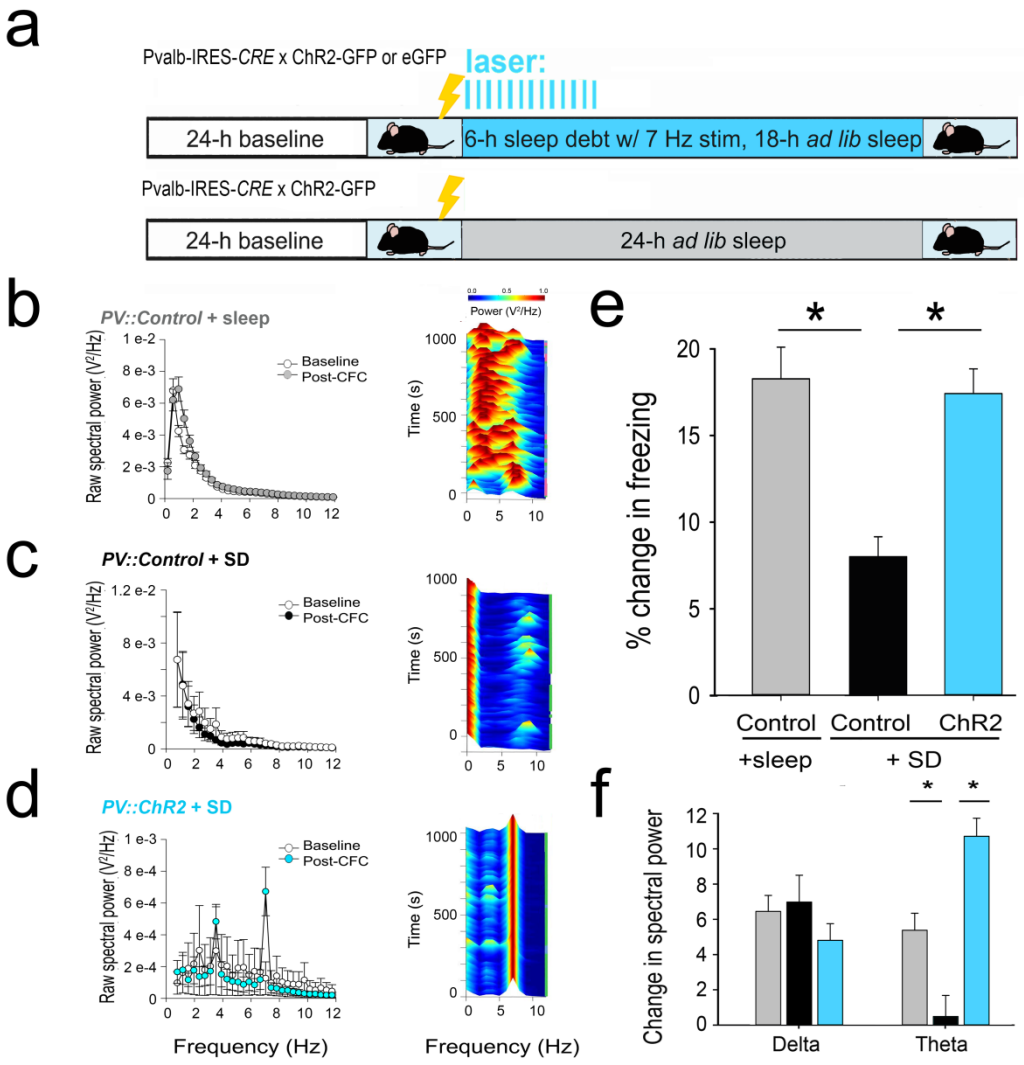

Figure 5.6: Theta stimulation during sleep deprivation rescues CFM. (a) Experimental paradigm: Double transgenic animals *PV::ChR2* or *PV::Control* following 24-h of baseline underwent CFC in a novel context. Following training, animals were optogenetically stimulated at 7Hz during 6-h SD. Starting at hour 6 post-CFC, mice were allowed to *ad lib* sleep. CFM was asses 24 hours after CFC. **(b-d)** Raw CA1 LFP spectral power during hours 0-6 of recording from representative animals (Mean ± SEM shown for all LFPs for each treatment n=28 for control + sleep, n=26 for control + SD, n=24 for ChR2 +SD) and representative LFP spectralgrams showing spectra power in delta and theta bands across 1000 seconds during 0-6 h manipulation. **(e)** CFM in was significantly reduced in control mice with post-CFC SD. PV+ interneuron stimulation at theta frequency during sleep debt is sufficient to rescue CFM to levels of control animals who were allowed to sleep. * indicates $p = 0.01$ Holm-Sidak *post hoc* test for control + sleep ($n = 8$) vs. control + SD ($n = 5$) and vs. ChR2 +SD ($n = 7$). Control + sleep vs. ChR2 +SD *N.S.* All error bars are SEM. **(f)** naturally occurring post-CFC increases in theta power in control animals who were allowed to sleep was surpassed by PV+-interneuron mediated theta power in ChR2 stimulated mice. Control mice that were sleep deprived has significant decreases in theta power compared to control + sleep and ChR2 +SD animals. Delta power changes were consistent across all treatments. * indicates $p = 0.001$ Holm-Sidak *post hoc* test for control + sleep ($n = 176$) vs. control + SD ($n = 140$) and vs. ChR2 +SD ($n = 92$). Control + sleep vs. ChR2 +SD *N.S.* All error bars are SEM for all LFPs across treatment.

Optogenetically-induced theta activity was equal to or greater that naturally-occurring post-CFC increases in theta power in freely-sleeping control mice. control has significant decreases in theta power during SD compared to both *PV:ChR2* mice and freely-sleeping *control* mice. **(Figure 5.6f)** This result suggests not only the sufficiency of theta to drive memory consolidation, but also the ability of a small population of PV+ interneurons to affect the activity of an entire network

5.3.4 Theta stimulation during post-CFC SD partially rescues lingering oscillatory deficits in recovery sleep

We also assessed CA1 LFP activity in the hours after optogenetic stimulation with SD **(Figure 5.7a-c, and Supplemental Figure 5.15).** While spectral power waxed and waned across bouts of sleep and wakes in *control* and *PV:ChR2* mice, there was lingering suppression of NREM and REM delta and theta activity, and NREM ripple occurrence, in the 6 h after SD in control mice. (**Figure 5.7d, g**) These oscillations were rescued with stimulation across SD in *PV:ChR2* mice. Theta power induced during stimulation seemed to coordinate subsequent NREM delta and REM theta. (**Figure 5.7e-f**). Enhancements of NREM delta power over hours 6-12 post-CFC predicted CFM consolidation for individual mice. **(Figure 5.7h)** These data suggest NREM sleep several hours after learning may be altered in a meaningful way by sleep-associated network activity patterns immediately following learning.

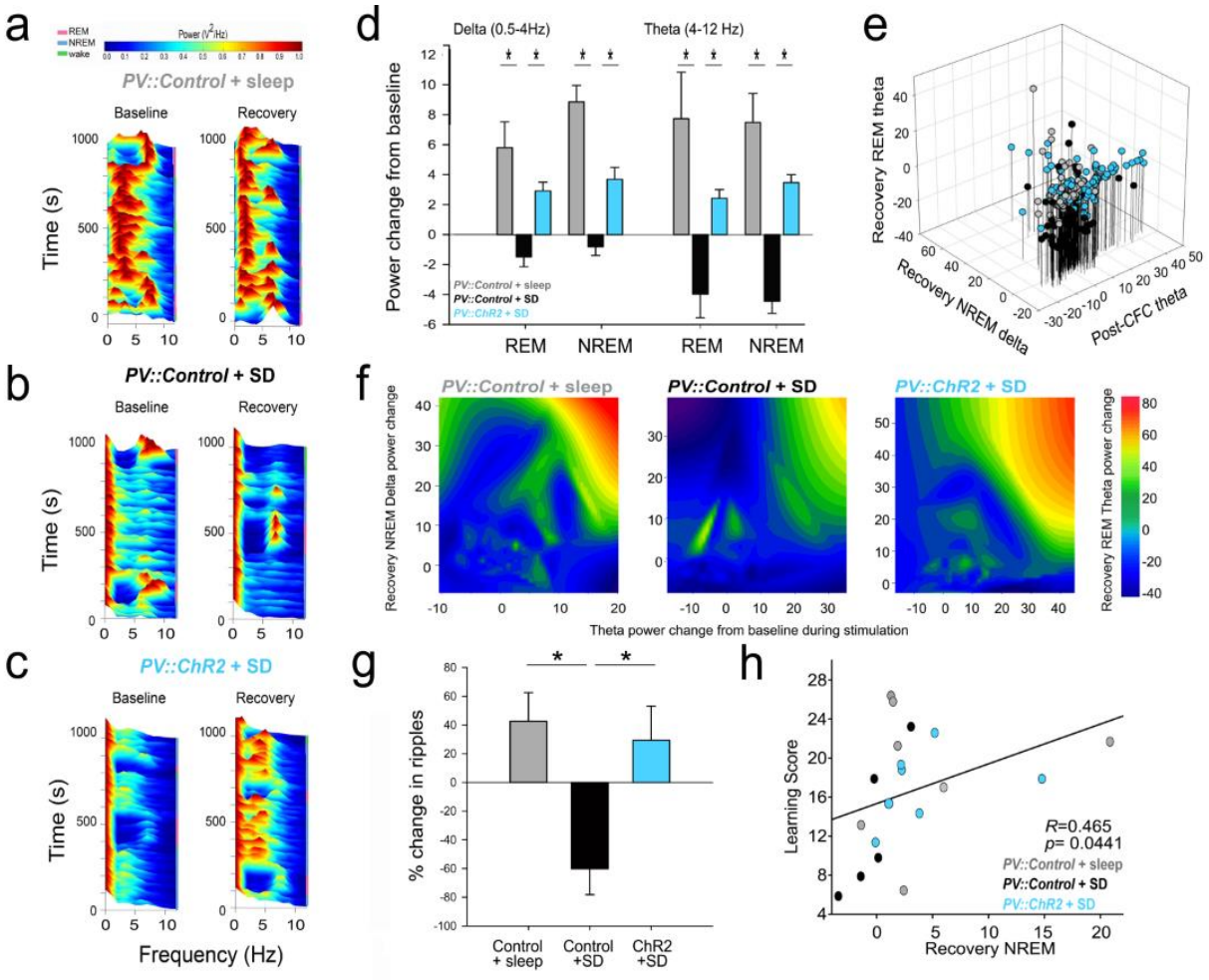

Figure 5.7: Theta stimulation following CFC in the absence of sleep partially rescues continued suppression of sleep-specific oscillatory activity during recovery period. (a-c) Representative LFP spectralgrams showing spectra power in delta and theta bands across 1000 seconds of hours 6-12 recording at baseline and post-CFC (matched for time of day). (b) Control mice + SD showed decreased oscillatory spectral power during recovery NREM and REM states (colored denotation on right) in delta and theta, respectively that was not seen in control animals that were allowed to sleep (a). ChR2 animals +SD showed a partial rescue of recovery oscillatory activity during sleep states (c). **(d)** Post-CFC increases in delta and theta power in control animals was partially rescued by PV+ interneuron stimulation at theta frequency in the absence of sleep. * indicates P<0.001 Pairwise multi-comparison Holm-Sidak *post hoc* test. (Mean + SEM is shown for all LFPs across treatments. Control + sleep (n = 176) vs. control + SD (n = 140) and vs. ChR2 +SD (n = 92). Control + sleep vs. ChR2 +SD *N.S.*. **(e)** 3D scatter plot of all sleep-specific oscillatory activity relationships. Control + sleep animals (gray) and ChR2 +SD animals (blue) increases in theta power during hours 0-6 is associated with recovery NREM delta and REM theta. **(f)** Filled contour maps for each treatment group showing the relationships for data shown in (e). **(g)** . PV+ interneuron stimulation at theta frequency during sleep debt is sufficient to rescue increased occurrence of ripples from baseline to levels of control animals who were allowed to sleep. * indicates p = 0.022 One way ANOVA. Holm-Sidak *post hoc* test for control + sleep (n = 8) vs. control + SD (n = 5) and vs. ChR2 +SD (n = 7). Control + sleep vs. ChR2 +SD *N.S.* All error bars are SEM. **(h)** Increases in NREM delta power during recovery was correlated with subsequent CFM consolidation (values indicate mean LFP changes per mouse; Spearman rank order).

5.3.5 Sleep-dependent oscillations, driven by PV+ interneurons, coordinate CA1 ensembles during consolidation

In addition to oscillatory changes following NREM inhibition of PV+ interneurons, we observe sustained, statistical decreases in firing rate of recorded (principal) cells in *PV::Arch* animals, specifically during NREM and REM states. **(Figure 5.8a)** To test the longer-term effects of PV+ interneuron-driven network oscillations and the altered firing patterns observed, we quantified FuNS changes during and after optogenetic manipulations of PV+ interneurons. After NREM-targeted inhibition in *PV:Arch* mice, we observed a trend for reduced FuNS, compared with a trend for increased FuNS following CFC in control mice. **(Figure 5.8b)** CFC also induced a long-lasting increase in the strength of network connections (quantified as the average mean temporal distance between neuronal pairs' spike trains, which was not seen after NREM inhibition. (See **Methods** for more details; **Figure 5.8c)** This data also shows trending relationship between increases in FuNS during NREM and behavioral measures of CFM consolidation 24 h after CFC. **(Figure 5.8d)**

Rhythmic PV+ interneuron stimulation during SD also resulted in sustained increases in firing rate in the recovery period following CFC that was not observed in SD control animals. Theta stimulation of PV+ interneurons during SD was also sufficient to drive CA1 FuNS increases during subsequent NREM sleep, a phenotype ameliorated by post-CFC SD. **(Figure 5.9b)** This manipulation also increased the strength of network connectivity following CFC, to a level comparable to what is observed in freely-sleeping animals. **(Figure 5.9c)** These increases in FuNS predict behavioral measures of CFM consolidation 24 h after CFC. **(Figure 5.9d)** Taken together, our data suggest

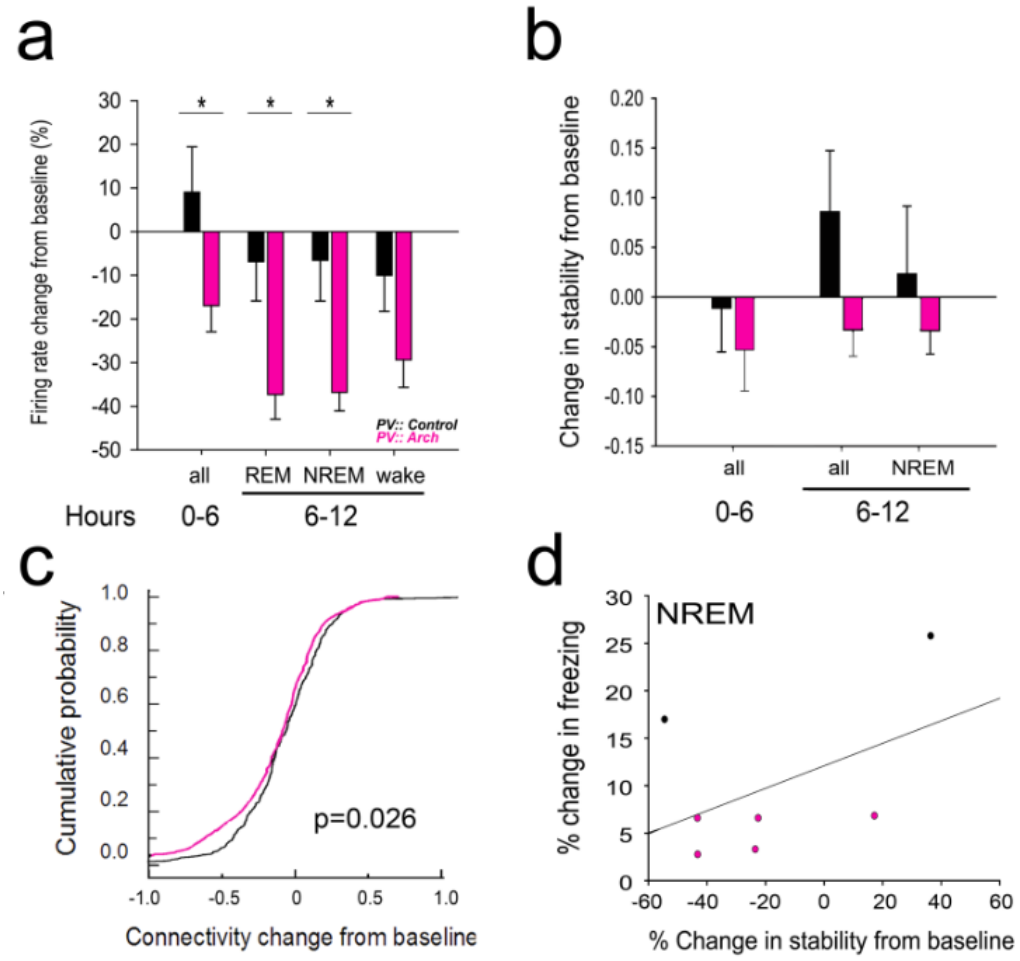

Figure 5.8: PV+ interneurons coordinate CA1 ensembles and increase FuNS during NREM sleep leading to consolidation. (a) Firing rate change from baseline across all states of inhibition and during 6-12 h recovery. Mean ± SEM shown for all animals within treatment group. * indicates p<0.03 One-way ANOVA, Holm-Sidak *post hoc* test **(b)** CA1 neuronal functional connectivity in control mice showed an increase in stability relative to baseline during recovery hours 6-12 that is lost in Arch NREM- inhibited animals. Data set is incomplete but is trending towards significance. Mean ± SEM shown for all animals within treatment group**. (c)** Neuronal functional connectivity strength also showed an increase in control mice relative to baseline. A similar change that was not seen in Arch mice during NREM inhibition. *p* value indicates results of Kolmogorov-Smirnov test. **(d)** Data set to this point shows trending relationship between increases in FuNS during NREM and behavioral measures of CFM consolidation 24 h after CFC p= 0.09.

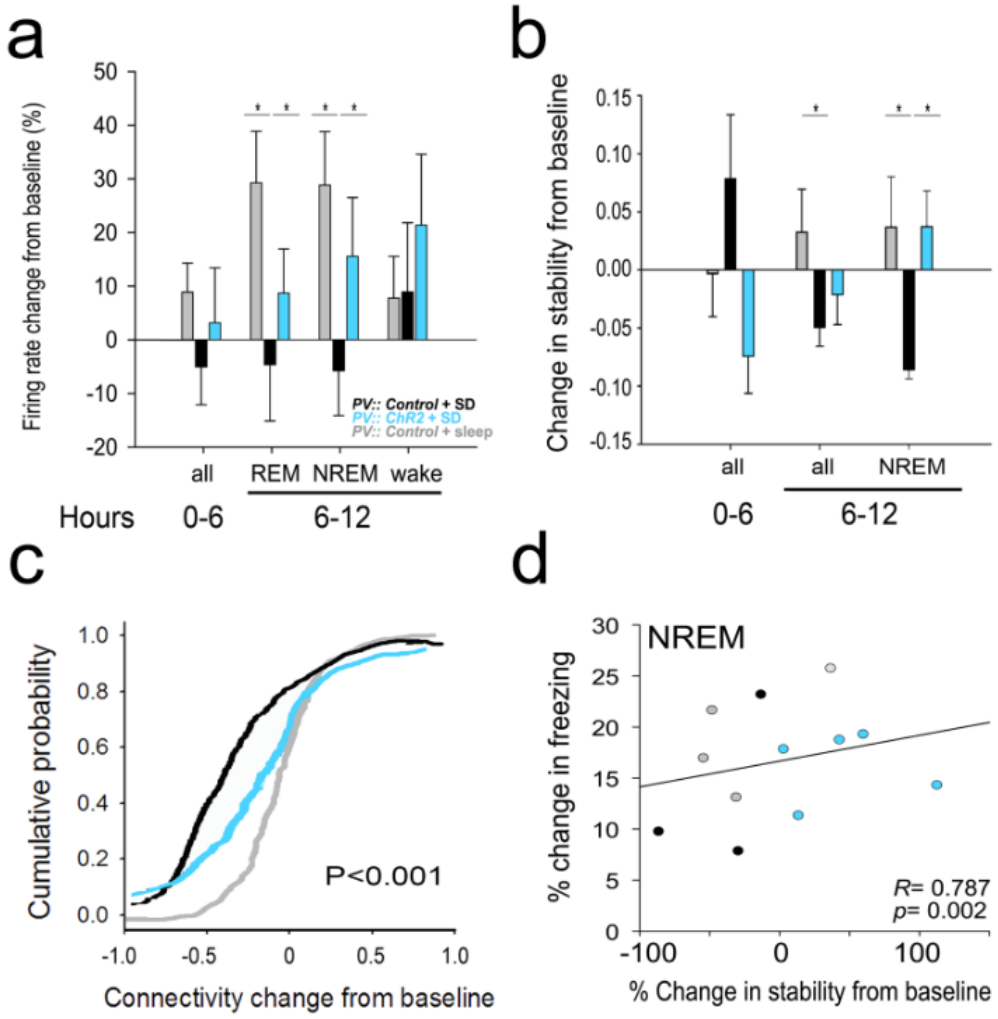

Figure 5.9: PV+ interneurons are sufficient to coordinate CA1 ensembles and increase FuNS during sleep deprivation. (a) Firing rate change from baseline across all states of inhibition and during 6-12 h recovery. Mean ± SEM shown for all animals within treatment group. * indicates p<0.02 One-way ANOVA, Holm-Sidak *post hoc* test **(b)** Stimulation of PV+ interneurons at 7 Hz induced a significant increase in CA1 network stability that lasted through the entire post-stimulation period, specifically during NREM sleep**. (c)** This manipulation also induced a long-lasting increase in the strength of network connections that partially recovers the effects seen in animals that were allowed to freely sleep. *p* value indicates results of Kolmogorov-Smirnov test **(d)** Increases in FuNS during NREM predict behavioral measures of CFM consolidation 24 h after CFC p= Spearman rank order

that NREM associated, rhythmic coordination of CA1 network activity by PV+ interneurons is necessary and sufficient for stabilizing network dynamics and promoting long-term memory formation.

5.4 Discussion

Learning of hippocampus-dependent tasks has been reported to lead to increases in neocortical slow oscillation synchrony, hippocampal ripple activity, and thalamocortical spindle oscillations during subsequent NREM. [17,25,45,93] REM theta oscillatory activity during the consolidation window is also increased and is a proposed mechanism by which spike timings of cells are coordinated to promote consolidation. [34,68,153] Both theta oscillations in REM and SPWRs in NREM have been hypothesized to mediate replay of activity patterns in hippocampal ensembles.[39] Here we show that PV+ interneurons regulate naturally occurring enhancements in both slow and fast NREM oscillations –delta, theta, and SPWRs - following learning and that disrupting these interneuron-mediated oscillations disrupts CFM consolidation. Together these NREM oscillations coordinate subsequent REM theta. (**Figure 5.4g-i)** REM theta increases following CFC are suppressed when PV+ interneurons are inhibited during prior bouts of NREM. Critically, however, REM- or wake-targeted PV+ interneuron inhibition does not disrupt CFM consolidation; NREM inhibition alone causes gross CFM deficits. This suggests that PV+ interneuron-mediated CA1 network oscillations could drive long-term plasticity, leading to subsequent changes in network dynamics (i.e., at later time points following CFC), alterations in REM theta-frequency oscillations, and long-term memory formation. In support of this idea, NREM-targeted interneuron inhibition leads to changes in all of these.

Critically, in sleep-deprived mice, theta frequency stimulation of CA1 PV+ interneurons rescues CFM to levels seen in freely-sleeping animals. This also restores persistent decreases in NREM delta power and SPWRs that extend into recovery sleep. This may reflect a multiple-step process during which information is stored in the hippocampus, where consolidation is initiated by REM theta-mediated coordination of spike-timings immediately after learning, and long term, stable storage of information is subsequently promoted by NREM slow oscillations and SPWRs. It is known that stabilization of functional connectivity persists over many hours, and can be quantified from just after learning until just before recall 24 h later. [68] The connections among ensembles of cells are strengthened as consolidation continues, possibly via stimulated reactivation during NREM SPWRs.[164] This primes these cells/ the rest of the network for reactivation during subsequent NREM sleep which leads to long term store of robust memories.

In wild-type animals, the formation of a behaviorally-accessible memory traces *in vivo* is accompanied by increased FuNS during NREM sleep in the CA1 network. tour current findings suggest that PV+ interneurons play a critical role in FuNS, and that early coordination of CA1 network activity through theta frequency oscillations is sufficient for subsequent FuNS increases. PV+ interneuron inhibition during post-CFC NREM sleep leads to decreases in FuNS measured in the recovery period 6-12h post-CFC. Augmentation or disruption of FuNS changes are associated with rescue or disruption of stable memory formation. In summary, this work demonstrates the necessity and sufficiency of PV+ interneuron-mediated network oscillations for successful, stable memory consolidation. Here we show that PV+ interneurons: 1) are

necessary during NREM sleep, but not REM sleep or wakefulness, immediately following CFC to establish fear memory, 2) coordinate NREM-REM oscillatory pattern coupling of delta, theta, and SPWR frequencies, 3) stimulation at theta frequency following CFC is sufficient to rescue network oscillatory and behavioral deficits due to sleep deprivation, and 4) can stabilize patterns of neuronal communication and induce long-lasting changes in the strength of functional connectivity relationships between CA1 neurons. We conclude that these neurons coordinate critical network dynamic changes following learning that lead to stable, long-term memory storage.

5.5 Supplemental Figures

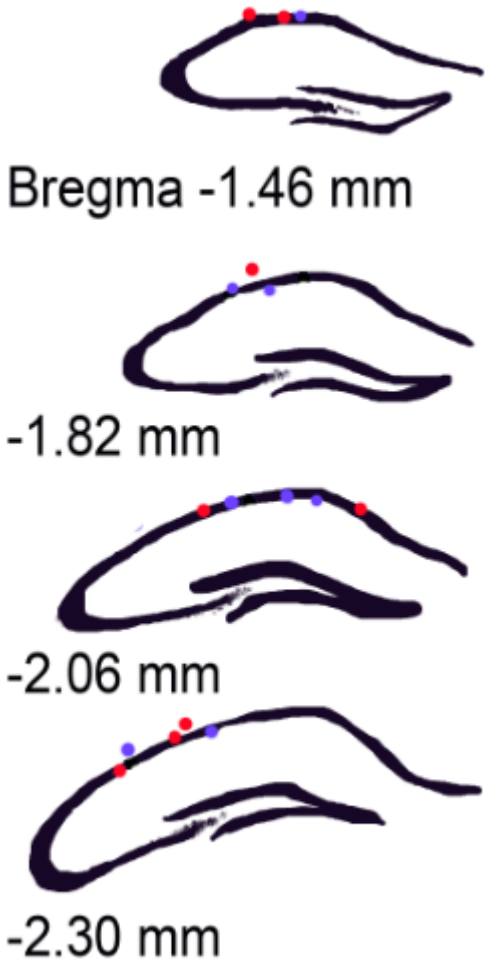

Supplemental Figure 5.1: Recording sites for C57BL/6J mice. Positions of electrode bundles for single-unit and LFP recordings for C57BL/6J mice used in CFC (*n* = 4 mice; red dots) and sham (*n* = 4 mice; purple dots) experiments.

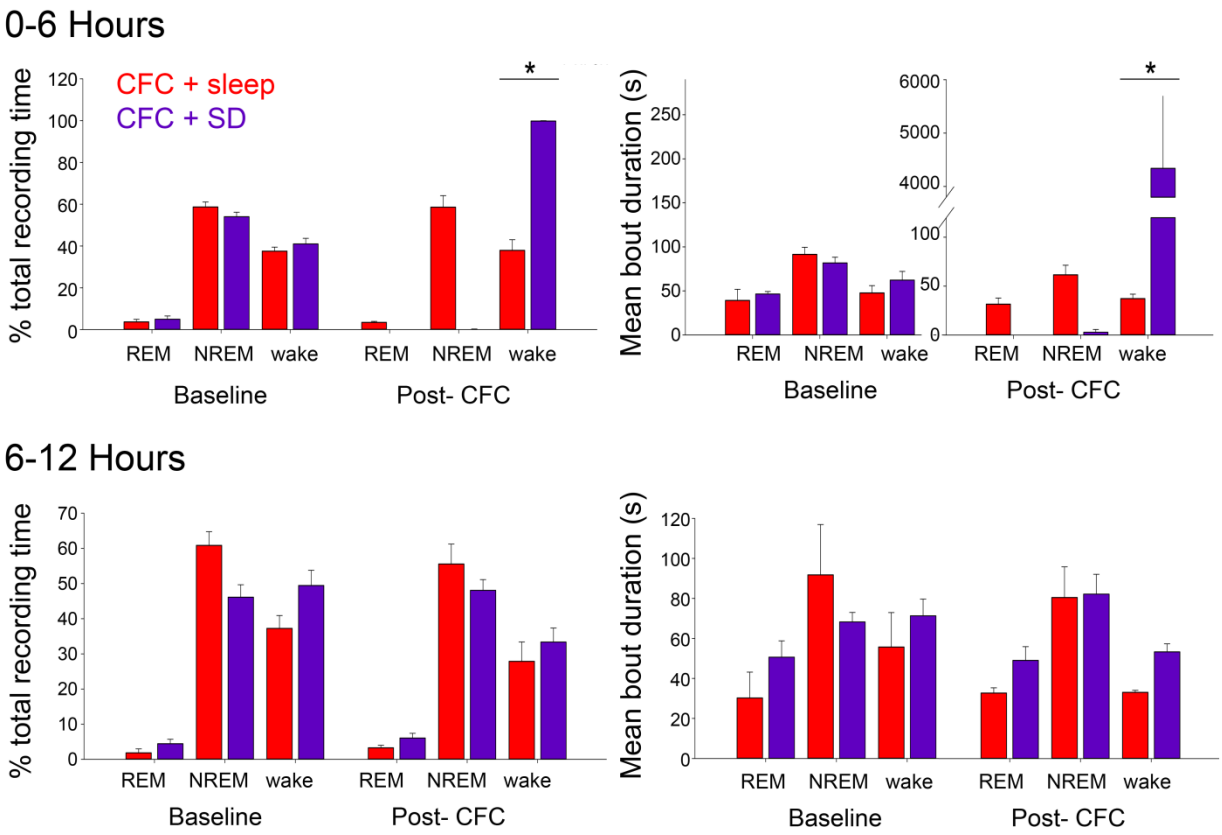

Supplemental Figure 5.2: Sleep architecture during C57BL/6J experiments. There was no significant effect of treatment on either percent of time spent in REM, NREM between baseline and following CFC during recovery time 6-12 hours after training for either % of total time in each state nor mean bout duration. For sleep deprived, there was an obvious increase in both % of total time spent in each state during handling period. Mean bout duration in Post-CFC recording reflects the SD. There was no significant effect of treatment on either percent of time spent in REM, NREM, and wake between baseline and following CFC during recovery time 6-12 hours after training for either % of total time in each state nor mean bout duration. Error bars are SEM for animals within each treatment and * denotes $p<0.005$ for Post-CFC differences between sleeping and sleep deprived animals.

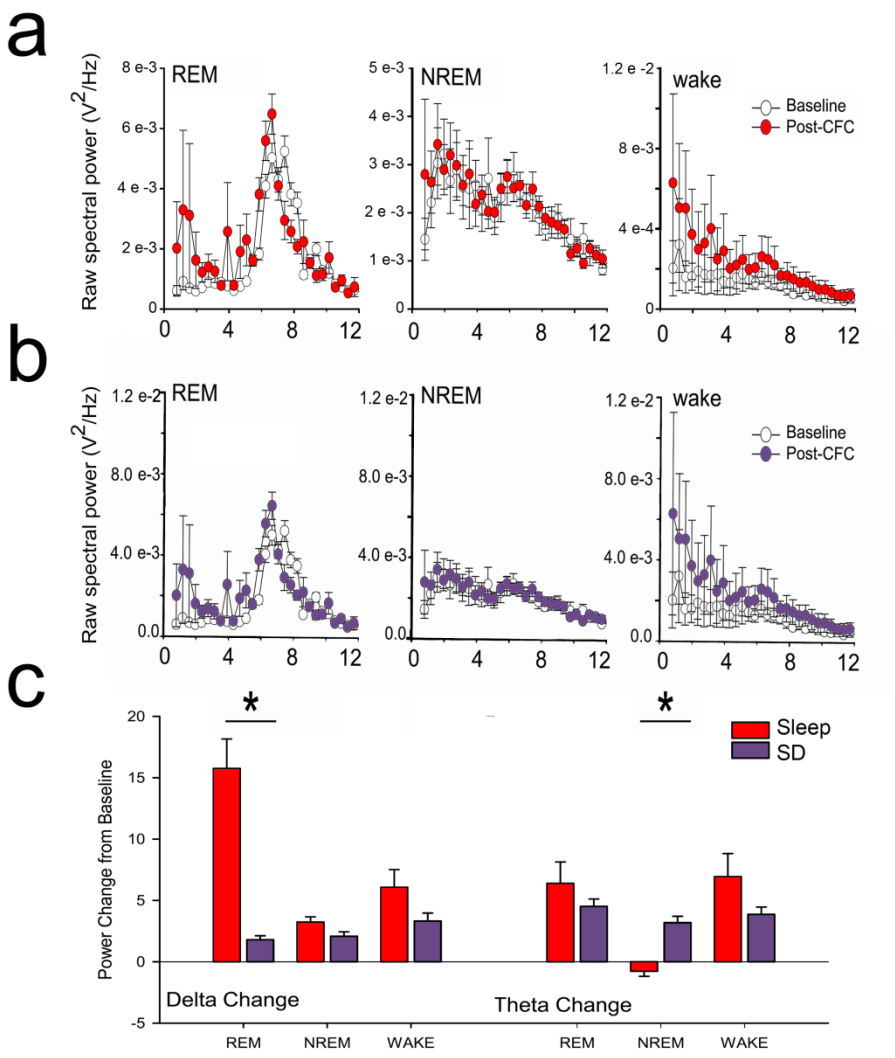

Supplemental Figure 5.3: CA1 LFP spectral power for C57BL/6J mice during recovery hours 6-12 post-CFC. Raw CA1 LFP spectral power during 6-12 hours of recording at baseline (white circles) and post-CFC (red circles and purple circles) for a representative C57BL/6J during REM sleep, NREM sleep, and wake for **(a)** sleeping animals (Mean ± SEM shown for local field potential values within animal n=28) and **(b)** sleep deprived animals (Mean ± SEM shown for local field potential values within animal n=22) **(c)** Quantification of power change within frequency bands corresponding to delta and theta during REM, NREM, and wakefulness. (Mean ± SEM shown for all LFPs for each treatment n=57 for sleeping, n=111 for SD). * indicates p< 0.05 Pairwise multi-comparison. Holm-Sidak *post hoc* test.

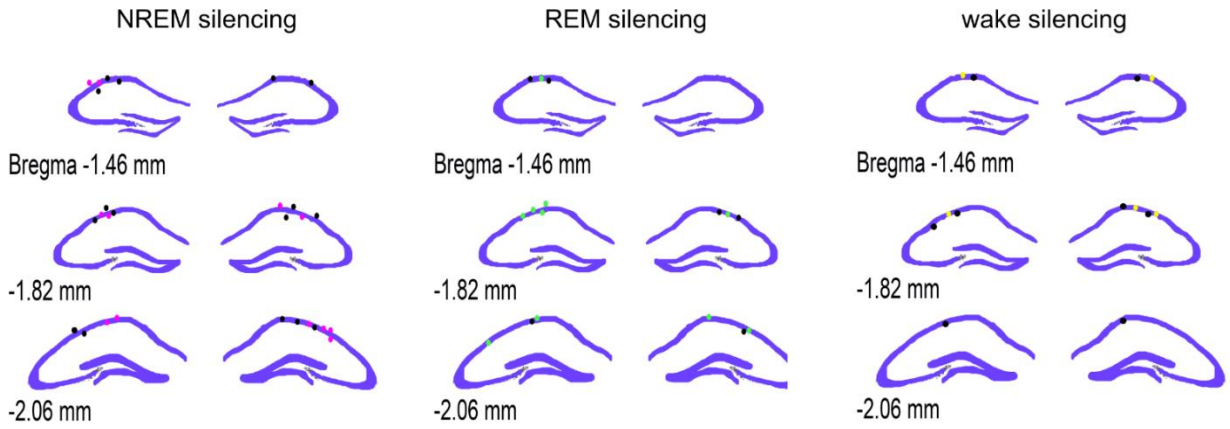

Supplemental Figure 5.4: Electrode placement for PV+ interneuron inhibition of each state. Positions of electrode bundles for single-unit and LFP recordings for *PV::Control* and *PV::Arch* mice during NREM inhibition (*n* = 5 mice; black dots for control, n=5 mice; pink dots for Arch), REM inhibition (*n* = 5 mice; black dots for control, n=4 mice; green dots for Arch), and wake inhibition (*n* = 5 mice; black dots for control, n=5 mice; yellow dots for Arch)

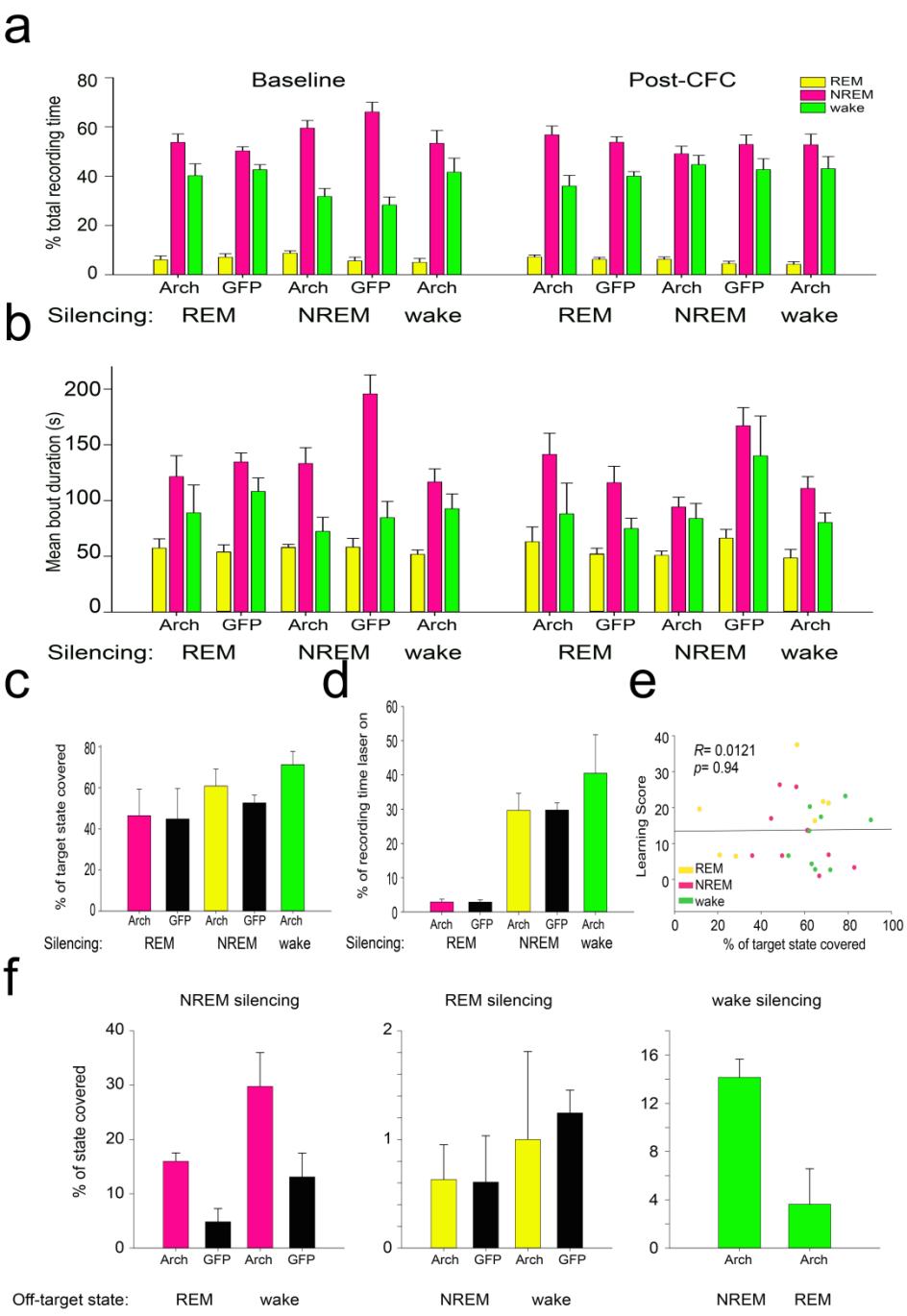

Supplemental Figure 5.5: Sleep architecture during inhibition experiments. There was no significant effect of treatment on either (**a**) percent of time spent in REM, NREM, and wake, (**b**) the mean duration of REM, NREM, and wake bouts, (**c**) Percent of target state covered between states inhibition, with and average coverage of 50% (**d**) the length of laser on time during targeted state was not different from the average time spent in that state. **(e)** % of target state covered was not predictive of learning behavior **(f)** % of off state targeting during laser. All error bars are SEM

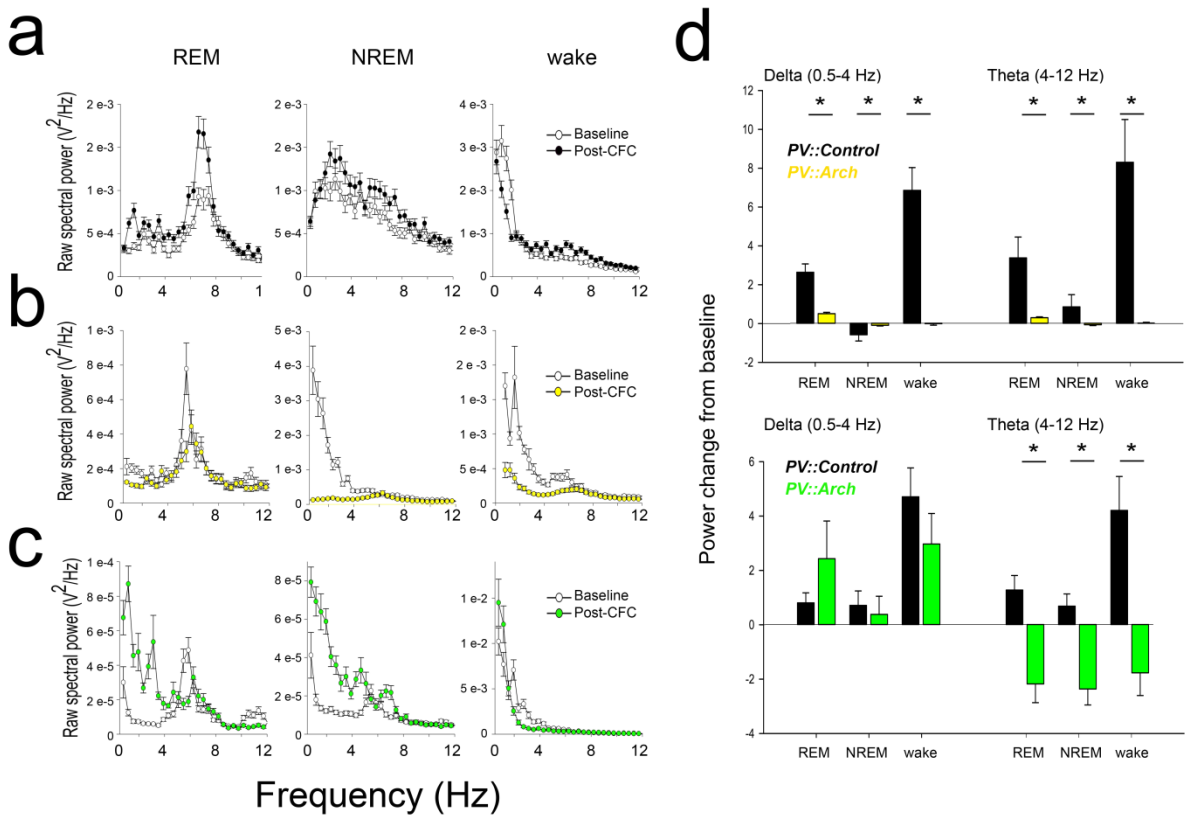

Supplemental Figure 5.6: CA1 LFP spectral power for Control and Arch mice during REM and wake-targeted inhibition. Raw CA1 LFP spectral power during hours 0-6 of recording at baseline) and post-CFC for a representative animals. (a) Control mouse with REM inhibition showing raw power in REM, NREM, and wake at baseline (white circles) and post-CFC (black circles) (Mean ± SEM shown for local field potential values within animal n=28). Raw PSD for control animals during waking looked similar to REM-inhibited controls and were not included. **(b)** Arch-expressing mouse with REM inhibition showing raw power in REM, NREM, and wake at baseline (white circles) and post-CFC (yellow circles) (Mean ± SEM shown for local field potential values within animal n=28) **(c)** Arch-expressing mouse with REM inhibition showing raw power in REM, NREM, and wake at baseline (white circles) and post-CFC (green circles) (Mean ± SEM shown for local field potential values within animal n=28 **(d)** Quantification of power change within frequency bands corresponding to delta and theta during REM, NREM, and wakefulness. (Mean ± SEM shown for all LFPs for each treatment n= 106 for control, n=88 for Arch during REM inhibition, n= 84 for Arch during wake inhibition. * indicates p< 0.05 Pairwise multi-comparison. Holm-Sidak *post hoc* test.

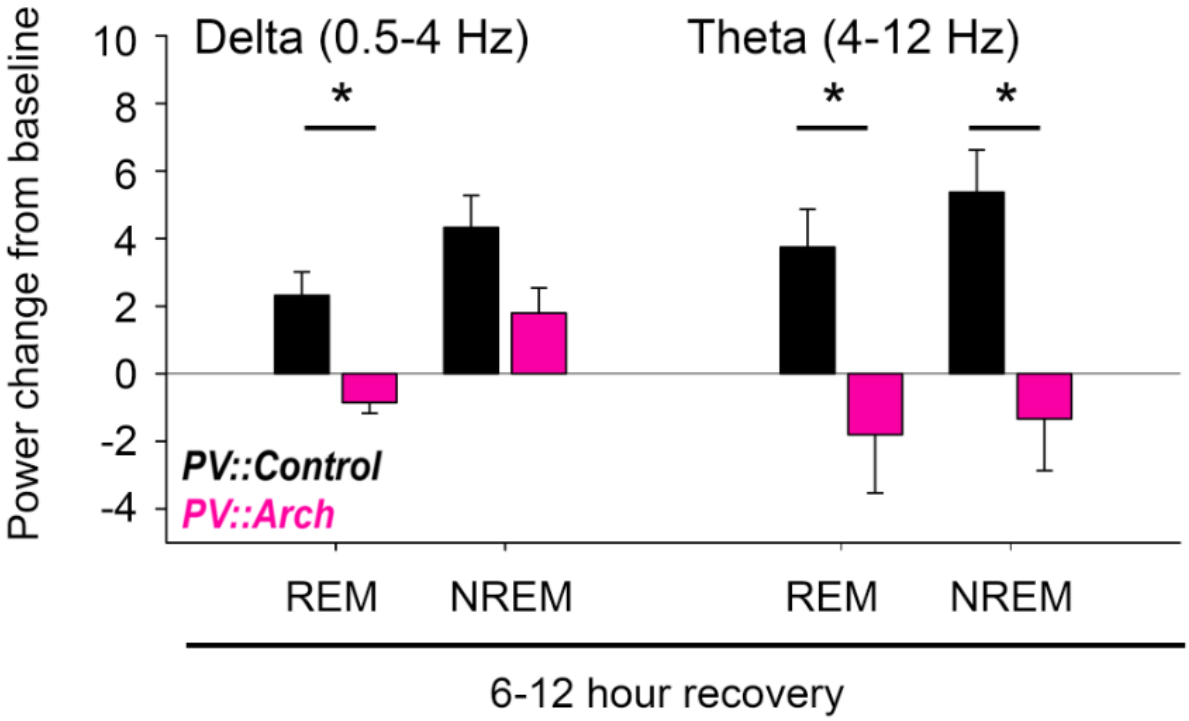

Supplemental Figure 5.7: CA1 LFP remains elevated at later time points, but is suppressed by 0-6 h Arch-inhibition during NREM. Quantification of power change within frequency bands corresponding to delta and theta during REM and NREM sleep. (Mean ± SEM shown for all LFPs for each treatment n= 72for control, n=128 for Arch during REM inhibition, n= 84 for Arch during wake inhibition. Mean ± SEM shown for all LFPs for each treatment * indicates p< 0.05 Pairwise multi-comparison. Holm-Sidak *post hoc* test.

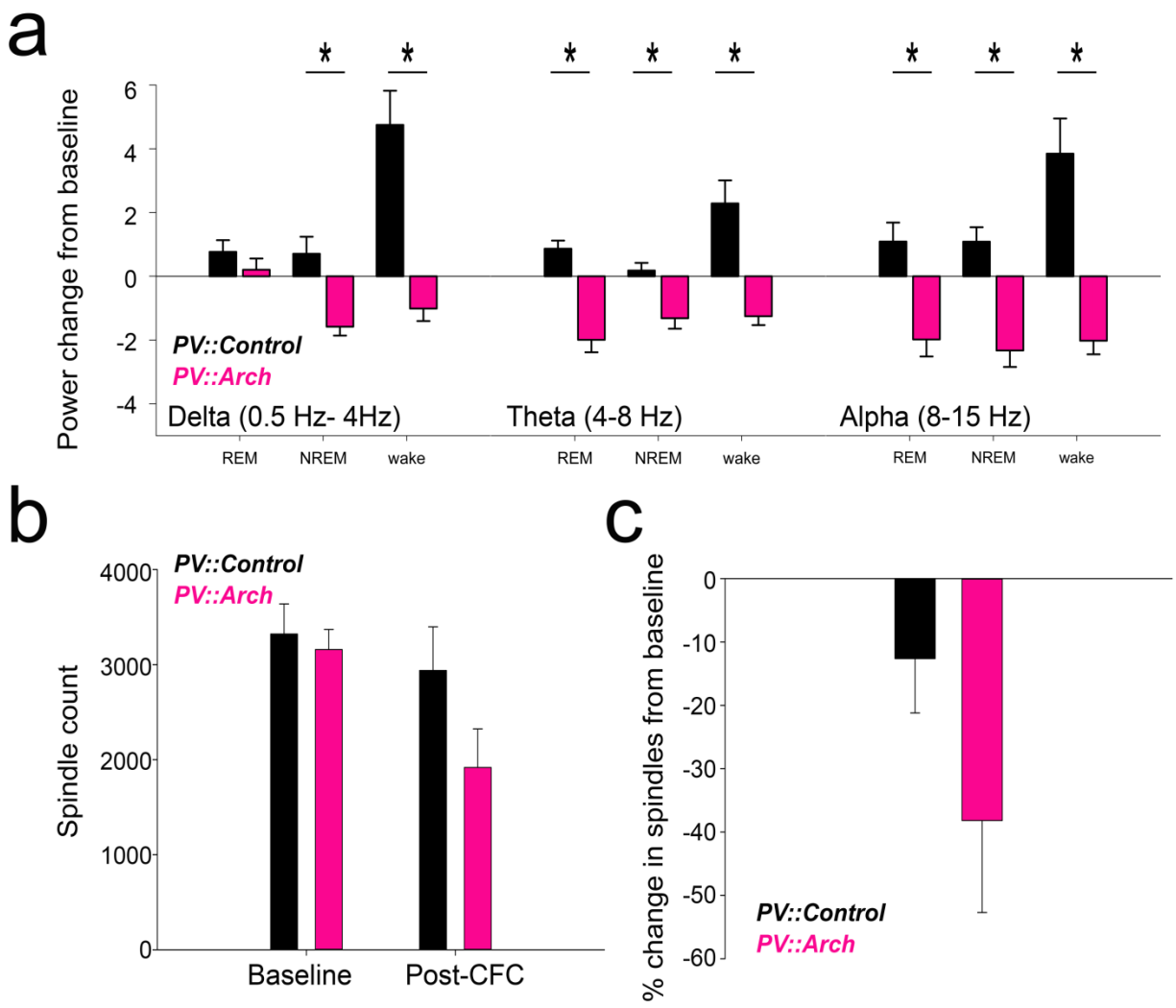

Supplemental Figure 5.8: PV+ inhibition during NREM sleep augments alpha power but has no effect on spindle power. **(a)** Because raw spectra power traces showed suppression of power in frequency bands beyond canonical 4-12 Hz frequency bands, we also analyzed narrower frequency bands for theta (4-8 Hz) and included alpha (8-15 Hz) analysis * indicates P<0.001 Pairwise multi-comparison. Holm-Sidak *post hoc* test. (Mean ± SEM shown for all LFPs for each treatment n= 103 for control and n=130 for Arch)

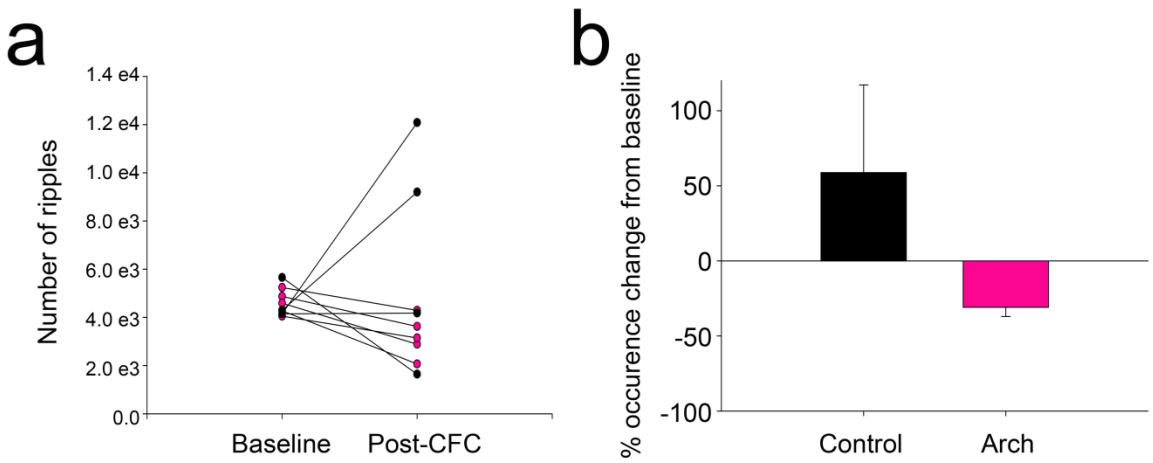

Supplemental Figure 5.9: PV+-interneuron inhibition following CFC shows increases in ripple occurrence. (a) Total number of ripples for each animal at baseline and 0-6 h post-CFC (control- black circles, Arch- pink circles) **(b)** There was no significant difference in occurrence of ripples from baseline when averaged across group. Mean ± SEM shown for all LFPs for each treatment

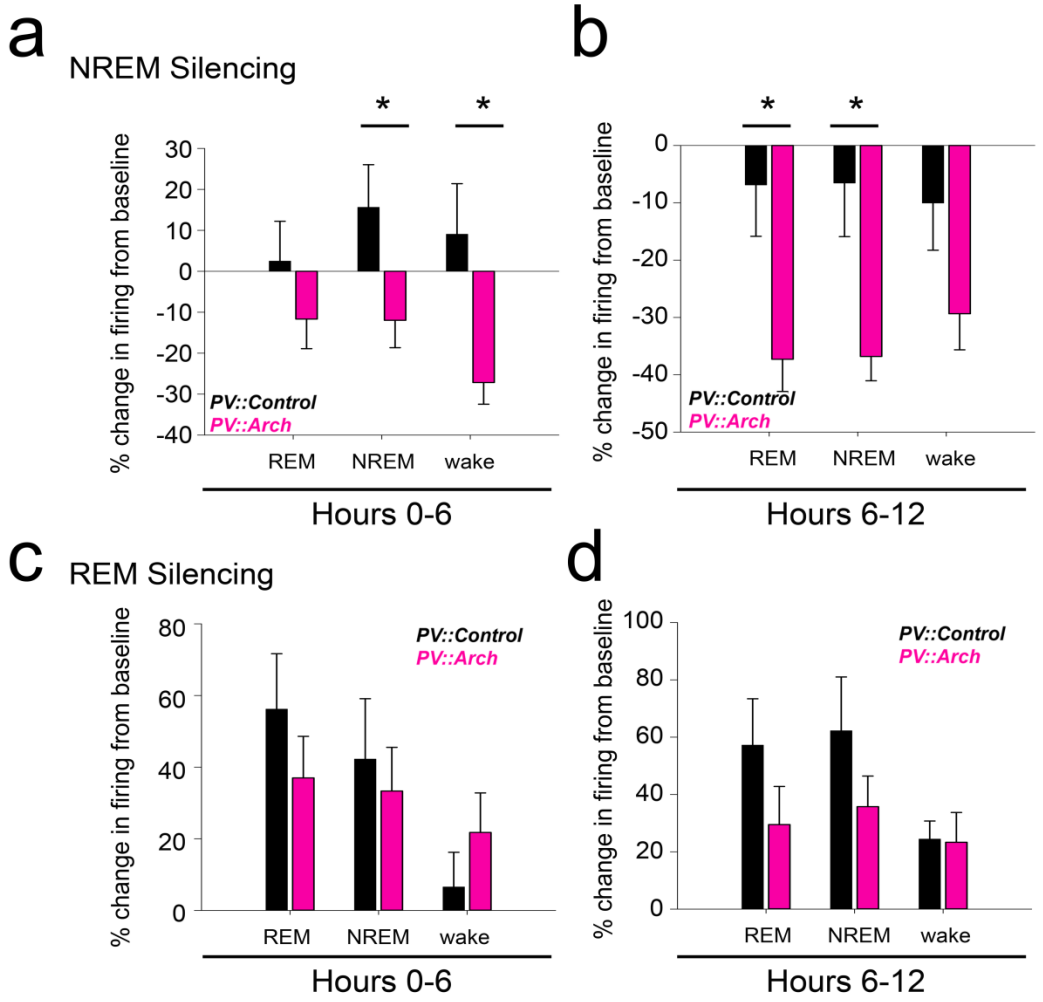

Supplemental Figure 5.10: CA1 firing rates are elevated following CFC, but is suppressed by 0-6 h Arch-inhibition during NREM. Quantification of firing rate change from baseline during REM, NREM, and wake during NREM inhibition (**a,b**; Mean ± SEM shown for all neurons for each treatment n= 35 for control and n= 56 for Arch. * indicates p< 0.05 Pairwise multi-comparison. Holm-Sidak *post hoc* test.) and REM inhibition(**c-d**; Mean ± SEM shown for all neurons for each treatment n= 42 for control and n= 38 for Arch.) **(a)** During the first 6 hours following training, control animals show increases in firing rate from baseline. Firing increases are suppressed by state-specific inhibition in NREM and wake states. **(b)** Firing rate changes later in recording time, as hours 6-12 show continued augmentation by PV-inhibition of firing in REM and REM states. (Mean ± SEM shown for all neurons for each treatment n= 35 for control, n=56 for Arch) during REM inhibition, n= 84 for Arch during wake inhibition. **(c-d)** No significant changes were noted in during REM-specific inhibition.

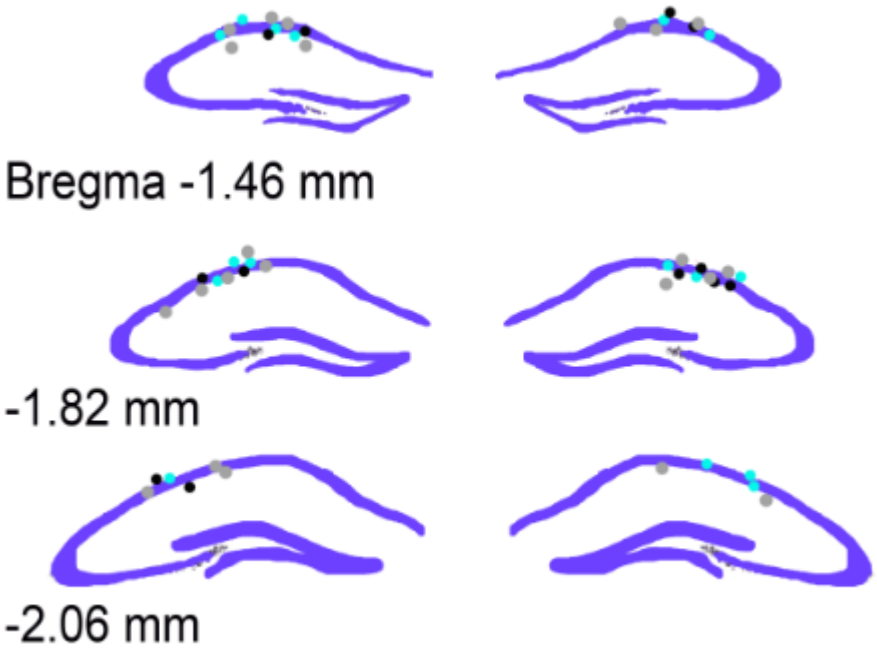

Supplemental Figure 5.11: Electrode placement for stimulation experiments. Positions of electrode bundles for single-unit and LFP recordings for *PV::Control* and *PV::ChR2* mice (*n* = 5 mice; black dots for control + SD, n=7 mice; blue dots for ChR2 + sleep, n=8 mice; grey dots for control + sleep)

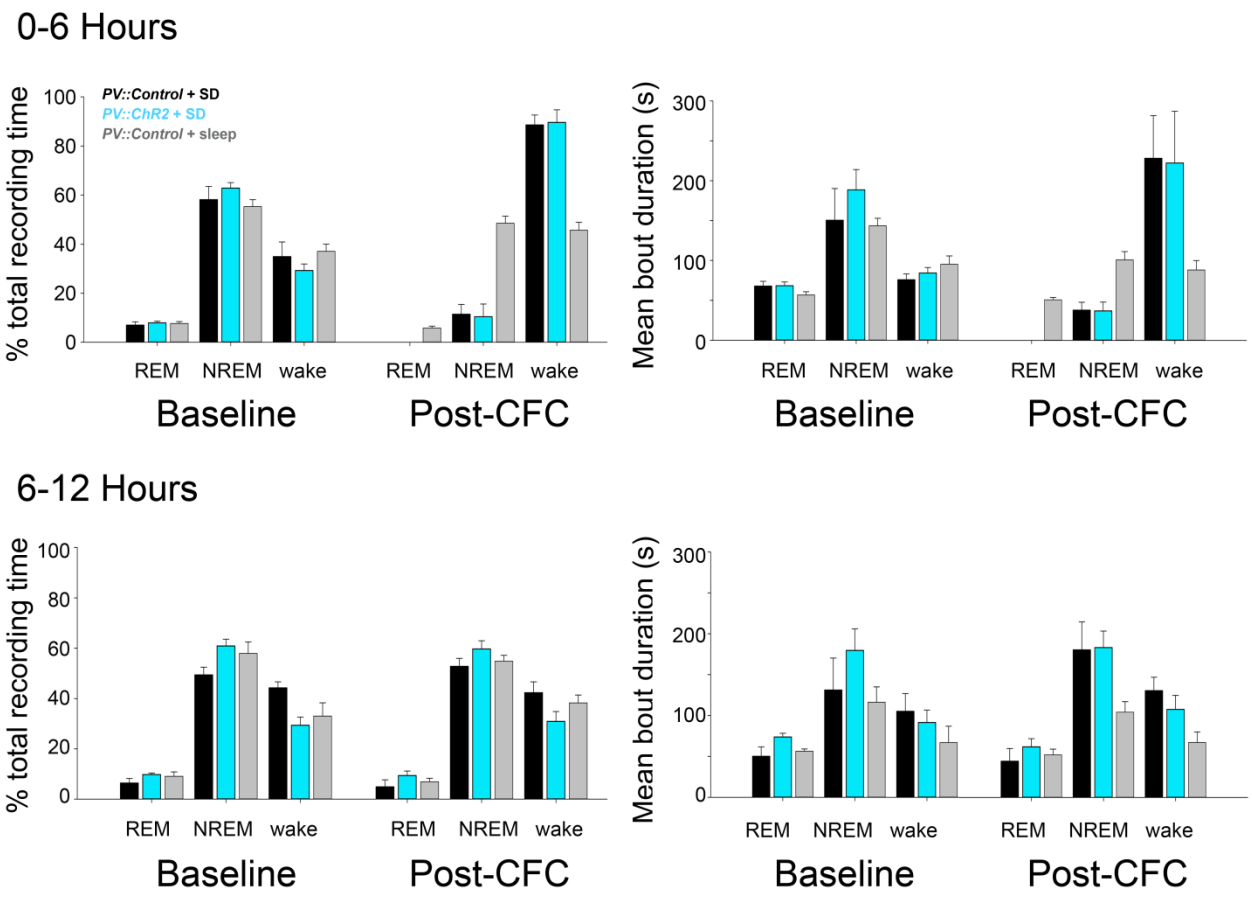

Supplemental Figure 5.12: Sleep architecture during stimulation experiments. There was no significant effect of treatment on either percent of time spent in REM, NREM between baseline and following CFC during recovery time 6-12 hours after training for either % of total time in each state nor mean bout duration. For sleep deprived, there was an obvious increase in both % of total time spent in each state during handling period. Mean bout duration in Post-CFC recording reflects the SD. There was no significant effect of treatment on either percent of time spent in REM, NREM, and wake between baseline and following CFC during recovery 6-12 hours after training for either % of total time in each state nor mean bout duration. Error bars are SEM for animals for each treatment,

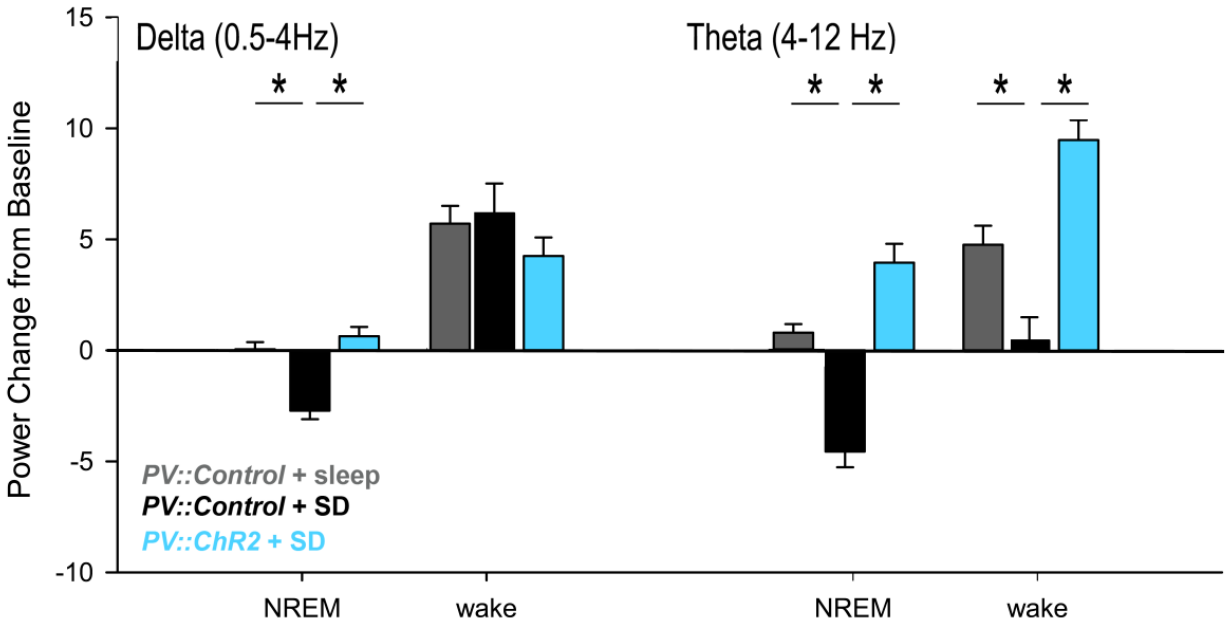

Supplemental Figure 5.13: CA1 LFP power in separate states during stimulation experiments. Quantification of power change from baseline within frequency bands corresponding to delta and theta during NREM sleep and wakefulness during hours 0-6. (Mean ± SEM shown for all LFPs for each treatment n= 92 for control + SD, n=140 for ChR2 + SD, and n=172 for control + sleep) * indicates $p < 0.05$ Pairwise multi-comparison, Holm-Sidak *post hoc* test. REM states not shown, because for animals never went into REM during SD manipulation.

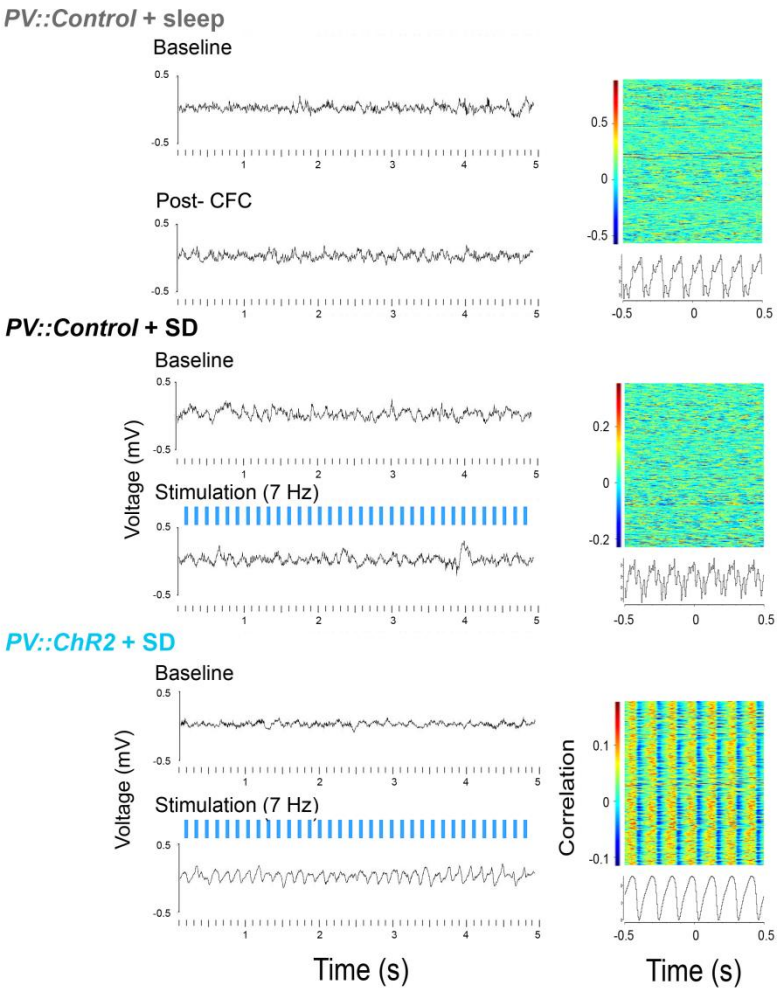

Supplemental Figure 5.14: Rhythmic optogenetic stimulation of PV+ interneurons in CA1. A representative 5-s LFP trace (***left***) and perievent LFP raster (***right***) for one of the recording sites from animals at in baseline and stimulation conditions.

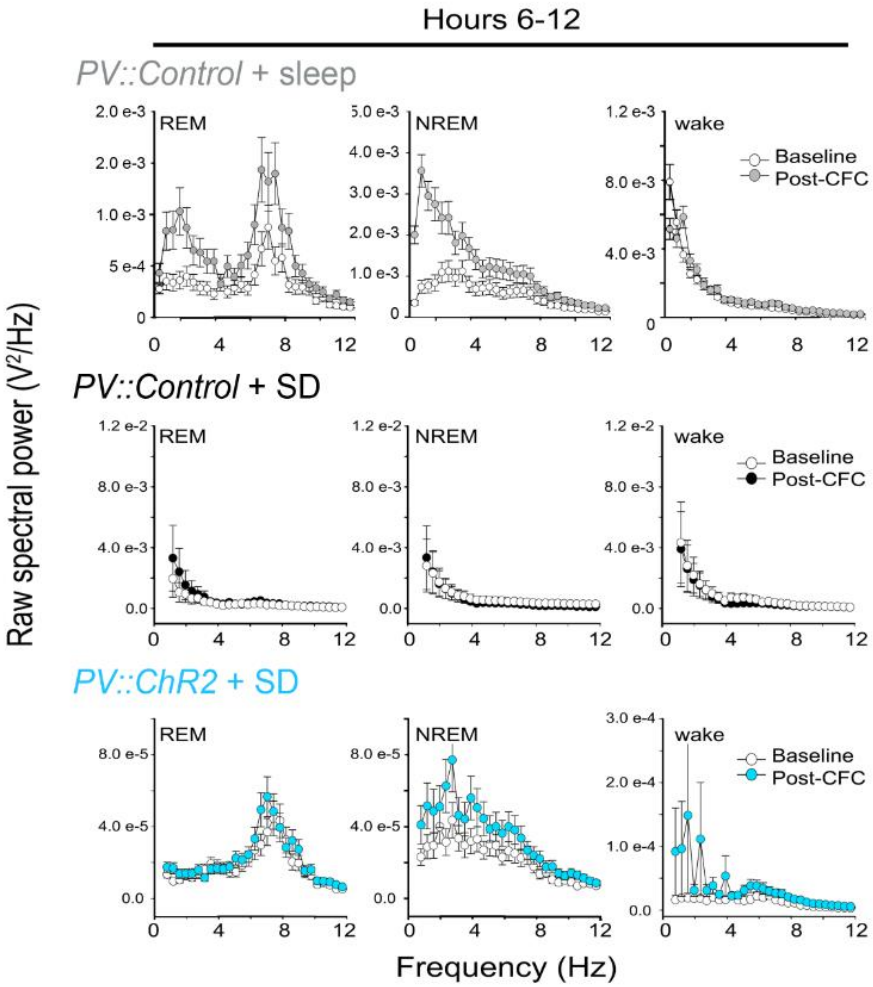

Supplemental Figure 5.15: Raw spectral power during recovery from rhythmic stimulation and sleep deprivation. Raw CA1 LFP spectral power during hours 6-12 of recording for a representative animals in REM, NREM, and wake at baseline (white circles) and post-CFC (colored circles). Mean ± SEM shown for local field potential values within each animal; n= 176 for control + sleep, n= 92 for control + SD, n=140 for ChR2 + SD.

CHAPTER VI:

Summary and conclusions

Sleep is thought to play a critical role in promoting various forms of learning and memory, and is also thought to regulate plasticity in brain circuits *in vivo*. In many human neuropathologies (e.g. Alzheimer's disease, schizophrenia, and epilepsy) there exist both cognitive deficits as well as disrupted sleep patterns, suggesting that sleep is critically linked to cognitive function. However, the mechanisms underlying this relationship are poorly understood.

Recent findings suggest a role for hippocampal activity patterns in episodic memory encoding. A significant body of evidence suggests that coordinated activation of specific populations of hippocampal neurons may promote subsequent recall, the so-called memory 'engram'. Lashley spent the entirety of his career seeking the location of the memory engram in the brain; however, what he neglected was that the importance of understanding memory is not so much *where* it is stored, but perhaps *HOW* memories are stored. Semon, the German scientist who initially coined the term engram described them as an 'enduring, though primarily latent modifications in the irritable substance produced by a stimulus', suggesting that the engram itself is reflected in the changes that ensue following learning. 'Irritable substance' is not single

cells, but rather the entire network of the brain. With respect to Lashley, this dissertation emphasizes the use of multiple methodologies to determine how network-wide activity patterns are the crux of memory understanding beyond individual, engram, cells and how these patterns affect the consolidation of contextual fear memory (CFM) in mice all within the context of sleep.

Characterization of activity pattern changes in CA1 hippocampus following learning show that many changes associated with proper consolidation are sleep-specific. [10,27,33] Chronic neuronal and network activity recordings in CA1 during CFM consolidation in Chapter II showed that there are multiple changes occurring in the network: increases in neuronal firing rate, increases in NREM delta (0.5-4 Hz), REM theta (4-12 Hz), and NREM sharp-wave ripple (SPWR, 150-250 Hz) oscillations. In addition, there are increasingly stable functional communication patterns between neurons during NREM sleep that persist over the 24-h of recording time. In the context of understanding memory, the first defining characteristic of an engram is *the persistent change in the brain resulting from a specific experience*. [71] The stabilization of cells' firing patterns following learning is manifestation of this change.

However, network stability measures are representative of a global change, a strengthening of multiple groups of cells that may or may not be a part of the original engram. Further understanding of the dynamics of network activity following learning was accomplished through collaborative efforts with the University of Michigan Department of Physics. We hypothesized that memory consolidation is systems-wide which promotes a globally – distributed representation of new memories. We developed the novel metric of Functional Network Stability (FuNS) to assess these

changes in biological networks. Analysis of these modeled networks have shown that there is a global stabilization, quantified as a persistence of functional connectivity over time, of network firing patterns upon introduction of a local heterogeneity (analogous to memory engram). **(Figure 3.3)** This is critical information for applying any metric to memory consolidation and the establishment of heterogeneity in biological systems, because we cannot always be certain that spike data is being collected from cells involved in the memory. Changes in functional stability due to introduction of heterogeneity can be calculated for heterogeneities of different strengths as well as for data recorded from neurons outside of the heterogeneity. For application to biological systems, these data show that a single memory engram can provide a substrate for systems-wide memory consolidation that could promote a globally-distributed representation of new memories.

The second defining characteristic of engrams is that they *have a behavioral property- automatic memory retrieval process engaged when a cue interacts with information stored in the memory.* Analysis in **Chapter III** of behavioral data in wild-type data show NREM-specific FuNS increases for individual mice were predictive of their behavioral performance during subsequent memory assessment. Since stability is a measure of network change, this correlation suggests an imparting of memory beyond the scope of individual engram cells. However, what drives this stability is still a matter of speculation. Numerous studies have demonstrated sequential replay of network activity patterns associated with prior experience. [81,83] Selective offline reactivation of neuronal populations activated during a learning experience has also been widely reported. [134–138] Reactivation appears to occur at a times immediately following new

experiences when it could play a pivotal role in consolidation. Behavioral state-dependent hippocampal oscillations such as sharp wave ripples (SPWRs) may support sequential replay, but it is still unclear whether hippocampal oscillations, replay, or reactivation are required for memory consolidation following novel learning. [139]

Employing our new FuNs metrics, we can quantify changes in functional connectivity between CA1 neurons in the hours following single-trial CFC and show that consolidation-related changes in CA1 network dynamics can be measured over a longer time window than previously reported for either sequential replay or ensemble reactivation (*i.e*., over several hours following learning, vs. tens of minutes). [42] This suggests replay may be necessary to initiate strengthening of the network, but is not sufficient.

In the course of this work in wild-type animals, it was observed that fast-spiking (FS) interneurons show greater firing coherence with CA1 network oscillations during CFM consolidation. The specific role of a subset of FS interneurons that were parvalbumin-expressing was investigated in Chapter IV. Transient inhibition of Parvalbumin-expressing (PV+) interneurons in mouse CA1 after learning abolishes CFM. This effect is associated with loss of three network changes associated with normal consolidation: 1) augmented sleep-associated delta, theta, and SPWR oscillations, 2) long-lasting stabilization of CA1 neurons' functional connectivity patterns and, 3) consistent NREM specific reactivation of ensembles of neurons in CA1.

Additionally, NREM stability following CFC was correlated with the occurrence of NREM ripples (particularly in the first 2 h following training; **Figure 4.7e**), but was not

predicted by NREM theta or delta changes (further supporting replay/reactivation may be an initiator of global stability). This suggests that PV+ interneurons play a critical role in stabilizing communication patterns throughout the CA1 network in the hours following CFC**,** but does not necessarily imply the need for PV+ interneurons to be in the engram itself. PV+ interneurons, whose extensive connectivity to principal cells in CA1 are thus hypothesized to play a critical role in controlling temporal dynamics during sleep-specific oscillations leading to memory formation. [62] Indeed, our data suggest that rhythmic coordination of network activity by PV+ interneurons - at frequencies that are significantly augmented following learning - has long-lasting effects on both the stability and strength of network connections. This is perhaps accomplished via theta-driven synchronous firing of large populations of cells, as enhanced neuronal spike-field coherence to theta rhythms were sufficient to induce long-lasting increases in stability.

To further separate the role of PV+ interneurons in CFM consolidation from sleep itself, during which most network stabilization occurs, PV+ interneurons were state-specifically inhibited in CA1 following learning. Chapter V shows that PV+ interneuron-mediated oscillations during sleep are specifically required for CFM, during NREM sleep, but not wake or REM sleep. This suggests that PV+ interneurons amplify NREM sleep-associated CA1 network oscillations to regulate spike timing in a manner that could promotes stability and systems-level memory consolidation. Additionally, NREM inhibition of PV+-interneurons alters subsequent REM oscillatory activity, but decreasing theta changes from baseline compared to controls **(Figure 5.5e)**. Very little work has been done in trying to understand NREM-REM transitions, However, bouts of REM always follow NREM, and cannot happen independently (for example when sleep

depriving an animal). Transition states between NREM-REM are often addressed in the literature as being of importance in consolidation, but these experiments are often done in larger rodents (i.e. rats). [165] Mouse models do not exhibit these transitory states and therefore there is impetus to study how these two states are connected. Future studies (in our lab or others) could address this question by assessing individual NREM-REM transitions following CFC during NREM-targeted inhibition of PV+- interneurons. Clarification of whether or not these REM-theta decreases happen across all REM bouts, or if it is a result of individual instances of large theta decreases in selected bouts.

In the absence of sleep, theta-frequency stimulation of PV+ interneurons drives frequency-specific, rhythmic activity in the CA1 LFP associated with stabilized functional communication between CA1 neurons. **(Figure 5.5b)** These increases in FuNS predict behavioral measures of CFM consolidation 24 h after CFC. **(Figure 5.5d)** Critically, rhythmic stimulation of CA1 PV+ interneurons in the immediate hours post-CFC is sufficient to rescue CFM from deficits caused by sleep deprivation. This rescue of This manipulation increased theta frequency band changes from baseline beyond that of normal sleeping animals. This also restores persistent decreases in NREM delta power and SPWRs that extend into recovery sleep. Differences in the oscillatory coordination of memory systems during sleep might be explained by differences in temporal processing, where consolidation is initiated by REM theta-mediated coordination of spike-timings early on in learning, and long term, stable store is facilitated later on via NREM slow oscillations and SPWRs. The connections between these ensembles of cells are strengthened as consolidation continues, possibly via galvanized reactivation

during NREM SPWRs.[164] I thus hypothesize that PV+-driven theta, not specific reactivation of engram cells, primes the entire network for reactivation during subsequent NREM sleep which leads to long term store of robust memories.

REM sleep, which is dominated by theta rhythms, is not a tonic behavioral state. Rather, it occurs in 30-60 second bouts intermittently throughout the day, totally only 5% of total recording time.[32,45] Putting this in perspective, mice spend just over an hour over the course of an entire day in REM sleep. Compared to the 6-h of theta drive we are imposing on the network, we are beyond the biological confines of the experiment. If I had continued the studies beyond the work in this dissertation, the real, biological sufficiency of theta in the absence of sleep would be assessed. REM is usually enriched in the latter half of a mouse's 12-h rest phase (assuming a 12/12 L/D cycle), so what is the biological relevance of having REM-specific oscillation immediately following training? [32] Future experiments may test the effects of more biologically-realistic theta stimulations, starting with a 60 second theta pulse every hour for 6-h in the context of SD. Assuming even distribution of REM states across the circadian day, this is approximately equal to 5% of total recording time. The main objective in this set of proposed experiments would not just be to see if temporally accurate theta stimulation is sufficient to rescue learning phenotype, but also to ensure that network oscillations in recovery sleep period are fully restored. Since network stabilization occurs over the course of recording time, and most of this is occurring during NREM sleep, we need to confirm normal baseline network rhythms following sleep deprivation can be rescued with limited theta drive in the 6-h post-CFC. Important questions such as 1) whether or not there is there a gradient of theta necessary to establish stability and 2) is stability

binary?- does it occur or not occur as a result of some gated threshold of pre-established (possibly theta-driven) synchrony- would be addressed with these experiments. Much of our understanding of these questions will result from further tailoring of our FuNS metric, which is currently being undertaken prior to public release of our metric for use by other investigators.

Lastly, new evidence out of the Zochowski lab suggests that in computational model during times of high acetylcholine (which mimics REM-like states) there is an increased advancement of spike timing. This drives synchrony of network activity more quickly because the network is trying to always get to a 0 phase shift. Theta could be this external drive on the network that synchronizes spike timings. Perhaps more interesting is that during periods of low acetylcholine (analogous to NREM states) when we biologically see a stabilization of network connectivity, computational models show that there is heterogeneity reinforcement via slow-waves (i.e. NREM delta), creating a distributed shadow of the memory across multiple groups of cells. The heterogeneity, as a computational analogue of a biological engram, supports the third defining characteristic of engrams that *the content of engram reflects what transpired at encoding and predicts what can be recovered in retrieval.* [71] Biological follow-up using data previously collected from wild-type mice could help our understanding of how slow waves and NREM sleep may thus lead to stabilization of a network. We would thus propose to amend our understanding of engrams, not just as the initial imparting of firing rate changes in individual cells (as first observed in **Chapter II**), but rather as a network-wide synchrony to REM-specific theta leading to subsequent strengthening during NREM sleep.

Together, this work would shed light on how sleep contributes to long-term memory formation, which has been a long-standing mystery in neuroscience. An understanding of these mechanisms may lead to targeted interventions for the multitude of neuropathologies where sleep quality and cognitive function are impaired.

BIBLIOGRAPHY

1. Squire, L. R. & Zola-Morgan, S. Memory: brain systems and behavior. *Trends Neurosci.* **11,** 170–5 (1988).

2. Lydic, R. & Biebuyck, J. F. Clinical Physiology of Sleep. (1988).

3. Lashley, K. In search of the engram. *Experimental Biology Symposium No. 4: Physiological Mechanisms in Animal Behaviour* 454–482 (1950).

4. Hübener, M. & Bonhoeffer, T. Searching for Engrams. *Neuron* **67,** 363–371 (2010).

5. Ryan, T. J., Roy, D. S., Pignatelli, M., Arons, a. & Tonegawa, S. Engram cells retain memory under retrograde amnesia. *Science.* **348,** 1007–1013 (2015).

6. Annese, J. *et al.* Postmortem examination of patient H.M.'s brain based on histological sectioning and digital 3D reconstruction. *Nat. Commun.* **5,** 1–9 (2014).

7. Scoviille, W. B. & Milner, B. Loss of recent memory after bilateral hippocampal leisons. *J Neurol Neurosurg Psychiatry* **20,** 11–21 (1957).

8. McGaugh, J. L. Neuroscience - Memory - a century of consolidation. *Science.* **287,** 248–251 (2000).

9. Squire, L. R. The Legacy of Patient H.M. for Neuroscience. **61,** 6–9 (2009).

10. Buzsáki, G. Theta Oscillations in the Hippocampus. *Neuron* **33,** 325–340 (2002).

11. Born, J. & Wilhelm, I. System consolidation of memory during sleep. *Psychol. Res.* **76,** 192–203 (2012).

12. Ebbinghaus, H. Memory; a contribution to experimental psychology. *Oxford Univ.***,** 352 (1859).

13. Jenkins, J. G. . & Dallenbach, K. M. . Obliviscence during Sleep and Waking. *Am. J. Psychol.* **35,** 605–612 (1924).

14. Ellenbogen, J. M., Hulbert, J. C., Stickgold, R., Dinges, D. F. & Thompson-Schill, S. L. Interfering with Theories of Sleep and Memory: Sleep, Declarative Memory, and Associative Interference. *Curr. Biol.* **16,** 1290–1294 (2006).

15. Havekes, R., Meerlo, P. & Abel, T. Animal Studies on the Role of Sleep in Memory: From Behavioral Performance to Molecular Mechanisms. *Curr. Top. Behav. Neurosci.* (2015)

16. Abel, T., Havekes, R., Saletin, J. M. & Walker, M. P. Sleep, plasticity and memory from molecules to whole-brain networks. *Curr. Biol.* **23,** R774-88 (2013).

17. Graves, L., Pack, a & Abel, T. Sleep and memory: a molecular perspective. *Trends Neurosci.* **24,** 237–43 (2001).

18. Stickgold, R. Sleep-dependent memory consolidation. *Nature* **437,** 1272–8

(2005).

19. Sara, S. J. Sleep to Remember. *J. Neurosci.* **37,** 457–463 (2006).

20. Walker, M. P. & Stickgold, R. Sleep-dependent learning and memory consolidation. *Neuron* **44,** 121–33 (2004).

21. Csicsvari, J., Hirase, H., Czurkó, a, Mamiya, a & Buzsáki, G. Oscillatory coupling of hippocampal pyramidal cells and interneurons in the behaving Rat. *J. Neurosci.* **19,** 274–87 (1999).

22. Benchenane, K. *et al.* Coherent theta oscillations and reorganization of spike timing in the hippocampal- prefrontal network upon learning. *Neuron* **66,** 921–936 (2010).

23. Feld, G. B., Weis, P. P. & Born, J. The Limited Capacity of Sleep-Dependent Memory Consolidation. **7,** 1–12 (2016).

24. Horne, J. A. & McGrath, M. J. The consolidation hypothesis for REM sleep function: Stress and other confounding factors - A review. *Biol. Psychol.* **18,** 165–184 (1984).

25. Mölle, M., Eschenko, O., Gais, S., Sara, S. J. & Born, J. The influence of learning on sleep slow oscillations and associated spindles and ripples in humans and rats. *Eur. J. Neurosci.* **29,** 1071–1081 (2009).

26. Sullivan, D., Mizuseki, K., Sorgi, a. & Buzsaki, G. Comparison of Sleep Spindles and Theta Oscillations in the Hippocampus. *J. Neurosci.* **34,** 662–674 (2014).

27. Steriade, M. Slow-wave sleep: Serotonin, neuronal plasticity, and seizures. *Archives Italiennes de Biologie* **142,** 359–367 (2004).

28. Headley, D. B. & Paré, D. Common oscillatory mechanisms across multiple memory systems. *npj Sci. Learn.* **2,** 1 (2017).

29. Mednick, S. C. *et al.* The restorative effect of naps on perceptual deterioration. *Nat. Neurosci.* **5,** 677–81 (2002).

30. Van Der Werf, Y. D. *et al.* Sleep benefits subsequent hippocampal functioning. *Nat. Neurosci.* **12,** 122–123 (2009).

31. Ahnaou, a, Huysmans, H., Jacobs, T. & Drinkenburg, W. H. I. M. Cortical EEG oscillations and network connectivity as efficacy indices for assessing drugs with cognition enhancing potential. *Neuropharmacology* 1–17 (2014).

32. Stickgold, R., Whidbee, D., Schirmer, B., Patel, V. & Hobson, J. A. Visual discrimination task improvement: A multi-step process occurring during sleep. *J. Cogn. Neurosci.* **12,** 246–254 (2000).

33. Girardeau, G., Benchenane, K., Wiener, S. I., Buzsáki, G. & Zugaro, M. B. Selective suppression of hippocampal ripples impairs spatial memory. *Nat.*

Neurosci. **12,** 1222–3 (2009).

34. Buzsáki, G. *et al.* Hippocampal network patterns of activity in the mouse. *Neuroscience* **116,** 201–11 (2003).

35. O'Keefe, J Dostrovsky, J. The hippocampus as a spatial map . Preliminary evidence from unit activity in the freely-moving rat. **34,** 171–175 (1971).

36. Buzsáki, G. The hippocampo-neocortical dialogue. *Cereb. Cortex* **6,** 81–92 (1996).

37. Wierzynski, C. M., Lubenov, E. V., Gu, M. & Siapas, A. G. State-Dependent Spike-Timing Relationships between Hippocampal and Prefrontal Circuits during Sleep. *Neuron* **61,** 587–596 (2009).

38. Eschenko, O. & Sara, S. J. Learning-dependent, transient increase of activity in noradrenergic neurons of locus coeruleus during slow wave sleep in the rat: brain stem-cortex interplay for memory consolidation? *Cereb. Cortex* **18,** 2596–603 (2008).

39. Girardeau, G. & Zugaro, M. Hippocampal ripples and memory consolidation. *Curr. Opin. Neurobiol.* **21,** 452–9 (2011).

40. Nguyen, P. V & Kandel, E. R. Brief theta-burst stimulation induces a transcription-dependent late phase of LTP requiring cAMP in area CA1 of the mouse hippocampus. *Learn. Mem.* **4,** 230–243 (1997).

41. Csicsvari, J., Hirase, H., Czurkó, a, Mamiya, a & Buzsáki, G. Fast network oscillations in the hippocampal CA1 region of the behaving rat. *J. Neurosci.* **19,** RC20 (1999).

42. Aton, S. J., Seibt, J. & Frank, M. G. *Sleep and Memory*. (John Wiley & Sons, Ltd: Chichester. DOI:, 2009).

43. Daumas, S., Halley, H., Francés, B. & Lassalle, J.-M. Encoding, consolidation, and retrieval of contextual memory: differential involvement of dorsal CA3 and CA1 hippocampal subregions. *Learn. Mem.* **12,** 375–82 (2005).

44. Graves, L. a, Heller, E. a, Pack, A. I. & Abel, T. Sleep Deprivation Selectively Impairs Memory Consolidation for Contextual Fear Conditioning. *Learn. Mem.* (2003).

45. Ognjanovski, N., Maruyama, D., Lashner, N., Zochowski, M. & Aton, S. J. CA1 hippocampal network activity changes during sleep-dependent memory consolidation. *Front. Syst. Neurosci.* **8,** 1–11 (2014).

46. Maras, P. M. *et al.* Preferential loss of dorsal-hippocampus synapses underlies memory impairments provoked by short, multimodal stress. *Mol. Psychiatry* **19,** 811–22 (2014).

47. Kotloski, R., Lynch, M., Lauersdorf, S. & Sutula, T. Repeated brief seizures induce progressive hippocampal neuron loss and memory deficits. *Prog. Brain Res.* **135,** 95–110 (2002).

48. Vyazovskiy, V. V, Cirelli, C., Pfister-Genskow, M., Faraguna, U. & Tononi, G. Molecular and electrophysiological evidence for net synaptic potentiation in wake and depression in sleep. *Nat. Neurosci.* **11,** 200–8 (2008).

49. Hebb, D. O. *The Organization of Behavior*. (1949).

50. Buzsáki, G. Two-stage model of memory trace formation: A role for 'noisy' brain states. *Neuroscience* **31,** 551–570 (1989).

51. Shimizu, E. NMDA Receptor-Dependent Synaptic Reinforcement as a Crucial Process for Memory Consolidation. *Science.* **290,** 1170–1174 (2000).

52. Tadavarty, R., Kaan, T. K. Y. & Sastry, B. R. Long-term depression of excitatory synaptic transmission in rat hippocampal CA1 neurons following sleep-deprivation. *Exp. Neurol.* **216,** 239–42 (2009).

53. Clarke, V. R. J., Collingridge, G. L., Lauri, S. E. & Taira, T. Synaptic kainate receptors in CA1 interneurons gate the threshold of theta-frequency-induced long-term potentiation. *J. Neurosci.* **32,** 18215–26 (2012).

54. Forro, T., Valenti, O., Lasztoczi, B. & Klausberger, T. Temporal Organization of GABAergic Interneurons in the Intermediate CA1 Hippocampus During Network Oscillations. *Cereb. Cortex* 1–13 (2013).

55. Lovett-barron, M. & Losonczy, A. Behavioral consequences of GABAergic neuronal diversity. *Curr. Opin. Neurobiol.* **26,** 27–33 (2014).

56. Klausberger, T. *et al.* Complementary roles of cholecystokinin- and parvalbumin-expressing GABAergic neurons in hippocampal network oscillations. *J. Neurosci.* **25,** 9782–93 (2005).

57. Kalueff, A. & Nutt, D. Role of GABA in Anxiety and Depression. *Depress. Anxiety* **24,** 495–517 (2007).

58. Klausberger, T. & Somogyi, P. Neuronal diversity and temporal dynamics: the unity of hippocampal circuit operations. *Science.* **321,** 53–7 (2008).

59. Freund, T. F. & Katona, I. Perisomatic inhibition. *Neuron* **56,** 33–42 (2007).

60. Freund, T. F. Interneurons of the Hippocampus. *Hippocampus* **6,** 347–470 (1996).

61. Andrioli, A. & Arellano, J. I. Quantitative analysis of parvalbumin-immunoreactive cells in the human epileptic hippocampus. *Neuroceince*. **149,** 131–143 (2007).

62. Hu, H., Gan, J. & Jonas, P. Fast-spiking, parvalbumin+ GABAergic interneurons: From cellular design to microcircuit function. *Science.* **345,** 1255263–1255263 (2014).

63. Bezaire, M. J. & Soltesz, I. Quantitative assessment of CA1 local circuits: knowledge base for interneuron-pyramidal cell connectivity. *Hippocampus* **23,** 751–85 (2013).

64. Huh, C. Y. L. *et al.* Excitatory Inputs Determine Phase-Locking Strength and Spike-Timing of CA1 Stratum Oriens/Alveus Parvalbumin and Somatostatin Interneurons during Intrinsically Generated Hippocampal Theta Rhythm. *J. Neurosci.* **36,** 6605–6622 (2016).

65. Sadowski, J. H. L. P., Jones, M. W. & Mellor, J. R. Sharp-Wave Ripples Orchestrate the Induction of Synaptic Plasticity during Reactivation of Place Cell Firing Patterns in the Hippocampus. *Cell Rep.* 1–14 (2016).

66. Chiovini, B. *et al.* Dendritic Spikes Induce Ripples in Parvalbumin Interneurons during Hippocampal Sharp Waves. *Neuron* **82,** 908–924 (2014).

67. Ferguson, K. a, Huh, C. Y. L., Amilhon, B., Williams, S. & Skinner, F. K. Experimentally constrained CA1 fast-firing parvalbumin-positive interneuron network models exhibit sharp transitions into coherent high frequency rhythms. *Front. Comput. Neurosci.* **7,** 144 (2013).

68. Ognjanovski, N. *et al.* Parvalbumin-expressing interneurons coordinate hippocampal network dynamics required for memory consolidation. *Nat. Commun.* **In Press,** (2017).

69. Moser, E. I., Kropff, E. & Moser, M.-B. Place cells, grid cells, and the brain's spatial representation system. *Annu. Rev. Neurosci.* **31,** 69–89 (2008).

70. Gerstein, G. L., Perkel, D. H. & Subramanian, K. N. Identification of functionally related neural assemblies. *Brain Res.* **140,** 43–62 (1978).

71. Josselyn, S. a., Köhler, S. & Frankland, P. W. Finding the engram. *Nat. Rev. Neurosci.* **16,** 521–534 (2015).

72. Fingelkurts, A. A., Fingelkurts, A. A. & Kähkönen, S. Functional connectivity in the brain - Is it an elusive concept? *Neurosci. Biobehav. Rev.* **28,** 827–836 (2005).

73. He, Y. Temporal Evolution Analysis of Functional Connectivity in Epilepsy Based on Weighted Complex Networks. 0–2 (2016).

74. Holmes, M. J. *et al.* Resting state functional connectivity of the hippocampus associated with neurocognitive function in left temporal lobe epilepsy. *Hum. brain Mapp.* **35,** 735–744 (2014).

75. Jeong, J. EEG dynamics in patients with Alzheimer's disease. *Clin. Neurophysiol.* **115,** 1490–1505 (2004).

76. Mary, A. *et al.* Resting-state Functional Connectivity is an Age-dependent Predictor of Motor Learning Abilities. 1–10 (2016).

77. Fujisawa, S. & Buzsáki, G. A 4-Hz oscillation adaptively synchronizes prefrontal, VTA and hippocampal activities. *Neuron* **71,** 153–165 (2011).

78. de Lanerolle, N. C. & Lee, T.-S. New facets of the neuropathology and molecular profile of human temporal lobe epilepsy. *Epilepsy Behav.* **7,** 190–203 (2005).

79. Bassett, D. S. *et al.* Dynamic reconfiguration of human brain networks during learning. *Proc. Natl. Acad. Sci. U. S. A.* **108,** 7641–7646 (2011).

80. Kudrimoti, H. S., Barnes, C. a & McNaughton, B. L. Reactivation of hippocampal cell assemblies: effects of behavioral state, experience, and EEG dynamics. *J. Neurosci.* **19,** 4090–4101 (1999).

81. Wilson, M. a & McNaughton, B. L. Reactivation of hippocampal ensemble memories during sleep. *Science* **265,** 676–9 (1994).

82. van de Ven, G. M., Trouche, S., McNamara, C. G., Allen, K. & Dupret, D. Hippocampal offline reactivation consolidates recently formed cell assembly patterns during sharp wave-ripples. *Neuron* 1–7 (2016). doi:10.1016/j.neuron.2016.10.020

83. Louie, K. & Wilson, M. a. Temporally structured replay of awake hippocampal ensemble activity during rapid eye movement sleep. *Neuron* **29,** 145–156 (2001).

84. Aton, S. J. *et al.* Visual experience and subsequent sleep induce sequential plastic changes in putative inhibitory and excitatory cortical neurons. *Proc. Natl. Acad. Sci. U. S. A.* **110,** 3101–6 (2013).

85. Aton, S. J. *et al.* Mechanisms of sleep-dependent consolidation of cortical plasticity. *Neuron* **61,** 454–66 (2009).

86. Seibt, J. *et al.* Protein synthesis during sleep consolidates cortical plasticity in vivo. *Curr. Biol.* **22,** 676–82 (2012).

87. McDermott, C. M., Hardy, M. N., Bazan, N. G. & Magee, J. C. Sleep deprivation-induced alterations in excitatory synaptic transmission in the CA1 region of the rat hippocampus. *J. Physiol.* **570,** 553–65 (2006).

88. Vecsey, C. G. *et al.* Sleep deprivation impairs cAMP signalling in the hippocampus. *Nature* **461,** 1122–5 (2009).

89. Bourtchouladze, R. *et al.* Different training procedures recruit either one or two critical periods for contextual memory consolidation, each of which requires protein synthesis and PKA. *Learn. Mem.* (1998).

90. Abel, T. & Lattal, K. M. Molecular mechanisms of memory acquisition, consolidation and retrieval. *Curr. Opin. Neurobiol.* **11,** 180–7 (2001).

91. Sindreu, C. B., Scheiner, Z. S. & Storm, D. R. Ca2+ -stimulated adenylyl cyclases regulate ERK-dependent activation of MSK1 during fear conditioning. *Neuron* **53,**

79–89 (2007).

92. Vecsey, C. G. *et al.* Genomic analysis of sleep deprivation reveals translational regulation in the hippocampus. *Physiol. Genomics* **44,** 981–91 (2012).

93. Popa, D., Duvarci, S., Popescu, A. T., Léna, C. & Paré, D. Coherent amygdalocortical theta promotes fear memory consolidation during paradoxical sleep. *Proc. Natl. Acad. Sci. U. S. A.* **107,** 6516–9 (2010).

94. Wetzel, W., Ott, T. & AMtthies, H. Post-training hippocampal rhythmic slow activity ('theta') elicited by septal stimulation improves memory consolidation in rats. *Behav. Biol.* **21,** 32–40 (1977).

95. McKay, B. M., Oh, M. M. & Disterhoft, J. F. Learning increases intrinsic excitability of hippocampal interneurons. *J. Neurosci.* **33,** 5499–506 (2013).

96. Mckay, B. M., Matthews, E. A., Oliveira, F. A. & Disterhoft, J. F. Intrinsic Neuronal Excitability Is Reversibly Altered by a Single Experience in Fear Conditioning. *J. Neurophysiol.* **102,** 2763–2770 (2009).

97. Feldt, S., Waddell, J., Hetrick, V., Berke, J. & Żochowski, M. Functional clustering algorithm for the analysis of dynamic network data. *Phys. Rev. E* **79,** 56104 (2009).

98. Power, J. M., Thompson, L. T., Moyer, J. R. & Disterhoft, J. F. Enhanced synaptic transmission in CA1 hippocampus after eyeblink conditioning. *J. Neurophysiol.* **78,** 1184–7 (1997).

99. O'Neill, J., Pleydell-Bouverie, B., Dupret, D. & Csicsvari, J. Play it again: reactivation of waking experience and memory. *Trends Neurosci.* **33,** 220–229 (2010).

100. McKay, B. M. *et al.* Increasing SK2 channel activity impairs associative learning. *J. Neurophysiol.* **108,** 863–70 (2012).

101. Pedarzani, P. *et al.* Specific enhancement of SK channel activity selectively potentiates the afterhyperpolarizing current IAHP and modulates the firing properties of hippocampal pyramidal neurons. *J. Biol. Chem.* **280,** 41404–41411 (2005).

102. Mackiewicz, M. *et al.* Macromolecule biosynthesis: a key function of sleep. *Physiol. Genomics* **31,** 441–57 (2007).

103. Feldman, D. E. The spike-timing dependence of plasticity. *Neuron* **75,** 556–71 (2012).

104. O'Connor, D. H., Wittenberg, G. M. & Wang, S. S.-H. Graded bidirectional synaptic plasticity is composed of switch-like unitary events. *Proc. Natl. Acad. Sci. U. S. A.* **102,** 9679–9684 (2005).

105. Leung, L. S. & Yu, H. W. Theta-frequency resonance in hippocampal CA1 neurons in vitro demonstrated by sinusoidal current injection. *J. Neurophysiol.* **79,** 1592–1596 (1998).

106. Penley, S. C. *et al.* Novel space alters theta and gamma synchrony across the longitudinal axis of the hippocampus. *Front. Syst. Neurosci.* **7,** 20 (2013).

107. Woo, N. H., Duffy, S. N., Abel, T. & Nguyen, P. V. Temporal spacing of synaptic stimulation critically modulates the dependence of LTP on cyclic AMP-dependent protein kinase. *Hippocampus* **13,** 293–300 (2003).

108. Hasselmo, M. E. What is the function of hippocampal theta rhythm?--Linking behavioral data to phasic properties of field potential and unit recording data. *Hippocampus* **15,** 936–49 (2005).

109. Kim, S., Putrino, D., Ghosh, S. & Brown, E. N. A Granger causality measure for point process models of ensemble neural spiking activity. *PLoS Comput. Biol.* **7,** 1–13 (2011).

110. Granger, C. Investigating Causal Relations by Econometric Models and Cross-spectral Methods. *Econometrica* **37,** 424–438 (1969).

111. Cadotte, A. J., DeMarse, T. B., He, P. & Ding, M. Causal measures of structure and plasticity in simulated and living neural networks. *PLoS One* **3,** (2008).

112. Bressler, S. L. & Seth, A. K. Wiener-Granger Causality: A well established methodology. *Neuroimage* **58,** 323–329 (2011).

113. Eschenko, O., Ramadan, W., Mölle, M., Born, J. & Sara, S. J. Sustained increase in hippocampal sharp-wave ripple activity during slow-wave sleep after learning. *Learn. Mem.* **15,** 222–228 (2008).

114. Schreiber, T. Measuring information transfer. *Phys. Rev. Lett.* **85,** 461–464 (2000).

115. Ito, S. *et al.* Extending transfer entropy improves identification of effective connectivity in a spiking cortical network model. *PLoS One* **6,** (2011).

116. Sepulcre, J., Sabuncu, M. R., Yeo, T. B., Liu, H. & Johnson, K. A. Stepwise Connectivity of the Modal Cortex Reveals the Multimodal Organization of the Human Brain. *J. Neurosci.* **32,** 10649–10661 (2012).

117. Bastos, A. M. & Schoffelen, J.-M. A tutorial review of functional connectivity analysis methods and their interpretational pitfalls. *Front. Syst. Neurosci.* **9,** 1–23 (2016).

118. Vinck, M., Battaglia, F. P., Womelsdorf, T. & Pennartz, C. Improved measures of phase-coupling between spikes and the Local Field Potential. *J. Comput. Neurosci.* **33,** 53–75 (2012).

119. Vyazovskiy, V. V. *et al.* Cortical firing and sleep homeostasis. *Neuron* **63,** 865–878 (2009).

120. Aton, S. J., Suresh, A., Broussard, C. & Frank, M. G. Sleep promotes cortical response potentiation following visual experience. *Sleep* **37,** 1163–70 (2014).

121. Gregoriou, G. G., Gotts, S. J., Zhou, H. & Desimone, R. High-frequency, long-range coupling between prefrontal and visual cortex during attention. *Science.* **324,** 1207–1210 (2009).

122. Bartlett, M. . S. . On the theoretical specification and sampling properties of autocorrelated time-series. *R. Stat. Soc.* **8,** 27–41 (1946).

123. Marsálek, P., Koch, C. & Maunsell, J. On the relationship between synaptic input and spike output jitter in individual neurons. *Proc. Natl. Acad. Sci. U. S. A.* **94,** 735–40 (1997).

124. Metropolis, N. & Ulam, S. The Monte Carlo Method. *J. Am. Stat. Assoc. ISSN* **44,** 335–341 (2012).

125. DiCiccio, T. J. & Efron, B. Bootstrap confidence intervals. *Stat. Sci.* **11,** 189–228 (1996).

126. Friston, K. J., Frith, C. D., Liddle, P. F. & Frackowiak, R. S. J. Functional Connectivity: The Principal-Component Analysis of Large (PET) Data Sets. *J. Cereb. Blood Flow Metab.* **13,** 5–14 (1993).

127. Tronson, N. C. *et al.* Mediating Conditioning and Extinction of Contextual Fear. *J. Neurosci.* **29,** 3387–3394 (2010).

128. Prince, T.-M. *et al.* Sleep deprivation during a specific 3-hour time window post-training impairs hippocampal synaptic plasticity and memory. *Neurobiol. Learn. Mem.* **109C,** 122–130 (2013).

129. Liu, X. *et al.* Optogenetic stimulation of a hippocampal engram activates fear memory recall. *Nature* **484,** 381–5 (2012).

130. Garner, a. R. *et al.* Generation of a synthetic memory trace. *Science (80-.).* **335,** 1513–1516 (2012).

131. Ramirez, S. *et al.* Creating a false memory in the hippocampus. *Science (80-.).* **341,** 387–391 (2013).

132. Matsuo, N. Irreplaceability of neuronal ensembles after memory allocation. *Cell Rep.* **11,** 351–357 (2015).

133. Ryan, T. J., Roy, D. S., Pignatelli, M., Arons, A. L. & Tonegawa, S. Engram cells retain memory under retrograde amnesia. *Science.* **348,** 1007–1013 (2015).

134. O'Neill, J., Senior, T. J., Allen, K., Huxter, J. R. & Csicsvari, J. Reactivation of experience-dependent cell assembly patterns in the hippocampus. *Nat. Neurosci.*

11, 209–15 (2008).

135. Dupret, D., O'Neill, J., Pleydell-Bouverie, B. & Csicsvari, J. The reorganization and reactivation of hippocampal maps predict spatial memory performance. *Nat. Neurosci.* **13,** 995–1002 (2010).

136. Valdes, J. M., Mc Naughton, B. L. & Fellous, J. M. Off-line reactivation of experience-dependent neuronal firing patterns in rat ventral tegmentum. *J Neurophysio* **114,** 1183–1195 (2015).

137. Bridi, M. C. D. *et al.* Rapid eye movement sleep promotes cortical plasticity in the developing brain. *Sci. Adv.* **1,** 1–8 (2015).

138. Chen, X., Rochefort, N. L., Sakmann, B. & Konnerth, A. Reactivation of the same synapses during spontaneous up states and sensory stimuli. *Cell Rep.* **4,** 31–39 (2013).

139. Sadowski, J. H. L. P., Jones, M. W. & Mellor, J. R. Ripples make waves: Binding structured activity and plasticity in hippocampal networks. *Neural Plast.* **2011,** (2011).

140. Sik, A., Penttonen, M., Ylinen, A. & Buzsaki, G. Hippocampal CA1 interneurons : Labeling study an in vivo intracellular. *J. Neurosci.* **75,** (1995).

141. Amilhon, B. *et al.* Parvalbumin interneurons of hippocampus tune population activity at theta frequency. *Neuron* **86,** 1277–1289 (2015).

142. Rogan, S. C. & Roth, B. L. Remote control of neuronal signaling. *Pharmacol. Rev.* **63,** 291–315 (2011).

143. Kim, J. J., Fanselow, M. S., DeCola, J. P. & Landeira-Fernandez, J. Selective impairment of long-term but not short-term conditional fear by the N-methyl-D-aspartate antagonist APV. *Behav. Neurosci.* **106,** 591–596 (1992).

144. Fanselow, M. S. Associative vs topographical accounts of the immediate shock-freezing deficit in rats: Implications for the response selection rules governing species-specific defensive reactions. *Learn. Motiv.* **17,** 16–39 (1986).

145. Daniel N. Hill, Mehta, S. B. & Kleinfeld, D. Quality metrics to accompany spike sorting of extracellular signals. *J. Neurosci.* **31,** 8699–8705 (2011).

146. Sato, T., Suzuki, T. & Mabuchi, K. Fast automatic template matching for spike sorting based on Davies-Bouldin validation indices. *Annu. Int. Conf. IEEE Eng. Med. Biol. - Proc.* 3200–3203 (2007).

147. Nicolelis, M. A. L. *et al.* Chronic, multisite, multielectrode recordings in macaque monkeys. *Proc. Natl. Acad. Sci.* **100,** 11041–11046 (2003).

148. Herry, C. *et al.* Switching on and off fear by distinct neuronal circuits. *Nature* **454,** 600–606 (2008).

149. Wheeler, D. W. *et al.* Hippocampome.org: A knowledge base of neuron types in the rodent hippocampus. *Elife* **4,** 1–28 (2015).

150. Graves, L. a, Heller, E. a, Pack, A. I. & Abel, T. Sleep deprivation selectively impairs memory consolidation for contextual fear conditioning. *Learn. Mem.* **10,** 168–76 (2003).

151. Stark, E. *et al.* Pyramidal cell-interneuron interactions underlie hippocampal ripple oscillations. *Neuron* **83,** 467–480 (2014).

152. Çalışkan, G. *et al.* Identification of Parvalbumin Interneurons as Cellular Substrate of Fear Memory Persistence. *Cereb. Cortex* **26,** 2325–2340 (2016).

153. Boyce, R., Glasgow, S. D., Williams, S. & Adamantidis, A. Causal evidence for the role of REM sleep theta rhythm in contextual memory consolidation. *Science (80-.).* **352,** 812–816 (2016).

154. Schlingloff, D., Kali, S., Freund, T. F., Hajos, N. & Gulyas, a. I. Mechanisms of sharp wave initiation and ripple generation. *J. Neurosci.* **34,** 11385–11398 (2014).

155. Donato, F., Rompani, S. B. & Caroni, P. Parvalbumin-expressing basket-cell network plasticity induced by experience regulates adult learning. *Nature* **504,** 272–276 (2013).

156. Havekes, R. *et al.* Sleep deprivation causes memory deficits by negatively impacting neuronal connectivity in hippocampal area CA1. *Elife* **5,** 1–22 (2016).

157. Tricoire, L. *et al.* A Blueprint for the Spatiotemporal Origins of Mouse Hippocampal Interneuron Diversity. *J. Neurosci.* **31,** 10948–10970 (2011).

158. Lopez De Armentia, M. *et al.* Development/Plasticity/Repair cAMP Response Element-Binding Protein-Mediated Gene Expression Increases the Intrinsic Excitability of CA1 Pyramidal Neurons. *J. Neurosci.* **27,** 13909–13918 (2007).

159. Diekelmann, S. & Born, J. The memory function of sleep. *Nat. Rev. Neurosci.* **11,** 114–26 (2010).

160. Dumoulin, M. C. *et al.* Extracellular Signal-Regulated Kinase (ERK) Activity During Sleep Consolidates Cortical Plasticity In Vivo. *Cereb. Cortex* **1,** 1–9 (2013).

161. Sheridan, G. K., Moeendarbary, E., Pickering, M., O'Connor, J. J. & Murphy, K. J. Theta-burst stimulation of hippocampal slices induces network-level calcium oscillations and activates analogous gene transcription to spatial learning. *PLoS One* **9,** e100546 (2014).

162. Grosmark, A. D., Mizuseki, K., Pastalkova, E., Diba, K. & Buzsáki, G. REM sleep reorganizes hippocampal excitability. *Neuron* **75,** 1001–7 (2012).

163. Jadhav, S. P., Kemere, C., German, P. W. & Frank, L. M. Awake hippocampal

sharp-wave ripples support spatial memory. *Science* **336,** 1454–8 (2012).

164. Malerba, P., Krishnan, G. P., Fellous, J.-M. & Bazhenov, M. Hippocampal CA1 Ripples as Inhibitory Transients. *PLOS Comput. Biol.* **12,** e1004880 (2016).

165. Poe, G. R. Sleep Is for Forgetting. **37,** 464–473 (2017).